LINEWIDTH AND RANGING CHARACTERIZATION OF A VERNIER-TUNED
DISTRIBUTED BRAGG REFLECTOR (VT-DBR) ALL-SEMICONDUCTOR
TUNABLE SWEPT LASER SYSTEM FOR
LIDAR IN AUTONOMOUS APPLICATIONS

A Thesis
presented to
the Faculty of California Polytechnic State University,
San Luis Obispo

In Partial Fulfillment
of the Requirements for the Degree
Master of Science in Electrical Engineering

by
Taewan Kim
June 2017

COMMITTEE MEMBERSHIP

TITLE: Linewidth and Ranging Characterization of a Vernier-Tuned Distributed Bragg Reflector (VT-DBR) All-Semiconductor Tunable Swept Laser System for Lidar in Autonomous Applications

AUTHOR: Taewan Kim

DATE SUBMITTED: June 2017

COMMITTEE CHAIR: Dennis Derickson, Ph.D.
Professor of Electrical Engineering

COMMITTEE MEMBER: Xiaomin Jin, Ph.D.
Professor of Electrical Engineering

COMMITTEE MEMBER: Vladimir Prodanov, Ph.D.
Associate Professor of Electrical Engineering

ABSTRACT

Linewidth and Ranging Characterization of a Vernier-Tuned
Distributed Bragg Reflector (VT-DBR) All-Semiconductor
Tunable Swept Laser System for Lidar in Autonomous
Applications

Taewan Kim

Linewidth and ranging experiments of a Insight packaged Vernier-Tuned Distributed Bragg Reflector (VT-DBR) laser across its wavelength output range of 1522.13 to 1566.18 nm is done in this work to characterize it for lidar applications. The purpose of this paper is to investigate the laser's potential to combine the advantages of lidar and FMCW radar for autonomous systems.

Linewidth measurements were done by using a Mach-Zehnder interferometer to set up a delayed self-homodyne measurement. The laser was set to output at a fixed wavelength across a range of 1523 to 1566 nm in 1 nm increments, and linewidth was captured each of these increments. For each of the linewidths, coherence time and length along with laser currents were associated. The minimum linewidth found in this test was found to be 50 MHz, leading to a maximum coherence time of 6.366 ns and a maximum coherence length of 129.92 cm. There was a somewhat linear, albeit low correlation, area of low linewidths depending on the front mirror and back mirror currents across the wavelength range.

Initial ranging experiments were performed using interference fringes caused by variable stationary path length differences introduced into a homemade Mach-Zehnder interferometer around the coherence lengths found in the linewidth test. The experimental path length differences indicated by the interference fringes seem to be accurate at very small ruler measured path length differences, but starts to stray away from the ruler measured as the path length differences get larger. Data taken suggests that there is a mathematical relationship in the error between the ruler measured and experimental path length differences leading to the belief that this error can be compensated for.

Keywords: Vernier-Tuned Distributed Bragg Reflector, VT-DBR, FMCW, linewidth, coherence, self-homodyne, Mach-Zehnder Interferometer, interference fringes

ACKNOWLEDGMENTS

TABLE OF CONTENTS

LIST OF TABLES

LIST OF FIGURES

Chapter 1. Introduction

With the onset of a more technologically focused future, the ability of everyday items to be "smart" is in demand more so than ever before. What is exactly a "smart" item? Something that can learn, something that can do tasks for a person, but all in all, something that further satisfies the human desire to do less in the pursuit of a "comfortable" future in which human involvement is minimized but productivity of that said person is the same or improved. In this pursuit of "smart" items or "comfortability" there is the drive for development of fully autonomous vehicles.

From a very high level, an autonomous vehicle can be defined as a vehicle that can drive or fly itself. Further delving into this concept, the vehicle would have to be able to safely transport itself from Point A to Point B with efficiency, comfortability, safety, and everything in between while completing tasks that it may be given. From drones to planes, rovers to cars, an automated future is in demand.

1.1 Example of Autonomy Technology: Driverless Cars

In the world today, especially in tech hubs such as Silicon Valley, driverless cars in particular are of huge interest. When presented with this challenge that can

rebound with large profits, top companies such as Google, Uber, and Tesla initiated research and development for driverless tech in the hopes of being the first company to create a common consumer purposed fully autonomous car. These companies all have different methods of approach for their goals. For example, Google has the autonomous car development as part of their Research and Development sector of the company called Waymo [1], Uber has bought out many faculty and facilities of Carnegie Mellon University to give them a head start [2], and Tesla is now producing cars that have full autonomous hardware in order to gather data from everyday drivers as they continue to develop the autonomous software needed for full autonomy in parallel [3].

Although all of these companies are in constant software development to develop the artificial intelligence needed for full autonomy, they seem to have convened on the hardware necessary for their software to be loaded unto. In other words, the hardware system necessary to receive data from the surroundings of said autonomous car and needed for actuation of received data has a commonality between all of these cars hoping to be self-driving. To provide a better understanding of this system, the hardware in this system will be listed and the use of each will be described.

Figure 1-1 highlights the hardware that is installed
on Google's self-driving cars along with the costs involved
for each piece.
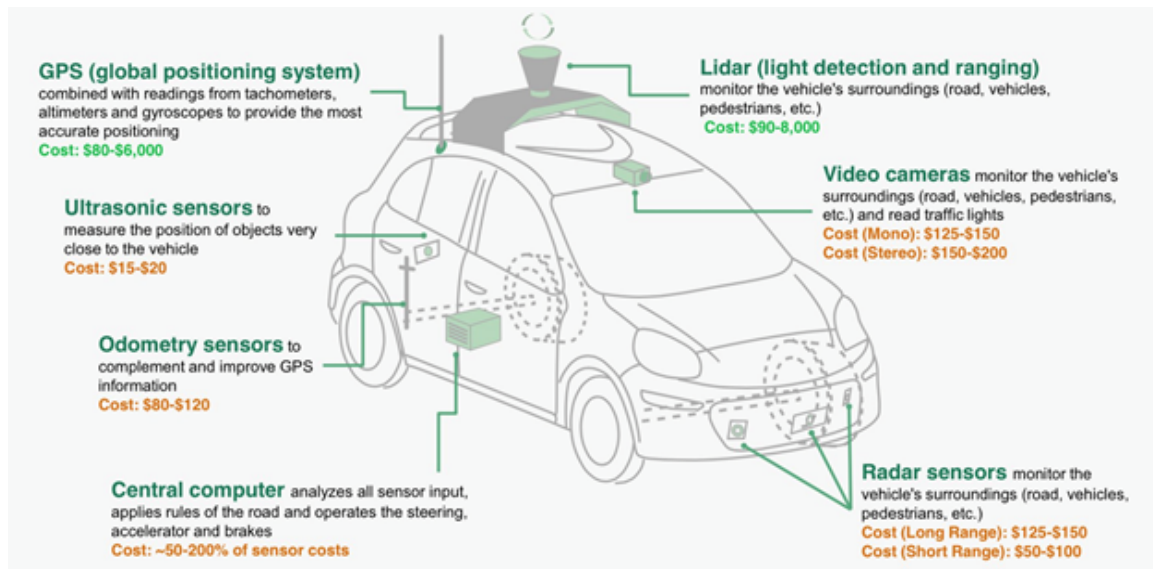
Figure 1-1 — A high-level overview of the hardware used on the Google Autonomous Car [4].

Observing what has been revealed by Google, the different
types of sensors in terms of hardware needed for a self-
driving car are GPS, Ultrasonic Sensor, Odometry Sensor,
Lidar, and Radar Sensor.

GPS, Short for Global Positioning System is used for
location identification. The problem with GPS becomes
resolution. GPS with the current technology available today
for the consumer and from a business analytics point of
view the most affordable GPS tech in terms of return on
investment is meter length resolution. Only very expensive
versions allow centimeter accuracy, though the push towards

innovation for less expensive highly accurate GPS is in the works [5].

Ultrasonic sensors are used for distance measurement and is composed of a transmitter and receiver and transmits a high frequency sound pulse and measures the amount of time it takes for that pulse to be received back after being reflected from another object to be able to estimate the distance between the ultrasonic sensor and said object [6].

Odometry Sensors are used to measure change in position over time. An example of how this might work is having rotary encoders on a wheel which will indicate how far the wheels have rotated, and knowing the wheel circumference, distance traveled can be found [7].

Lidar uses a surveying method used for object detection by illuminating said object with a laser light. An array of detectors or a timed camera can read in light reflections from the short pulses of light emitted, to create a 3D point "cloud" for vector information and volume identification [8].

Radar sensors, which are commonly frequency-modulated continuous-wave (FMCW) radar, is composed of a transmitter and receiver and uses RF technology to determine speed, proximity, range, and object size. Both lidar and radar are

4

used commonly used in autonomous systems to cross validate what they're seeing and to predict motion [9].

With the many technologies available for the purpose of an autonomous vehicle briefly outlined, it would be of great interest to be able to explore technology that is able to combine the benefits of a two into a new sensor. Given that radar and lidar are commonly used to cross validate, if there was a method of utilizing a laser and its benefits of angular accuracy along with the benefits of the FMCW method of radar, it could be extremely beneficial to the arsenal of hardware that may be needed for autonomous systems in the future.

1.2 Frequency Modulated Continuous-Wave (FMCW)

Ordinary pulsed radar detects an object by emitting a short pulse and calculating the time of flight of the reflected pulse off the object. This practice of using short pulses requires the radar to have a high instantaneous transmit power which results in a larger and more expensive physical apparatus for the radar [10]. Frequency Modulated Continuous-Wave (FMCW) radars, on the other hand, can achieve similar results as ordinary pulsed radars but with a lesser instantaneous transmit power and thus physical apparatus by using continuously emitting continuous pulses whose frequencies vary over time [10].

Further, the continuous wave sweep nature of FMCW allows it to detect velocity as well, while ordinary pulsed radars cannot continuously monitor and as a result, cannot accurately measure velocity of a detected object. Called a linear FM sweep, the range to the object of interest is found by detecting the frequency difference between the transmitted and received signals. As such, the range between the radar and the object is proportional to the difference in frequencies (called the beat frequency) [11].
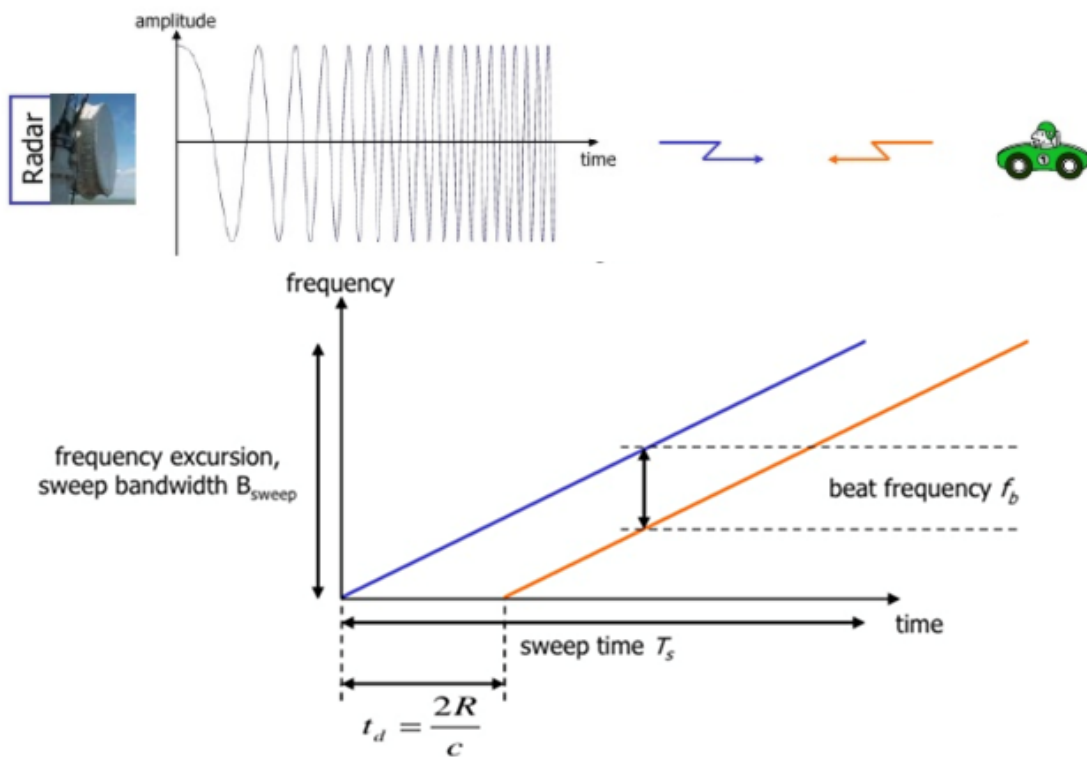
Figure 1-2 — The concept of FMCW with a linear sweep of frequencies transmitted [11].

Figure 1-2 provides a visual representation of FMCW. As illustrated, the transmitter of the radar sends out

pulses of linearly increasing frequencies over time and this repeats at a rate commonly called the sweep rate. These pulses are reflected off the object of interest and the receiver receives a frequency which is indicative of the round-trip delay as shown which is proportional to the distance of the object from the radar.

Further explaining, how this would work is that with each repetition of the frequency sweeps (governed by the sweep rate), there is a range of frequencies (governed by the sweep bandwidth) that is sent out. Following those frequencies to the object of detection, they will reflect off the object, and return to the receiver of the radar. As these frequencies return to the receiver, the difference in frequencies transmitted vs. received is called the beat frequency and can be correlated with a difference in time called the delay time. With this frequency and time difference data received and utilizing the speed of light, the distance to the object can be calculated. In equation form, the relationship between all these factors that determine the distance between the radar and the object is shown as follows [11]:

$$\frac{t_d}{T_s} = \frac{f_b}{B_{sweep}}$$

$$R = \frac{cT_s f_b}{2 * B_{sweep}}$$

where:

$$c = speed\ of\ light$$

$$t_d = delay\ time\ (s)$$

$$f_b = beat\ frequency\ (Hz)$$

$$R = distance\ between\ antenna\ and\ the\ reflecting\ object\ (m)$$

$$T_s = sweep\ time\ (s)$$

$$B_{sweep} = sweep\ bandwidth\ (Hz)$$

With this distance detection also comes the ability for detection of a moving object, or the velocity of this object; however, Doppler frequency must be taken into account as well for this calculation. The radar in this application must not only measure the difference in frequencies between the transmitted and received, but also the Doppler frequency which is caused by the speed of the object.
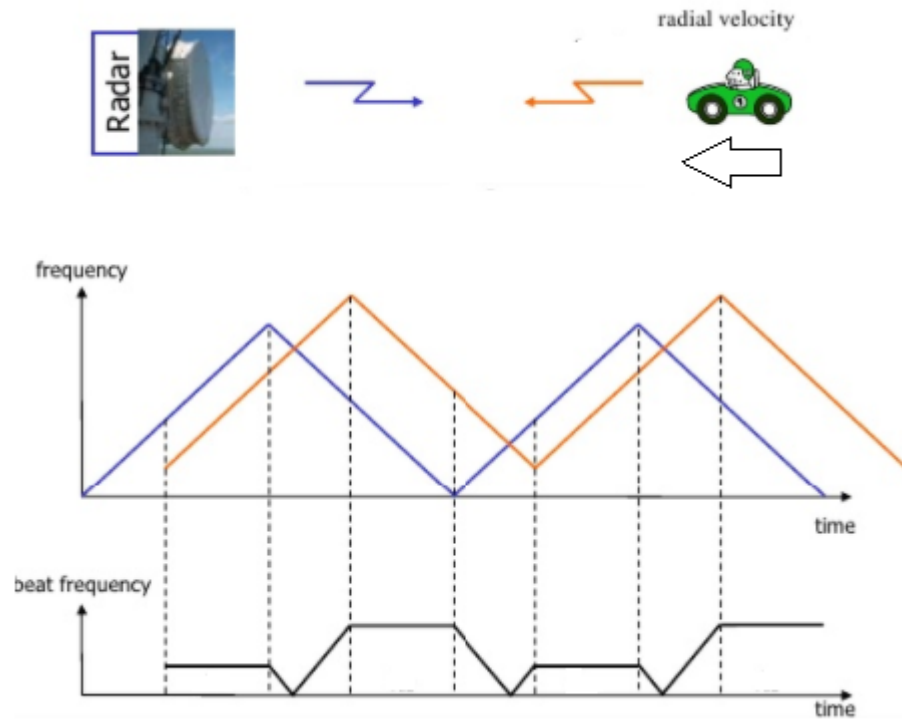
Figure 1-3 — The concept of FMCW with the Doppler effect showing a linear increase and decrease sweep of frequencies transmitted [11].

Figure 1-3 provides a visual representation of FMCW with the Doppler effect. As illustrated, the transmitter of the radar outputs a linear increase and decrease of frequencies, and as they reflect off the object of interest approaching the radar, the beat frequency is higher or lower depending on the increasing or decreasing sweep of frequencies received at the receiver.

The Doppler effect can be explained further at a high level using a simple example. If one is an observer to an ambulance that is emitting its siren sound at a certain constant frequency, and that ambulance is approaching the

observer, the frequency of the sound to the approached observer is higher than the true emitted frequency of the moving ambulance. However, on the flip side, to an observer that the ambulance is departing from, the frequency of the sound is lower than the true emitted frequency. A visual representation of this can be found in Figure 1-4.

Figure 1-4 – Ambulance caused Doppler effect with an approached and departed observer [12].

Along with the simple concept of ranging both still and moving objects with the FMCW method, comes another benefit, which is security from jamming. With autonomous systems reliant on their sensors as much as humans are reliant on their senses to move around, it is extremely important that the sensors are resistant to those who may want to trick them into sensing something false, bringing them offline, or worse, causing an accident. Because in FMCW, the frequency is constantly changing, it stands as a formidable system to trick. In order for one to jam the radar, they would first have to know the operating range of

frequencies (sweep bandwidth) and operate within that range
so that a receiver can acknowledge the false frequency as
within its bandwidth. Furthermore, the jammer would also
have to know the step frequency (slope of the linear
increase) of the signal transmitted by the radar it is
trying to jam and would have to successfully emulate such a
signal. Compared to another sensor such as lidar, where
there is simply a short pulse of light that is sent out and
received, FMCW is much more difficult to emulate, and as a
result, jam.

1.3 Swept Laser in Optical Coherence Tomography (OCT)

OCT is an imaging technique used for translucent and
partially opaque materials first demonstrated in the early
1990s [13]. It is commonly used for biomedical imaging in
cardiology, optometry, dermatology, and early cancer
detection where it can offer sub-micrometer isotropic
resolution images [13]. OCT can be seen as a optical
ultrasound where highly coherent light instead of sound is
used. OCT can be performed in or ex vivo, as shown in
Figure 1-5 allowing a dynamic imaging modality that is
minimally invasive and can offer high resolution imaging
[13].
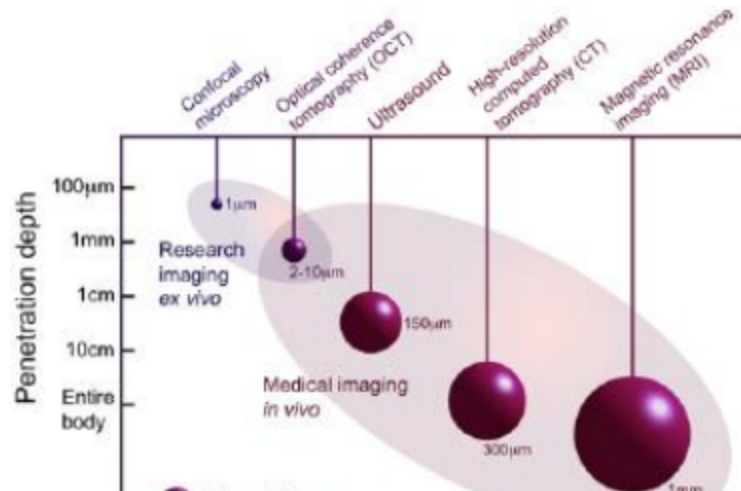
Figure 1-5 – Biomedical imaging techniques and the unique niche of OCT [13].

Recent developments of OCT have brought upon several different methods with unique advantages, and among them, there in source-swept OCT (SSOCT). In SSOCT, a broadband swept light source is required [13]. Figure 1-6 illustrates a high-level block diagram of an SSOCT system.
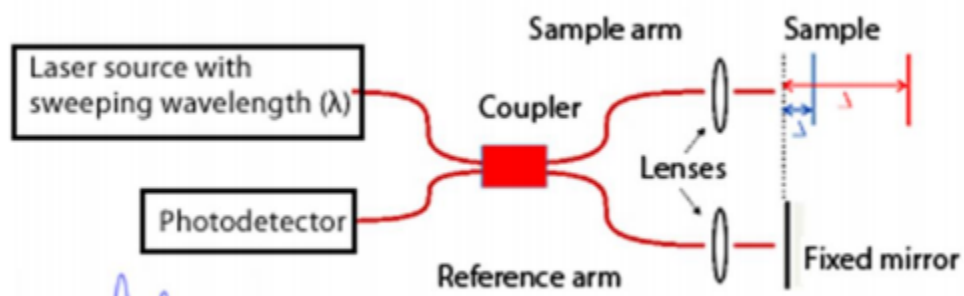
Figure 1-6 — A typical SSOCT test setup with a sampling output going to the photodetector and two sample arms, one of which is a reference with a fixed mirror [13].

Figure 1-6 is implemented as a fiber-coupled Michelson interferometer and the sample arm is used for imaging something such as an artery, tooth surface, or skin [13]. This method, also know as Fourier Domain OCT (FDOCT) has been shown to have a sensitivity advantage over traditional time domain OCT [13]. Swept frequency lasers are an ideal source for this approach and have continually demonstrated success.

1.4 Purpose of Study

This study uses an Insight Photonics packaged Vernier-Tuned Distributed Bragg Reflector (VT-DBR) which is an all-semiconductor, high-speed, tunable laser. Tunable meaning that the wavelength can be controlled over a certain range [13]. As such, just like how FMCW radar sweeps across a range of frequencies, this can be done with the tunable laser to sweep across its range of wavelengths. The VT-DBR so far has demonstrated success in achieving high-resolution images of the human body in OCT applications [13].

The purpose of this study is to investigate into the feasibility of using this laser for ranging purposes similar to how the FMCW method works for radar in order to combine the benefits of both a lidar and radar into one FMCW lidar sensor. The overall goals of such a sensor and

the potential benefits of FMCW lidar over conventional time of

flight lidar is summarized in Table 1.

Table 1 – Goals of FMCW lidar sensor and comparison of FMCW method vs conventional time of flight method.

Parameter	Goal Value	Comments	FMCW Specific	Time of Flight Specific
Range/Sensitivity	100 m	Should be able to sense something like a stop sign at 100 m with adequate signal to noise ratio.	Heterodyne detection is used.	Requires Geiger-Mode detectors.
Distance Resolution	10 cm	N/A	Requires sweep bandwidth B_{sweep} of 5 GHz	$t = \dfrac{d}{v}$ $= \dfrac{10\,cm}{3\times10^8\,m/s}$ $\approx 333\,ps$
Time to take a single data point.	$2\,\mu s$	Corresponds to taking 500 kSamples/s	N/A	N/A
Security of system against other lidars.	TBD	Must be able to work in an environment with many simultaneous LIDARs in operation, with little interference.	Robust	Vulnerable (easier to jam with pulses or CW)
Security against intentional jamming.	TBD	Must still work even with intentional laser jamming signal.	Robust	Vulnerable (easier to jam with pulses or CW)
Cost	TBD	Minimal part of autonomous system cost	TBD	TBD
Eye Safety	IEC Class 1	Class 1 lasers are very low risk and "safe under reasonably foreseeable use" [14].	N/A	N/A

The extent to which this FMCW lidar application of the VT-DBR differs from a typical OCT application is summarized in Table 2.

Table 2 – Comparison of VT-DBR Laser for OCT vs FMCW Lidar.

Parameter	OCT	FMCW Lidar	Comments
Tunability Range	$5000\ GHz$	$5\ GHz$ ← Easy	Easy
Sweep Rate	$\dfrac{5000\ GHz}{10\ \mu s}$	$\dfrac{5\ GHz}{2\ \mu s}$ ← Moderate Challenge	Moderate Challenge
Distance Resolution	$10\ \mu m$	$10\ cm$ ← Easy	Easy
Range	$1-2\ cm$	$100\ m$ ← Key Challenge	Key Challenge (Subject of this thesis)

An example of factors that come into play to test the potential success of an FMCW laser and reaching the goal of a range/sensitivity of 100 m as shown in Table 1 and Table 2 is the range of wavelengths chosen to be swept over. Depending on how the laser is tuned, some wavelengths may yield to lower spectral width than others leading to longer or more accurate ranging measurements. Also from there, extracting the theoretical maximum range of the laser would be useful to determine what applications the current configuration of the Insight VT-DBR laser would be most fitted for.

Another example of factors that come into play is how accurate the laser ranging is when an object is in its theoretical range. Is the resolution error large? Table 1 indicates a desired distance resolution of 10 cm. If the

resolution error is too large, is there an error trend so that this resolution problem can possibly be compensated for? These are some of the questions that can be asked from the ranging accuracy point of view.

1.5 Thesis Summary

Chapter 2 provides more info on the VT-DBR laser and its tuning mechanism along with a basic theoretical background on linewidth needed to aid in understanding the experiments performed in Chapter 3 and Chapter 4.

Chapter 3 outlines an experiment done to capture the laser linewidths across the laser's sweep range and analysis of what those linewidths indicate along with how one may achieve minimum linewidth.

Chapter 4 outlines an experiment done to test the feasibility of ranging by the laser within optical fibers. Analysis of how one can calculate range from the data retrieved and how accurate the ranging is, is discussed.

Chapter 5 shares conclusions with regards to the investigation done and future work that is necessary to further investigate into the feasibility of an FMCW laser on future autonomous systems.

Chapter 2. The Insight VT-DBR Laser and Linewidth

In order to discuss aspects of the device under test, the Insight VT-DBR akinetic laser, it would be helpful to understand what the VT-DBR akinetic laser is before describing the specific capabilities of the Insight packaged laser. After discussing the capabilities of the Insight laser, the characteristics of interest of the laser in the application of ranging is discussed to be able to give a basic theoretical basis for the experiments found in the following Chapters, 3 and 4.

2.1 Laser Components and the VT-DBR Laser

Three main components are necessary for a conventional laser to produce an optical output and they include a gain medium, an optical resonator, and a pump. First, the gain medium is a medium which amplifies the power of light in order to compensate for resonator losses. Different types of material with the necessary properties such as a gas, liquid, or solid can be used, but in the VT-DBR laser specifically, a semiconductor is used. Second, the optical resonator is placed around the gain medium to act as a source of a feedback for the system and is composed of two parallel mirrors, one which is fully reflective and another which is partially reflective to allow light to escape the laser cavity. Last, the pump is the source of energy for

the laser and injects electrical or optical energy into the medium to stimulate the process of light emission [13]. Figure 2-1 illustrates the configuration of a gain medium, optical resonator, and pump of a laser.
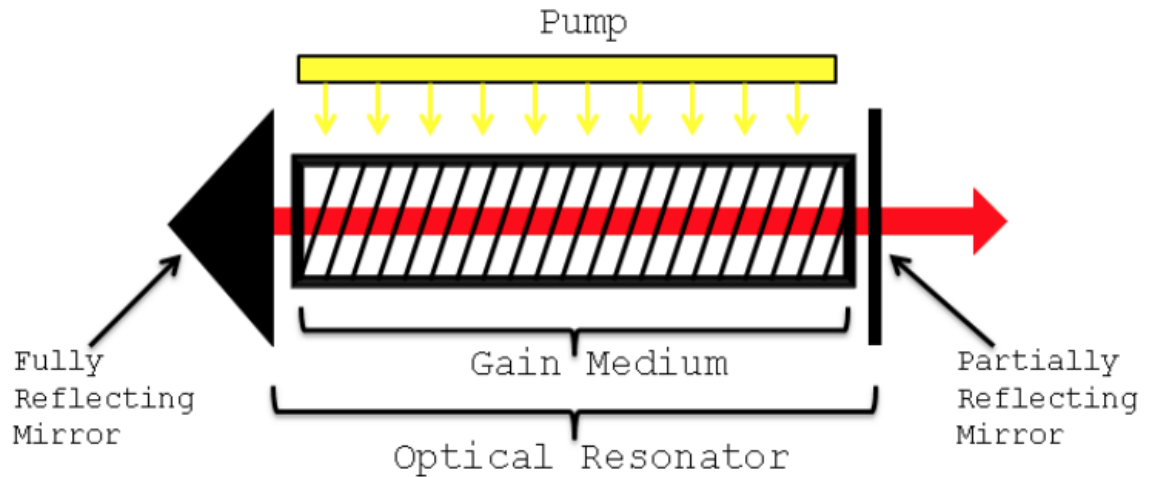
Figure 2-1 – A conventional laser configuration of a gain medium, pump, and optical resonator consisting of a fully reflective mirror and partially reflective mirror [13].

The Vernier-Tuned Distributed Bragg Reflector (VT-DBR) akinetic laser source is a high-speed, all-semiconductor, tunable laser (controllable over a certain wavelength range) [15]. Because this laser wavelength is controllable, it is ideal for a sweep of frequencies, inherent in the FMCW method commonly found today in radar.

Moving on from the conventional laser, and discussing the specific laser used in this study, The VT-DBR laser's foundation works by using two distributed Bragg-reflector (DBR) mirrors on each end of its optical cavity to select the oscillatory wavelength [16]. The mirrors reject the

transmission of a harmonically related set of wavelengths, depending on the length of separation of the two mirrors, and the rejected light resonates within the laser cavity in the electrically pumped gain medium where a single mode commonly reflected by the mirrors is amplified [15].

The distance between the DBR mirrors of the VT-DBR laser is altered by application of different electric currents into the semiconductor materials the mirrors are composed of, changing their refractive index [17]. Reflective angle of incidence is changed from a change in refractive index of a material, which ultimately changes the distance seen by light between the two mirrors. In turn, this affects the light to be rejected by the mirrors, changing the wavelength output of the laser.

The VT-DBR has 5 control currents to perform wavelength tuning which include the back mirror (bm), gain amplifier, phase, front mirror (fm), and semiconductor optical amplifier currents (soa) which can be seen in Figure 2-2.
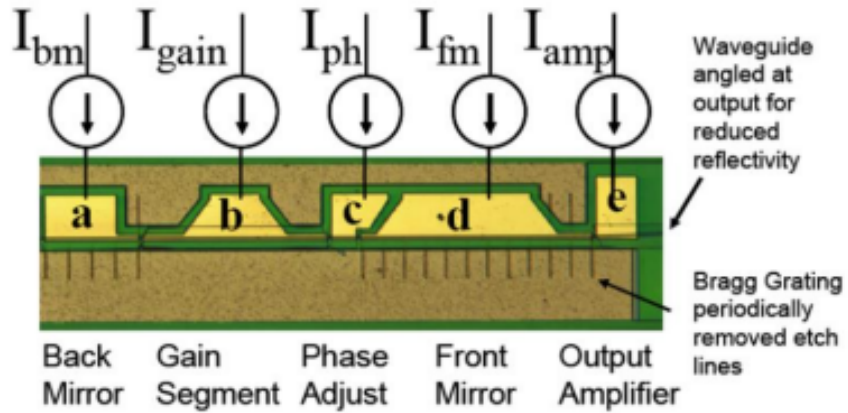
Figure 2-2 – The 5 control currents of the VT-DBR to control wavelength tuning [18]

The front mirror (fm), back mirror (bm), and phase sections which can also be seen in Figure 2-2, are responsible for wavelength selection [19]. These currents can change the refractive index of the DBR mirrors. The semiconductor optical amplifier (soa) and gain sections allow control of the power output of the laser. "Vernier" in VT-DBR refers to the Vernier effect used in tuning the laser from the comb reflection spectra found in the DBR structures [15].

What makes this laser superior to other tunable lasers is the "akinetic" in "VT-DBR akinetic laser source" title which means that there are no moving parts. The advantage of this is that because there are no moving parts the wavelengths can be controlled more quickly.

2.2 Capabilities of Insight Laser

The Insight Akinetic Laser source, which is the laser used throughout the experiments in Chapters 3 and Chapter 4, provides the user interface and packaging of the VT-DBR laser discussed in the previous section. Digital control is utilized to change the control current pumps against time in order to provide an accurate control of optical wavelengths. A default sample clock of 400 MHz is used and trigger signals are generated by the laser to indicate when measurements are valid to be taken. Figure 2-3 gives a visual representation of the front panel of the Insight laser source.

Figure 2-3 – Front Panel of the Insight Akinetic Laser source [20].

As can be seen in Figure 2-3, "Laser out" is the laser output of the laser while "Laser in" in is the input to a internal acquisition device. "Start Sweep" is a digital signal output that allows one to know the duration of a

21

laser sweep and "Data Valid" output is also a digital
signal output that notifies the user when points in a laser
sweep are valid or not. The outputs of the laser can be
seen in a LABVIEW oscilloscope via use of 5105 PCI
Digitizer ADC and a 5105 Acquisition program as seen in
Figure 2-4.

Waveform Graph 2 "Start Sweep"

Waveform Graph 3 "Data Valid"
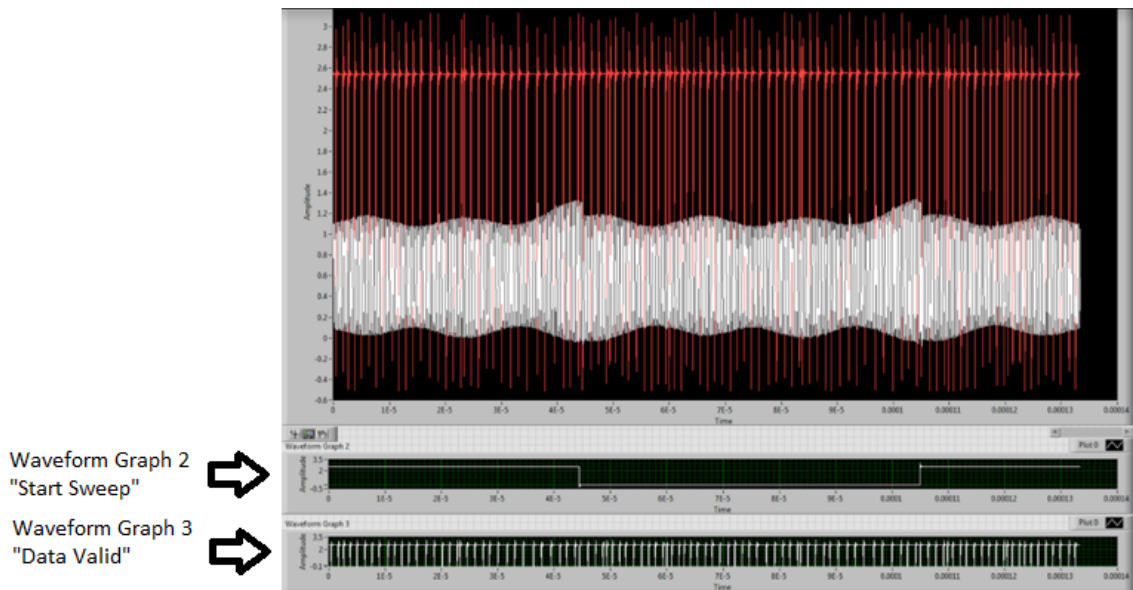
**Figure 2-4 – 5105 Acquisition program with time domain
waveform data and waveforms of laser outputs including
"Data Valid" and "Start Sweep".**
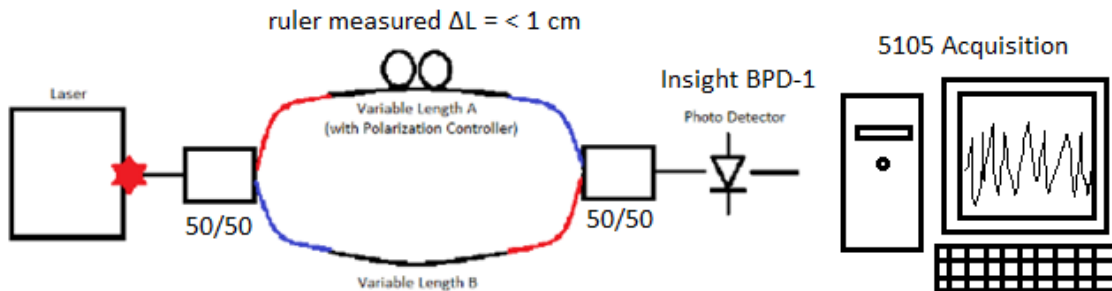
**Figure 2-5 — Interference fringe test setup for a ruler
measured path length difference of 1 cm.**

The white waveform seen in Figure 2-4 is an example of a time domain waveform that is under analysis which is the output of the interference fringe test setup shown in Figure 2-5. The red waveform overlapped with the white waveform is the digital data valid signal that is high to indicate valid laser output and low to indicate invalid laser output. Waveform Graph 2 shows the waveform of the "Start Sweep" output of the Insight laser and as can be seen is indicating the beginning and end of sweeps at its rising and falling edges. Waveform Graph 3 is the data valid output of the laser in a separate graph from the time domain waveform under analysis.

The specific Insight laser model used throughout this thesis is Model SLE-101 and has a sweep range of 1522.13 to 1566.18 nm.

2.3 Linewidth and Coherence

The linewidth Δv of a laser is the width of its optical spectrum 3 dB down from the peak or at half power. A laser spectrum usually has Lorentzian-shaped central peak, small sidebands located closer to the central peak caused by relaxation oscillations, and small sidemodes (cavity frequencies) located farther from the central peak [21]. A typical optical spectrum is shown in Figure 2-6 below.
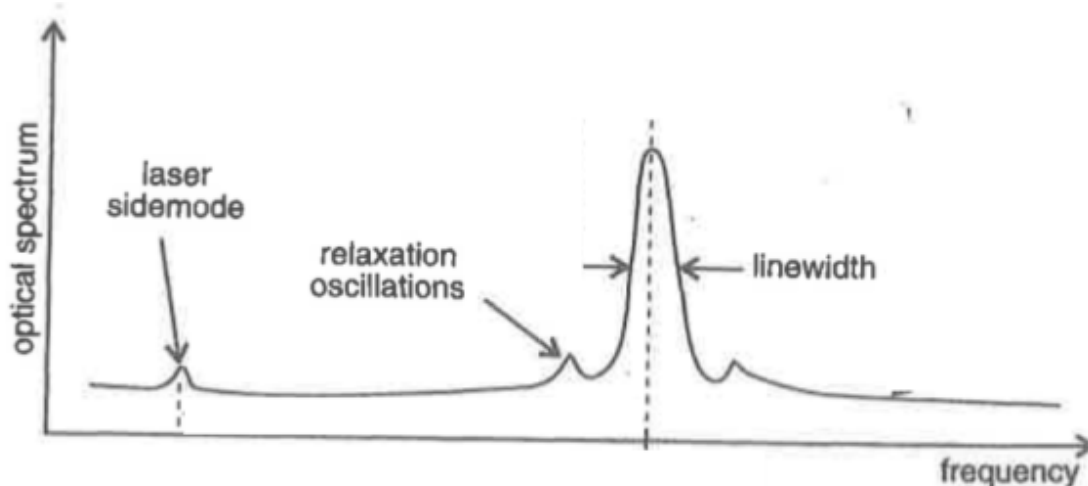
Figure 2-6 – Typical Lorentzian-shaped central peak laser spectrum with relaxation oscillations and sidemodes [21].

In the case of linewidth for our specific application, the narrower the better. For example a range/sensitivity of 100 m as was outlined in Table 1 of Section 1.3 in Chapter 1 within optical fiber requires a narrow linewidth of 649.6 kHz. Larger range/sensitivity, translates to a shorter required linewidth. This is due to the fact that linewidth is related to temporal coherence, which is characterized by coherence time or coherence length. Coherence time is a measure of spectral purity of a laser wavelength or frequency over time and a narrower linewidth is related to a longer coherence time and coherence length. The mathematical relationship between linewidth and coherence time τ_c is shown as follows:

$$\tau_c = \frac{1}{\pi \Delta v}$$

The coherence length is the coherence time multiplied by

the velocity of light within optical fiber which is:

$$v_g = \frac{c}{n_g}$$

Where the group velocity index n_g for optical fiber is 1.47,

leading to the coherence length equation of:

$$L_c = \tau_c v_g$$

Coherence time/length can be reduced by random events

like spontaneous emission in the laser cavity, which can

alter phase or frequency of the laser output. This concept

is illustrated in Figure 2-7.
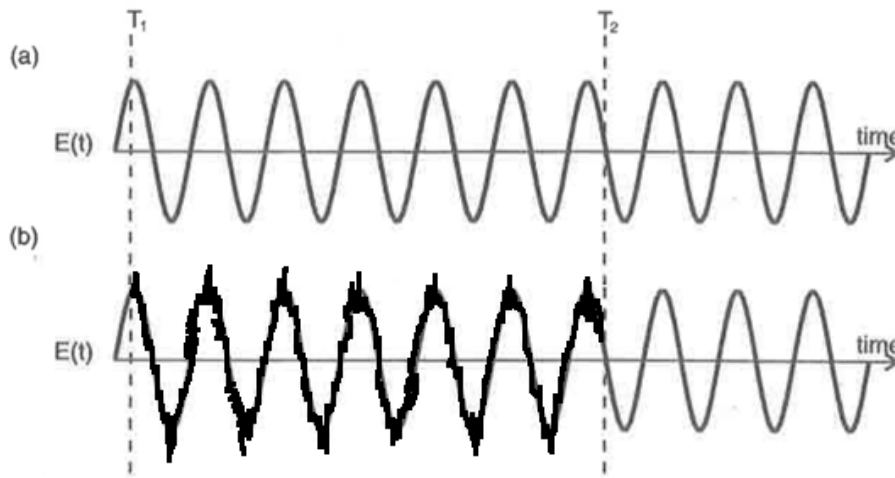
**Figure 2-7 – Concept of coherence time with an example of
(a) coherent light, and (b) short coherence [21].**

As can be observed in Figure 2-7, the coherence is longer

in (a) and shorter in (b). Looking between the time

intervals of T_1 and T_2, the coherence is longer in (a)

because phase is predictable across the interval, while in

(b) there are random phase or frequency jumps which causes the phase to be unpredictable across the interval.

In two path interferometers, the degree to which an optical wave interferes with a delayed version of itself depends on the coherence time of the wave with respect to the optical delay [21]. As such, coherence length and coherence time plays a large role in the ranging with interference fringes experiment done in Chapter 4 and due to that large role played, linewidth is the subject of investigation in Chapter 3.

Chapter 3. Laser Linewidth Characterization

With the importance of linewidth emphasized in Section 2.4 of Chapter 2, and the goals outlined in Table 1 in Section 1.3 of Chapter 1, an experiment was done to be able to efficiently characterize the Insight Laser's linewidth. For FMCW, the laser must be swept at range of frequencies. As such, it made sense to step the laser across a range of frequencies that could be possible candidates for a sweep range to be selected that would utilize wavelengths with minimal linewidth compared to say wavelengths in another range with larger linewidths.

3.1 Laser Linewidth Test Setup and Theory

With the Insight Laser Control Program the laser can be set in fixed wavelength mode. The interface is shown in Figure 3-1.
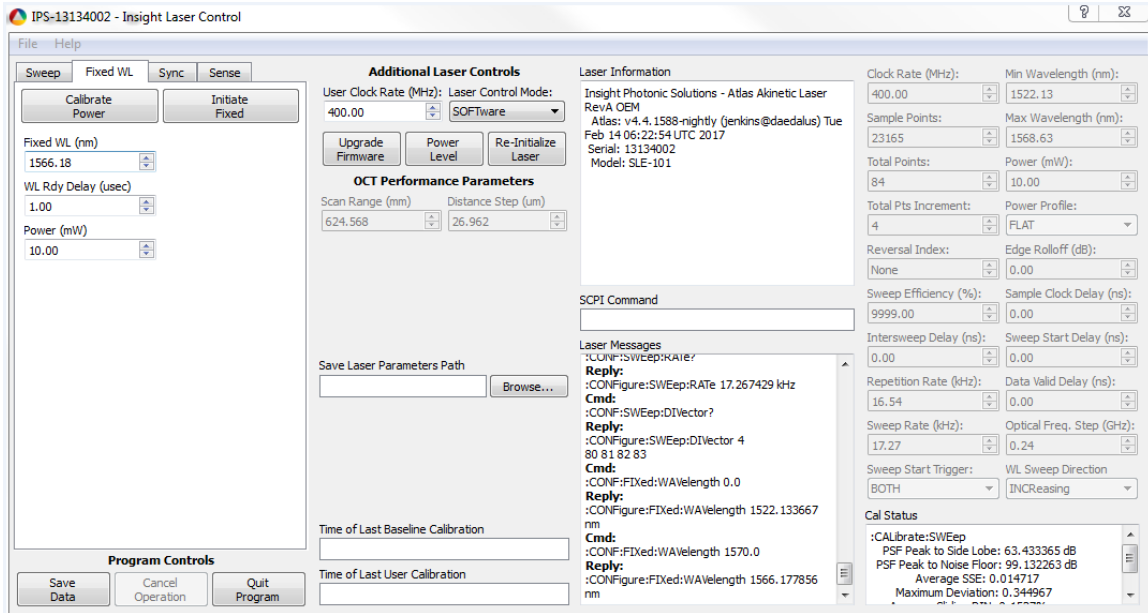
Figure 3-1 - Insight Laser Control Program fixed wavelength output interface [20].

The fixed wavelength interface allows the user to output the laser at a fixed wavelength with modifiable power. The output of the laser in this mode can range from wavelengths of 1522.13 nm to 1566.18 nm. The output of the laser at a wavelength of 1540 nm and at a power of 5 dBm is shown in a Optical Spectrum Analyzer (Agilent 86140B) to visually highlight the characteristics of the laser in the frequency spectrum in Figure 3-2.
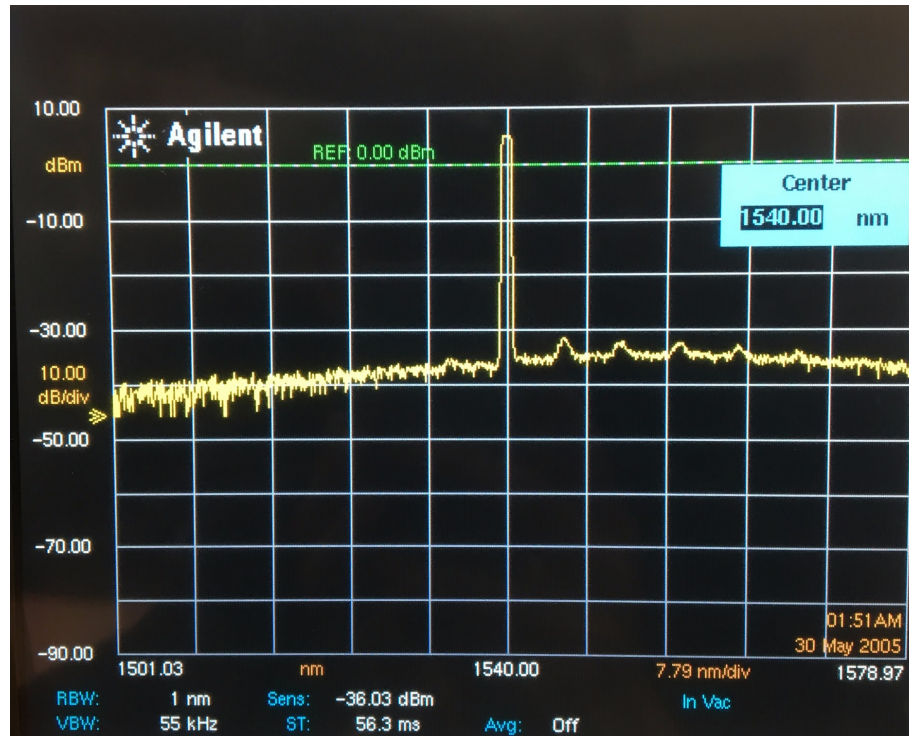
Figure 3-2 - Fixed 1540 nm output of laser shown in optical spectrum analyzer.

Because there is a large number of different wavelengths that can be output, in order to get a characteristic of the entire range of the laser in the most efficient way possible, it was determined that 1 nm step would be sufficient to get an understanding of linewidth variability across the range. More specifically, the laser linewidth would be observed across the range of 1523 to 1566 nm in 1 nm increments.

With the laser under test settings determined and basic methodology for the how the laser is to be tested figured out, the next step was to determine the method of measuring the linewidth of the laser and the delayed self-

homodyne method was chosen. The delayed self-homodyne
method is a simple way to measure the linewidth of a laser
and offers a very high resolution compared to other methods
of measuring linewidth due to the simple usage of an
optical interferometer with low-loss fiber optic delays
[21]. In this method, there is a photodetector that must
receive a combined optical field, consisting of one field
which is delayed and another that is minimally delayed,
which is why an interferometer is necessary. There are many
different types of interferometers that can be used for the
purpose of delayed self-homodyne including Mach-Zehnder,
Micheson, and Fabry-Perot interferometers [21]. Visual
representations of the different types of interferometers
can be seen in Figure 3-3 [21], however a Mach-Zehnder
interferometer was chosen to move forward with due to
simplicity and availability.
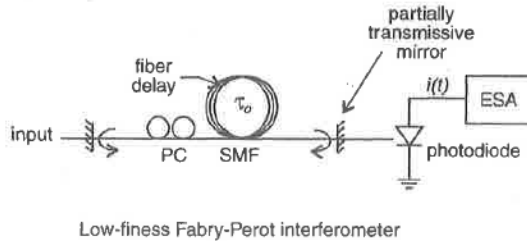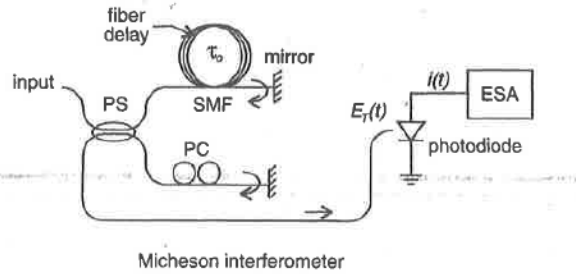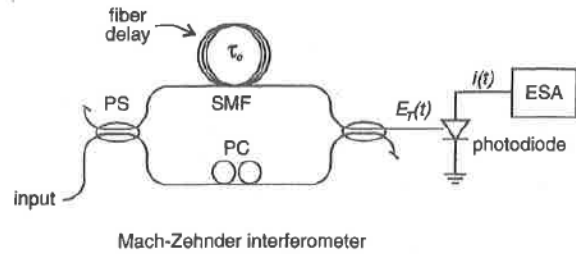
Figure 3-3 – Mach-Zehnder, Micheson, and Fabry interferometers seen in delayed self-homodyne measurement setups [21].

The translation from optical to electrical spectrum can be seen in Figure 3-4 [21]. The spectrum shape of semiconductor lasers can be approximated by a Lorentzian-shaped profile and for such shapes such as Lorentzian and Gaussian, lineshapes are preserved from the optical to the electrical through the autocorrelation operation [21].
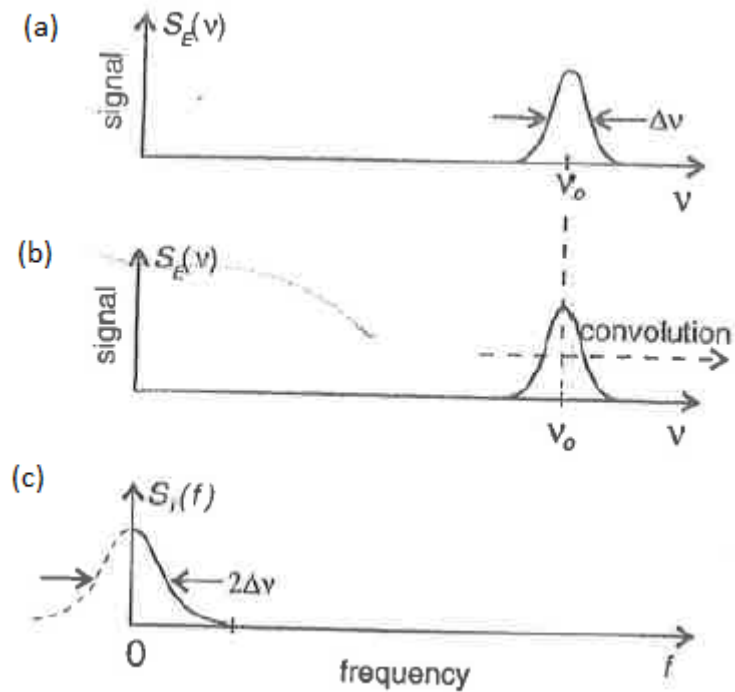
**Figure 3-4 — (a) Laser lineshape mixing with (b) delayed
self for (c) output electrical spectrum shape [21].**

As can be seen in Figure 3-4, the linewidth appears in
the electrical spectrum with half of the full spectral
shape shown (due to the mixed spectrum centered about 0 Hz)
of which the width of the half spectrum at 3dB down is the
linewidth.

3.2 Laser Linewidth Test

With a basic theoretical background and a method of
capturing linewidth determined, the experimental setup to
capture the linewidths of fixed wavelengths across the
wavelength range able to be output by the Insight laser was
begun. As hinted, the experimental setup for the delayed
self-homodyne is simple. The Insight laser was connected to

an off the shelf 3.5 μs delay Mach-Zehnder Interferometer

with a knob for polarization (Hewlett Packard 11980A) for

the summation of the laser output with itself. This was

then connected to the input of a photodetector to convert

from the optical to the electrical spectrum (optical power

into electrical current). The output of the photodetector

was then input into an off the shelf electrical spectrum

analyzer (Agilent Technologies N9000A) for display of the

electrical spectrum to the user. A visual representation of

the experimental setup for linewidth characterization of

the Insight laser can be seen in Figure 3-5.
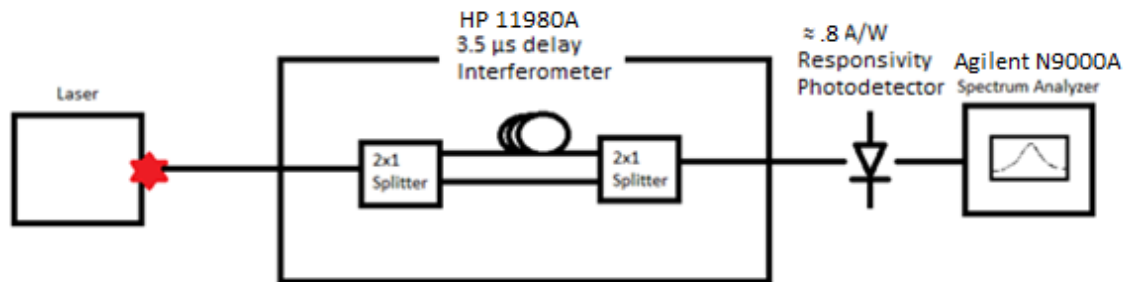
Figure 3-5 - Insight laser delayed self-homodyne experimental test setup: laser is output into interferometer for mixing with delayed self into photodetector to observe output spectrum in electrical spectrum analyzer.

With the experimental setup ready, the output

wavelength range of the laser was run through. As mentioned

before, steps of 1 nm of fixed wavelength were done across

the range of 1523 to 1566 nm. It must be noted that the

Insight laser fixed wavelength interface was not able to

output at exactly 1556 and 1561 nm and in order to keep

consistency of data, they were skipped.

As mentioned before on why linewidth is important for

laser ranging in Section 2.4 in Chapter 2, linewidth has a

relation to coherence time and as a result coherence

lengths. As such, after the laser linewidth spectrum was

captured for the range of the laser, linewidth was

extracted. With the linewidth Δv, coherence time τ_c and

coherence length L_c was calculated as follows:

$$group\ velocity\ index\ n_g = 1.47, for\ optical\ fiber$$

$$velocity\ of\ light\ within\ fiber\ v_g = \frac{c}{n_g}$$

$$coherence\ time\ \tau_c = \frac{1}{\pi \Delta v}$$

$$coherence\ length\ L_c = \tau_c v_g$$

Further, in order to gain an understanding of how the

laser currents play into the linewidth, the laser currents

at play during each of the fixed wavelength outputs were

gathered from factory data provided by Insight Photonics

[22]. Please refer to Appendix A for the results of this

experiment in tabular format for the linewidths captured

from 1523 nm to 1566 nm and the corresponding coherence

times, coherence lengths, and laser currents. Figure 3-6

highlights the format in which the data was taken for

example purposes for a fixed wavelength output of 1523 nm.

$$wl \; = 1523 \; nm$$
$$\Delta v \; = 50 \; MHz$$
$$\tau_c = 6.366 \; ns$$
$$L_c = \; 129.92 \; cm$$
$$fm \; = 13016$$
$$bm \; = 49647$$
$$phase \; = 11712$$
$$soa \; = \; 14657$$
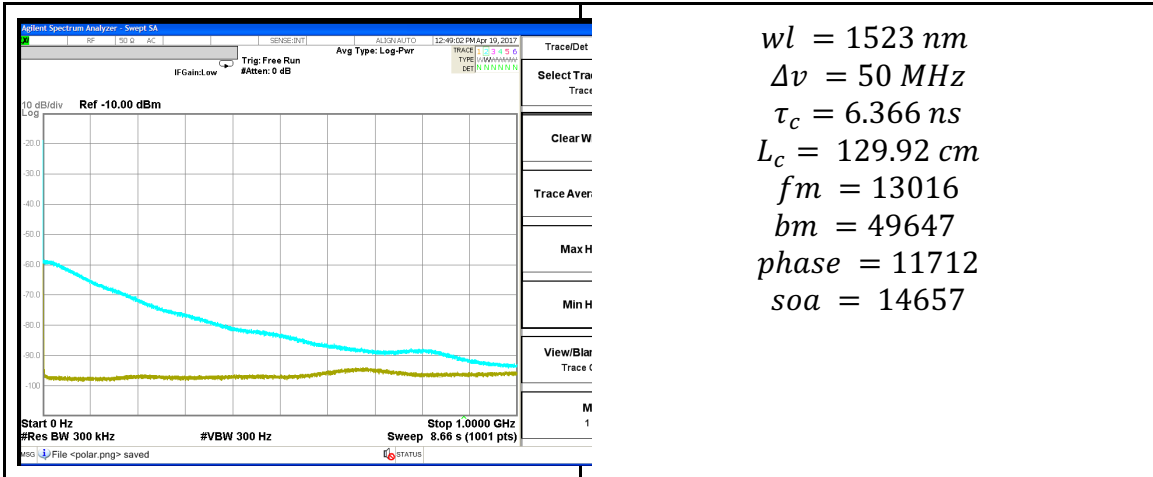
Figure 3-6 – Example of experimental data taken for fixed wavelength output of 1523 nm.

Although the linewidth Δv provides the width of the lineshape at 3dB down from the peak, it is not enough to highlight the rest of the lineshape that is shown. For example, the 3dB point will only show how close the lineshape is hugging the 0 Hz peak but does not highlight how much the lineshape spreads out the further from 0 Hz one may get. In order to capture this data, the width from 0 Hz was captured in terms of dB points. So instead of capturing just the linewidth (3dB down), the width from 0 Hz was captured at 10 dB down, 20 dB down, and 30 dB down and was compared with the theoretical values of a Lorentzian spectral shape, which were calculated utilizing Figure 3-7.

Measured Point	Displayed Width
−3 dB	Δv
−10 dB	$\sqrt{9}\ \Delta v$
−20 dB	$\sqrt{99}\ \Delta v$
−30 dB	$\sqrt{999}\ \Delta v$

Figure 3-7 – Theoretical Lorentzian spectral shape at measured points of –3 dB, –10 dB, –20 dB, and –30 dB [21].

The frequencies at these points were captured and this experimental data for the fixed wavelengths of 1523 to 1566 nm along with the theoretical Lorentzian values calculated in tabulated form can be found in Appendix B. Figure 3-8 highlights the format in which the data was recorded for example purposes for a fixed wavelength output of 1523 nm.

Laser Wavelength	Experimental Laser Lineshape	Lorentzian Laser Lineshape
$1523\ nm$	$\Delta v = 50\ MHz$ $\Delta v_{10dB} = 160\ MHz$ $\Delta v_{20dB} = 350\ MHz$ $\Delta v_{30dB} = 700\ MHz$	$\Delta v = 50\ MHz$ $\Delta v_{10dB} = 150\ MHz$ $\Delta v_{20dB} = 497.5\ MHz$ $\Delta v_{30dB} = 1580\ MHz$

Figure 3-8 – Example of experimental data recorded of width at various dB down from peak for fixed wavelength output of 1523 nm.

3.3 Laser Linewidth Test Results and Analysis

As can be initially observed from the laser linewidth test tabulated in Appendix A, it can be seen that there is a large variation between the different wavelengths in terms of linewidth with the largest linewidth captured to be 300 MHz at a fixed wavelength laser output of 1562 nm leading to a calculated minimum coherence time of 1.061 ns and coherence length of 21.65 cm. The smallest linewidth captured to be at 50 MHz found at fixed wavelength laser outputs of 1523, 1525, 1539, 1545, and 1546 nm leading to a maximum coherence time of 6.366 ns and coherence length of 129.92 cm .

Thus, the largest linewidth captured by this experiment is 600% that of the smallest linewidth captured. In order to gain a clearer representation of how linewidth varied with wavelength output by the laser, they were graphed against each other and can be seen in Figure 3-9.
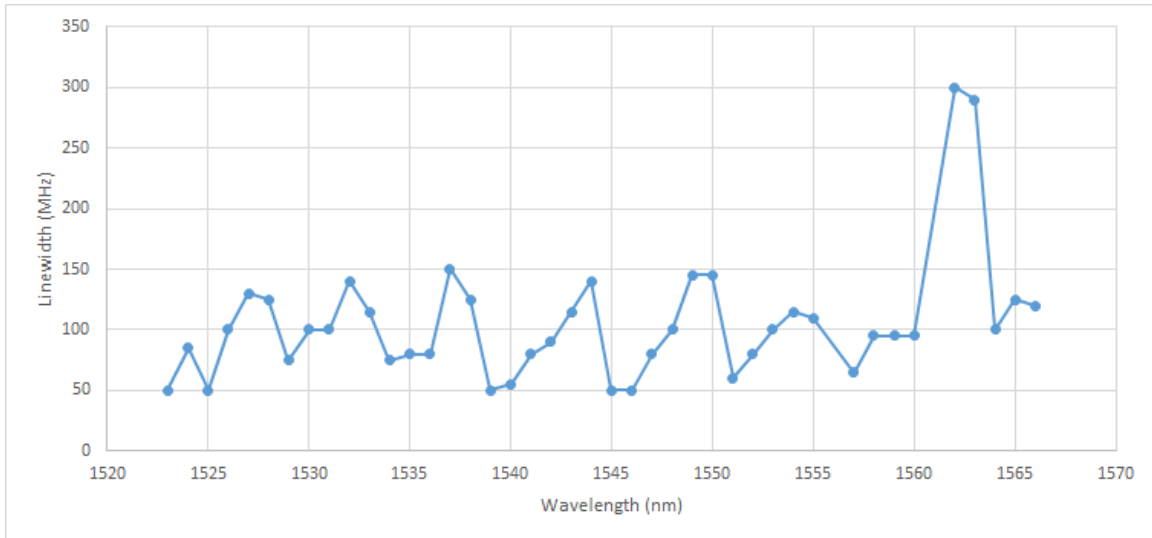
Figure 3-9 – Laser linewidth graphed against fixed wavelength laser output.

As can be observed in Figure 3-9, across the range there is a large up and down variability of the linewidth from 1523 to 1566 nm. What is immediately obvious from the graph however, is how far out the linewidth is at 1562 and 1563 nm compared to the linewidth at the rest of the wavelengths. Besides 1562 and 1563 nm with linewidths of 300 and 290 MHz, the next largest linewidth is found to be 150 MHz at 1537 nm which is approximately half of the linewidth of the two maximum. The wavelengths and corresponding linewidths at which there is an obvious peak and the wavelengths at which there is a obvious trough compared to data points in the vicinity in the up and down linewidth nature of Figure 3-9 is captured in Table 3 and Table 4 respectively. Please note 1549 and 1550 nm were both

included in Table 3 due to their equivalence in linewidth. For

the same reason 1545 and 1546 were both included in Table 4.

Table 3 – Peaks in linewidth found at various wavelength outputs of laser.

λ	Δv
1524 nm	85 MHz
1527 nm	130 MHz
1532 nm	140 MHz
1537 nm	150 MHz
1549 nm	140 MHz
1550 nm	145 MHz
1554 nm	145 MHz
1562 nm	300 MHz

Table 4 – Troughs in linewidth found at various wavelength outputs of laser.

λ	Δv
1523 nm	50 MHz
1525 nm	50 MHz
1529 nm	75 MHz
1534 nm	75 MHz
1539 nm	50 MHz
1545 nm	50 MHz
1546 nm	50 MHz
1551 nm	60 MHz
1557 nm	65 MHz
1564 nm	100 MHz

Observing the peaks in linewidth as shown in Table 3, the initial trend that is somewhat apparent is how much the magnitude of the peaks increases over the wavelength range. For example, the first peak is seen at 1524 nm with a linewidth of 85 MHz, while the last peak is seen at 1562 nm with a linewidth of 300 MHz which is over 3 times larger than the first peak. The general trend from the first peak to the last peak can be found in Figure 3-10.
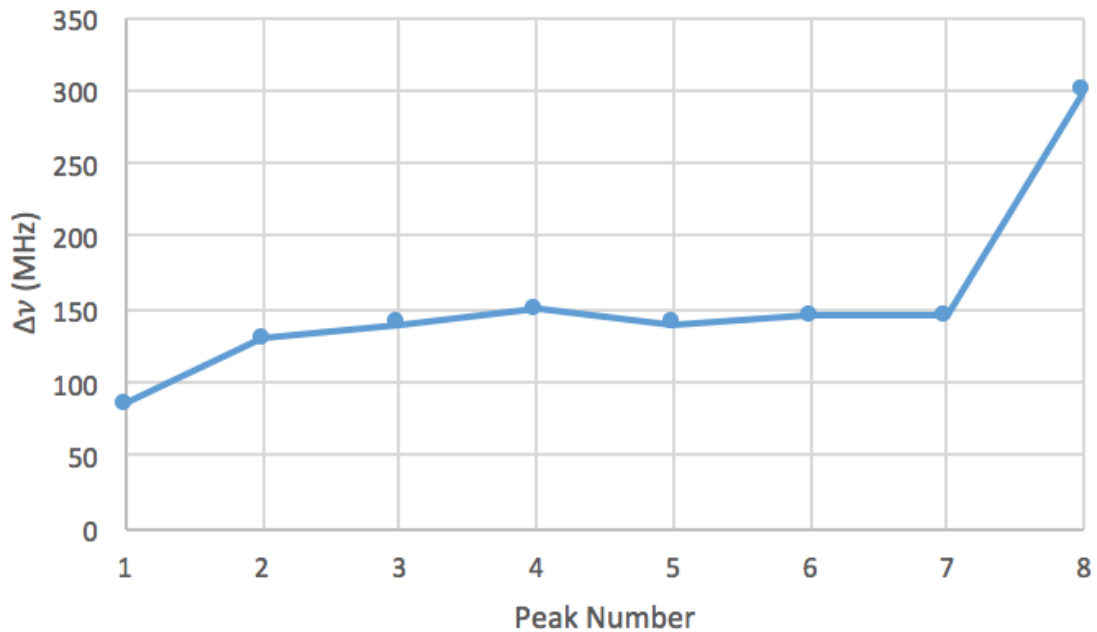
Figure 3-10 – Peak linewidths across the 1523 to 1566 nm wavelength range under test.

Observing the troughs in linewidth as shown in Table 4, there isn't a very obvious trend besides the fact that the last trough has a higher linewidth than the troughs before it, though not nearly as dramatically as is seen in the linewidth peaks. Otherwise, the rest of the troughs

seem to hover around 60 MHz. The general trend from the first trough to the last trough can be found in Figure 3-11.
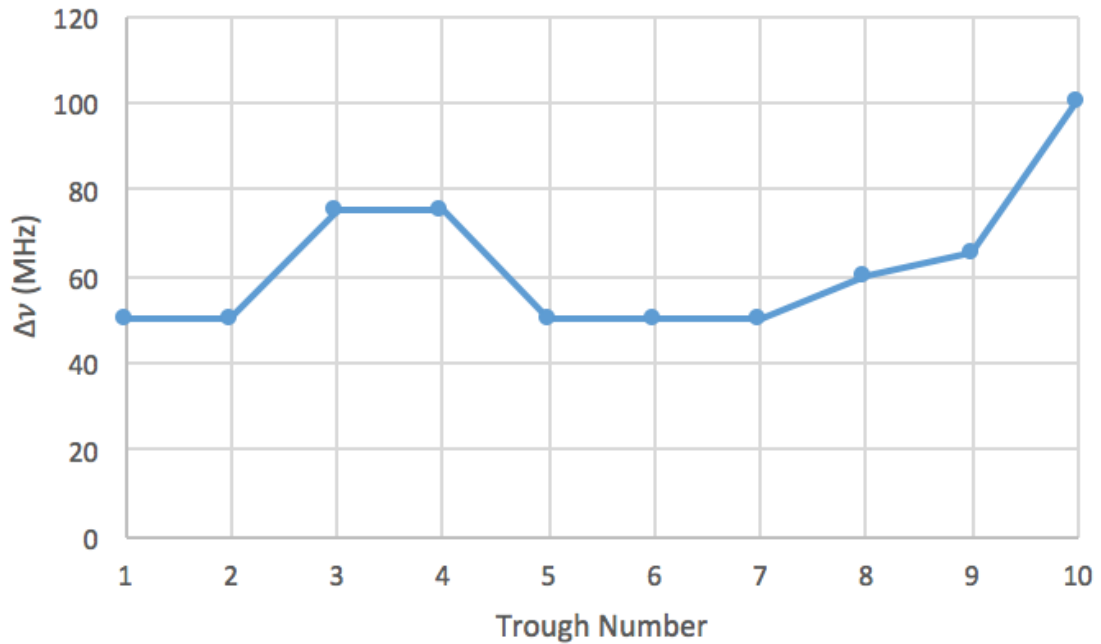
Figure 3-11 - Trough linewidths across the 1523 to 1566 nm wavelength range under test.

Variation in linewidth is evident with the changes in wavelength, and to get a further understanding of what might cause these changes in linewidth, it was mentioned that the different magnitudes of laser current that are active for a set wavelength may play a factor. To get a visual representation of how these laser currents come into play, the four currents were graphed against wavelength, shown in Figure 3-12.

(a)

(b)

42
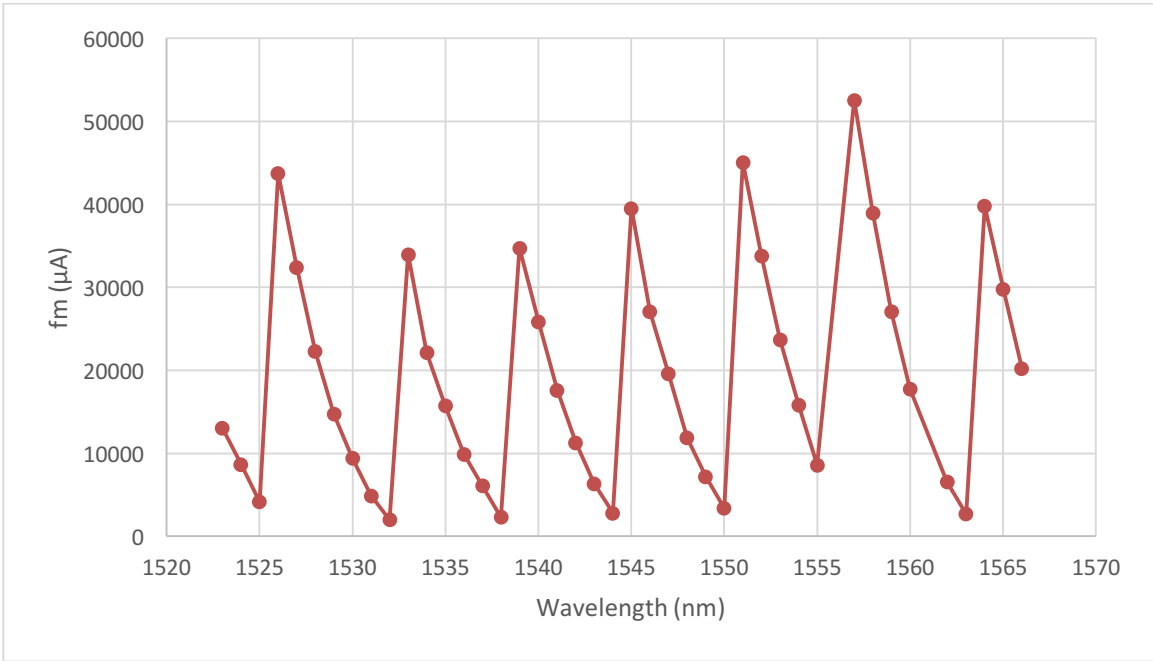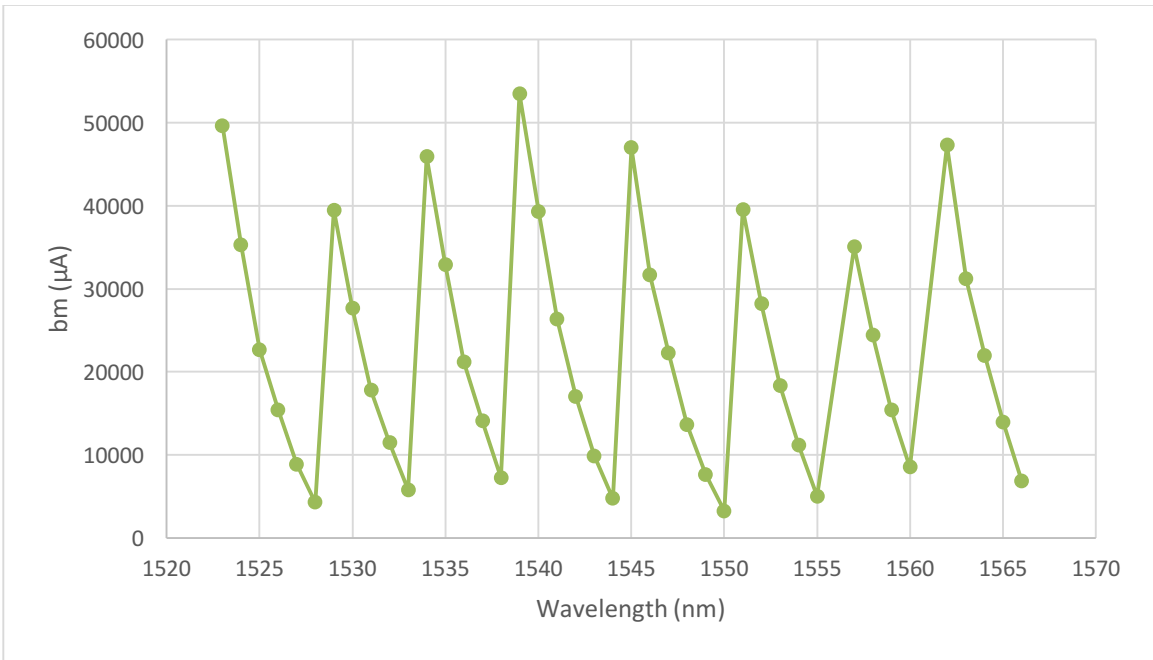
(c)
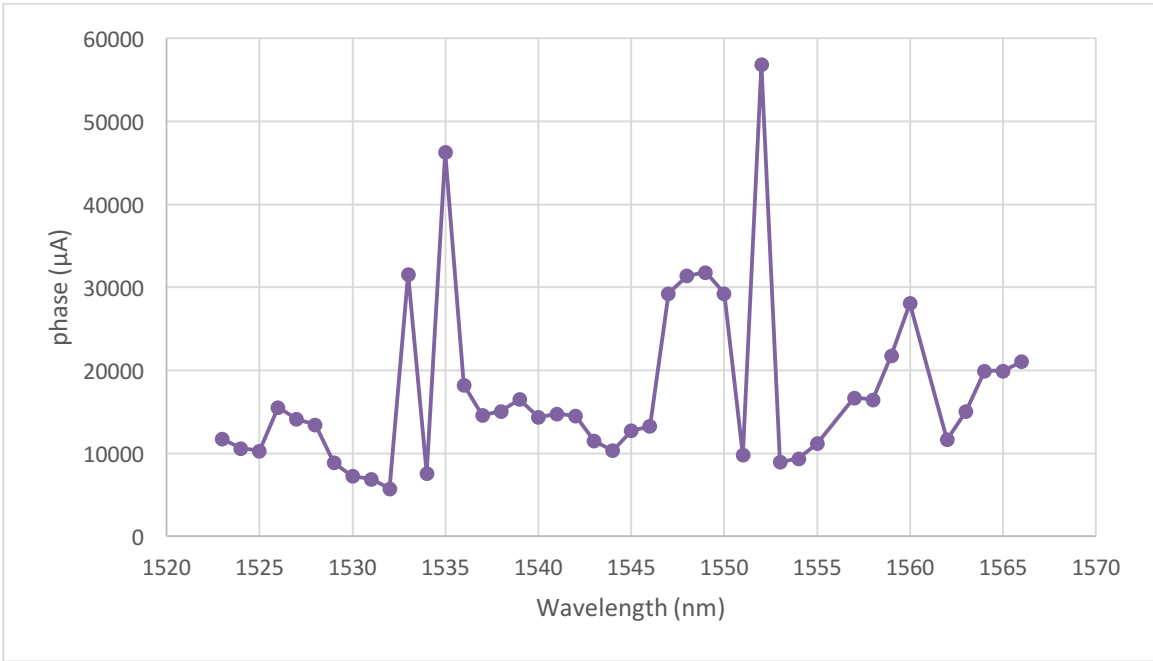
(d)
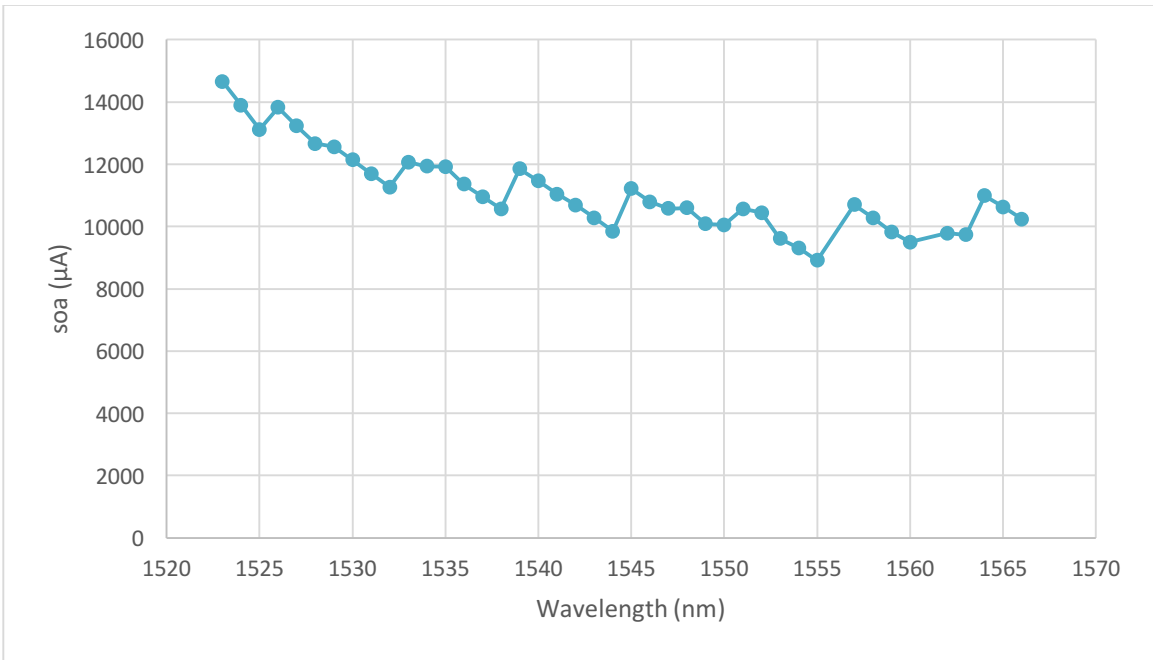
Figure 3-12 – (a) Front mirror (fm), (b) back mirror (bm), (c) phase, and (d) semiconductor optical amplifier (soa) currents variability across the wavelength output range.

As can be observed in Figure 3-12, the first attributes that are apparent are the large up and down variability of

both the front mirror and back mirror currents of the laser. The maximum current for the front mirror case being $52534\,\mu A$ at a fixed wavelength of 1557 nm and the minimum current for the front mirror case being $2022\,\mu A$ at a fixed wavelength of 1532 nm. For the back mirror case the maximum current in this test is $53504\,\mu A$ at a fixed wavelength of 1539 nm, and the minimum current found is $3213\,\mu A$ at a fixed wavelength of 1550 nm. There is also large variability seen with the phase current; however, there does not seem to be an obvious pattern in how the the phase current changes over the range. This is due to the limited amount of data being taken at one nm increments; an increment which is too large for the phase currents. According to the factory data provided by Insight, the phase current in reality also illustrates an up and down pattern across the wavelength range [22]. In the case of the soa current, its general up and down shape across the wavelength range is similar to the fm and bm currents, but the magnitude of its variability is minimal compared to that of the other currents. Initial observation of the current graphs seem to indicate that the front mirror and back mirror currents with their variability and pattern might be the bigger influences on linewidth.

With a visual representation of all of the laser currents and linewidth against wavelength output by the laser, the wavelengths at which there were peak and trough linewidths can be observed to get a better indication of the magnitude of the different laser currents at those points. Using the graphs in Figure 3-12 as reference, Table 3 and Table 4 can be expanded with the currents at these wavelengths and is shown in Table 5 and Table 6.

Table 5 – Peaks in linewidth found at various wavelength outputs of laser with their corresponding laser currents.

λ	$\varDelta\nu$	fm(μA)	bm(μA)	phase(μA)	soa(μA)
1524 nm	85 MHz	8689	35317	10602	13899
1527 nm	130 MHz	32425	8872	14129	13233
1532 nm	140 MHz	2022	11437	5732	11264
1537 nm	150 MHz	6108	14066	14583	10958
1549 nm	140 MHz	7220	7629	31801	10086
1550 nm	145 MHz	3377	3213	29276	10050
1554 nm	145 MHz	15857	11153	9362	9316
1562 nm	300 MHz	6572	47277	11626	9787

Table 6 – Troughs in linewidth found at various wavelength outputs of laser with their corresponding laser currents.

λ	$\varDelta\nu$	fm	bm	phase	soa
1523 nm	50 MHz	13016	49647	11712	14657
1525 nm	50 MHz	4173	22664	10276	13119
1529 nm	75 MHz	14717	39474	8864	12563
1534 nm	75 MHz	22116	45904	7610	11932

1539 nm	50 MHz	34736	53504	16493	11849
1545 nm	50 MHz	39503	46982	12729	11218
1546 nm	50 MHz	27048	31647	13278	10796
1551 nm	60 MHz	45088	39538	9810	10567
1557 nm	65 MHz	52534	35049	16698	10696
1564 nm	100 MHz	39771	21950	19923	10987

Further observation of the currents that make a wider linewidth as seen in Table 5, seem to indicate no obvious trend. A visual representation of these currents can be found in Figure 3-13.
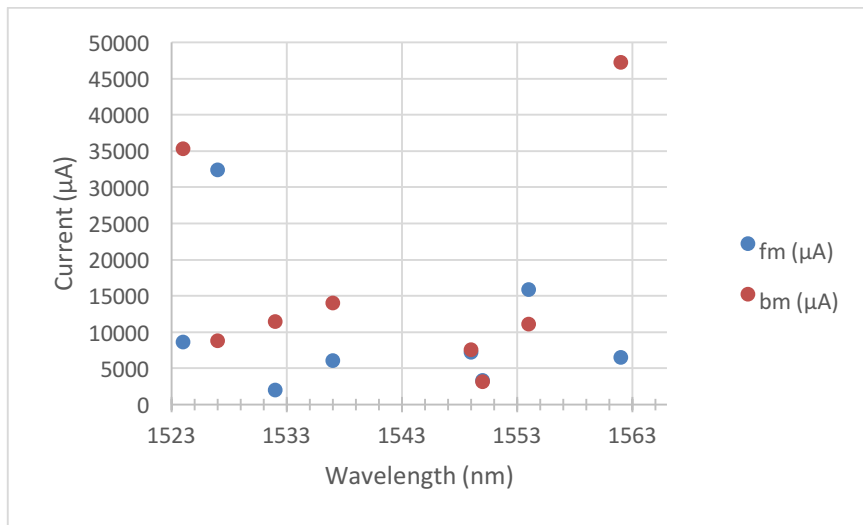
Figure 3-13 - Front mirror (fm) and back mirror (bm) currents at linewidth peaks across the tested wavelength range.

However, further observation of the currents that make a narrower linewidth as seen in Table 6, seem to indicate a somewhat vague trend, but a trend nonetheless. In the lower end of the wavelength range, there is lower front mirror

current then back mirror current. Around the middle of the

wavelength range, there is closer to equal front mirror and

back mirror current. At the higher range of the wavelength

range, the front mirror current is higher than the back

mirror current. The trend can be seen in Figure 3-14. The

linear fit shown in Figure 3-14 shows the general trend but

in no way indicates a good fit in which a mathematical

model can be derived.
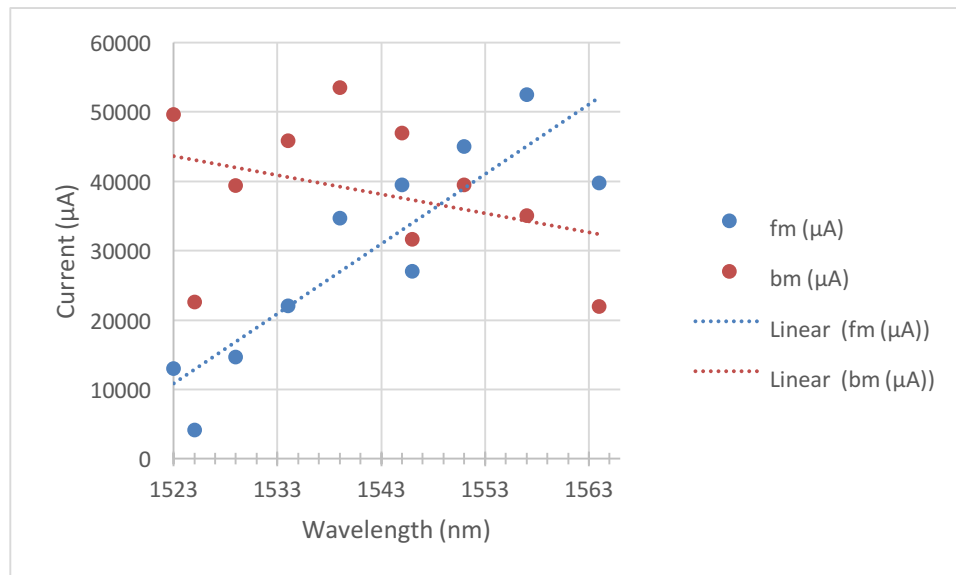
Figure 3-14 - Trend of the front mirror (fm) and back mirror (bm) currents at linewidth troughs across the tested wavelength range.

With a proposed trend for narrower linewidths as seen

in Figure 3-14, the front mirror currents of peak and

trough linewidths can be plotted on one graph to see how

much the front mirror currents at a wider linewidth deviate

from the trend and this can be seen in Figure 3-15. This

can be done with the back mirror currents as well and can
be seen in Figure 3-16. Although plotting on one graph
might be helpful in order to see how both the front mirror
and back mirror currents at a certain wavelength comply
with their respective trends, they were decided to be
graphed separately in order to keep the graphs less
difficult to read.
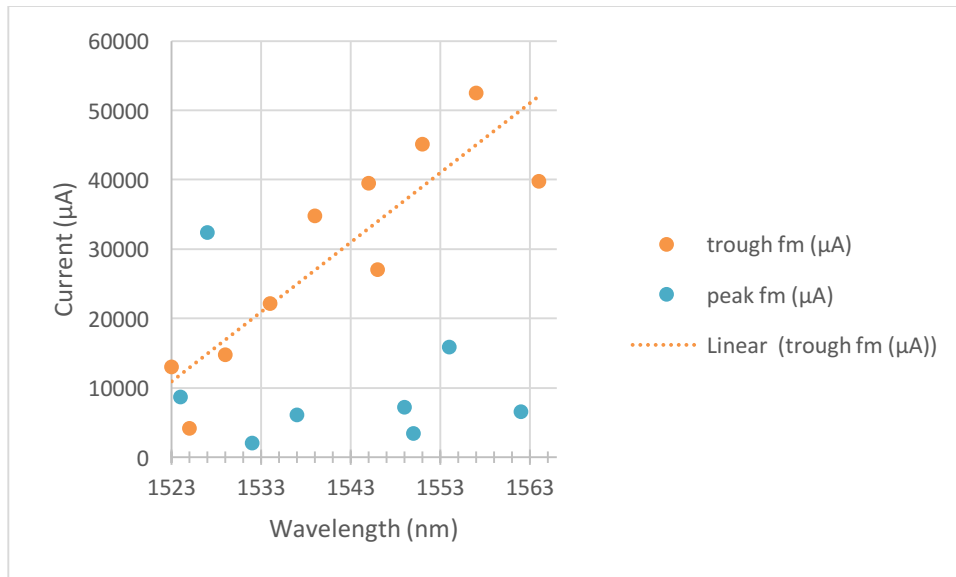
**Figure 3-15 – Trough front mirror (trough fm) and peak
front mirror (peak fm) currents plotted on same graph to
highlight deviation from proposed trend.**
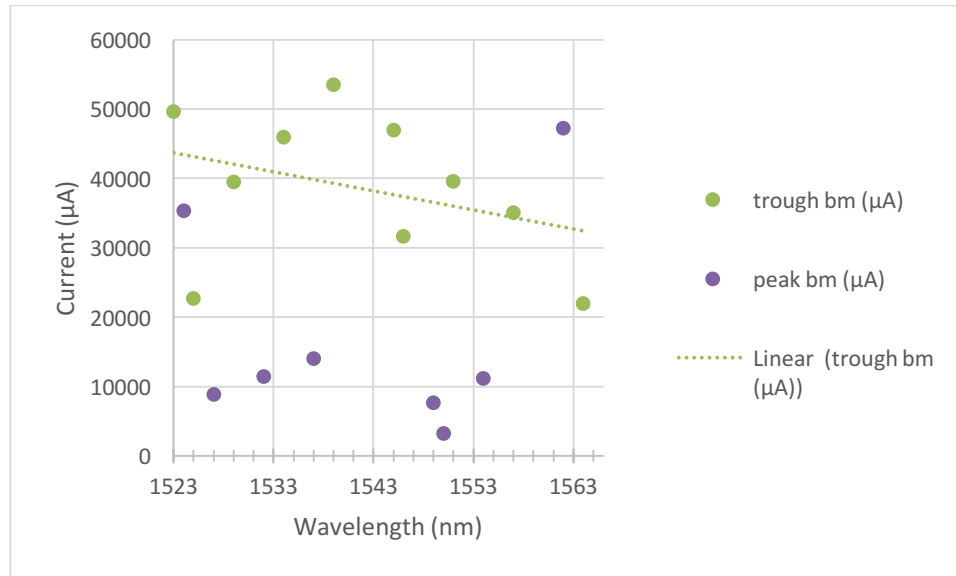
Figure 3-16 – Trough back mirror (trough bm) and peak back mirror (peak bm) currents plotted on same graph to highlight deviation from proposed trend.

As seen in both Figure 3-15 and 3-16, there is indication that the peak front mirror and back mirror currents deviate from the proposed trend. However, upon further observation it can be seen that there is one wavelength that seems to contradict the trend. The front mirror and back mirror currents at the wavelength of 1524 nm hug the respective proposed trends closely but has been labeled as a peak linewidth. Upon further investigation, using Table 5 as a reference, the linewidth at that wavelength is 85 MHz. It was labeled as a peak linewidth due to the lower linewidth on each side of it, which was a linewidth of 50 MHz at 1523 and 1525 nm. Thus an argument for the original proposed trend can be that although in the data set that was taken, the 85 MHz is labeled as a peak,

it is not technically a high linewidth when compared

against the other linewidths found in the range under test.

Moving on to more of the rest of the lineshape, upon

initial observation of the captured tabulated results

regarding lineshape as can be found in **Appendix B,** the

spectral shapes of the various wavelengths seem to

expectedly follow a pattern in which a narrower linewidth,

defined as 3dB down from peak Δv, leads to a narrower width

from 0 Hz at 10 dB down Δv_{10dB}, 20 dB down Δv_{20dB}, and 30 dB

down Δv_{30dB} from peak. What is interesting however is the

difference in lineshapes even though the Δv's are the same.

For example, 1523 nm and 1525 nm have an equivalent

linewidth of 50 MHz, but the lineshape is noticeably

different between the two wavelengths. This is further

highlighted quantitatively in Figure 3-17 along with the

rest of the wavelengths across the range.
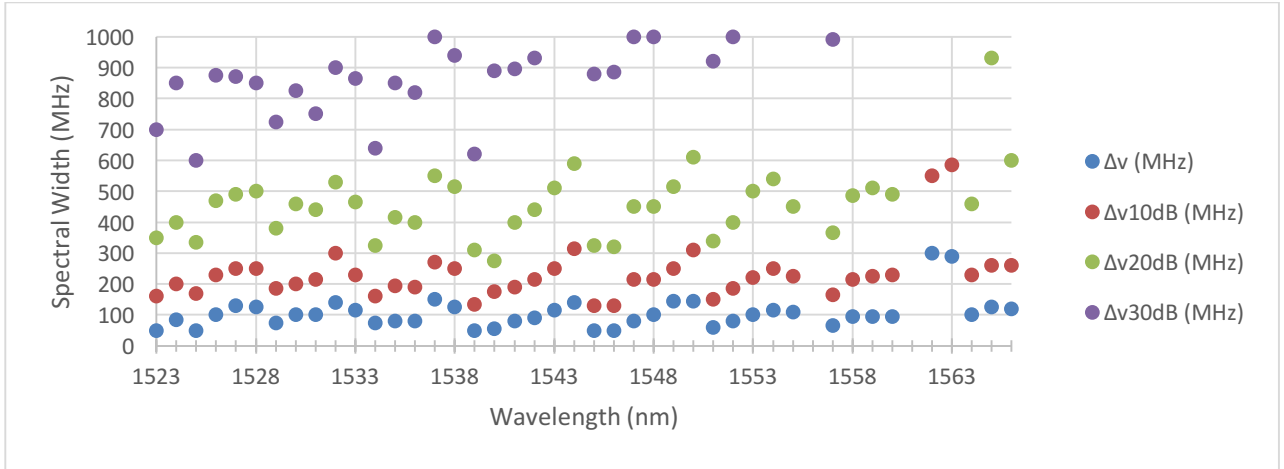
Figure 3-17 – Frequencies at 3 dB (Δv), 10 dB (Δv_{10dB}), 20 dB (Δv_{20dB}), and 30 dB (Δv_{30dB}) down from peak for wavelengths across the range of 1523 to 1566 nm.

Regarding the comparison of the experimental lineshapes to the theoretical Lorentzian lineshape values found in Appendix B, there is a large difference especially when comparing the frequencies at Δv_{20dB} and Δv_{30dB}. The lineshape found in this experiment is much narrower at these points than the theoretical Lorentzian values, and is more similar to a Gaussian shape. A Gaussian and Lorentzian comparison is visually illustrated in Figure 3-18.
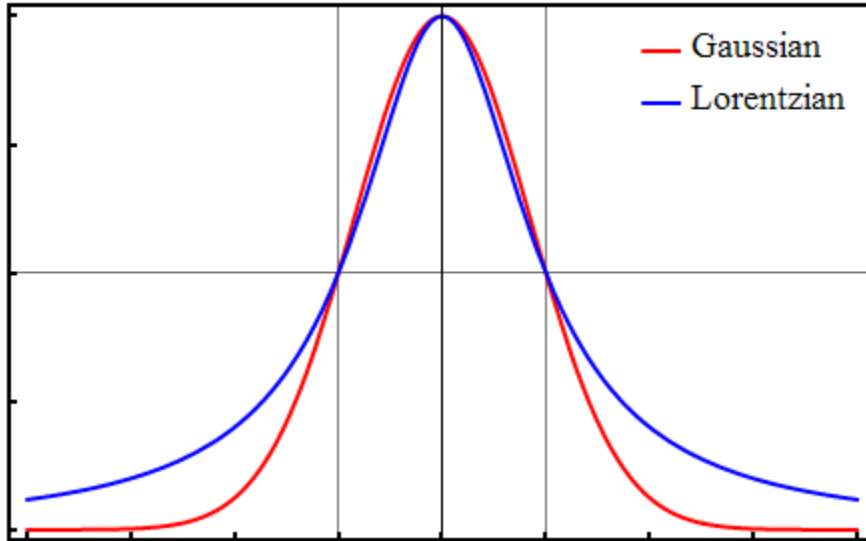
Figure 3-18 – Lorentzian spectral shape and a Gaussian spectral shape overlaid [23].

Chapter 4. Ranging with Interference Fringes

     With investigation into the linewidths of the
wavelengths across the Insight laser output range of 1523
to 1566 nm, coherence times and coherence lengths were
calculated for fixed wavelengths as can be seen in Appendix
A. In order to test the laser's ability to abide by those
calculations, but more importantly, get a general trend for
how effective the laser might be at ranging, an
interference fringe test was done. For initial test
purposes, the laser was chosen to be swept across the
entire wavelength range, 1522.13 to 1566.18 nm, that was
available to be output by laser in the fixed wavelength
mode as seen in Section 3.1 of Chapter 3, in order to keep
the two tests consistent with each other so that
comparisons can be drawn.

4.1 Interference Fringe Test Setup and Theory

     With the Insight Laser Control Program the laser can
be set in swept wavelength mode. The interface is shown in
Figure 4-1.
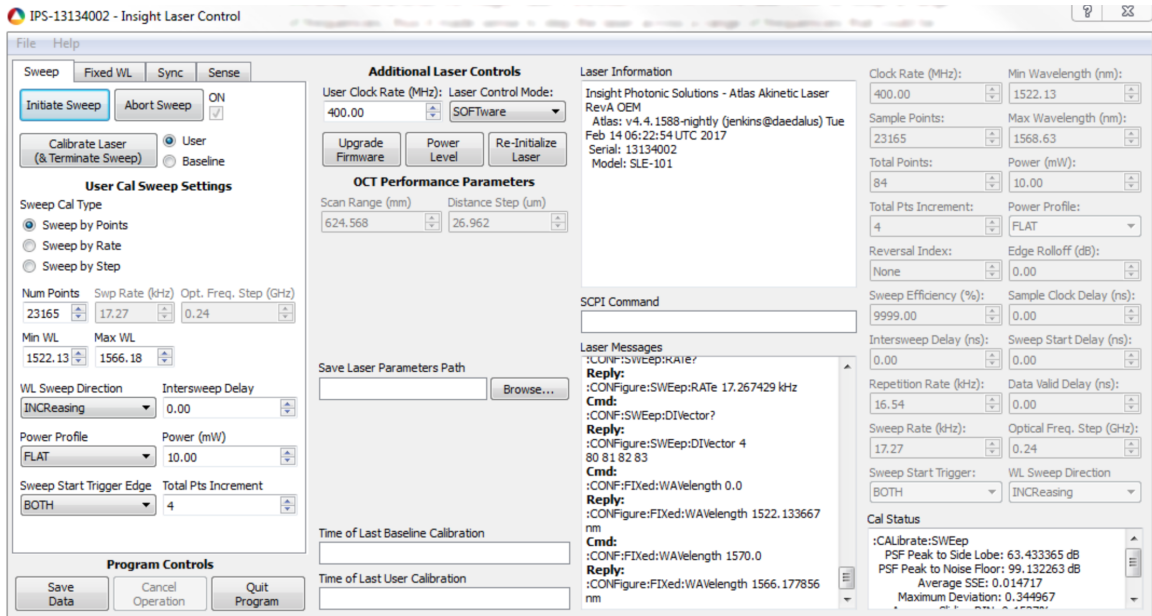
Figure 4-1 - Insight Laser Control Program swept wavelength output interface [20].

The swept wavelength interface of this laser allows the user to sweep across a chosen range of frequencies between 1522.13 nm and 1566.18 nm with modifiable power and various other modifiable characteristics of the sweep as shown in Figure 4-1. The output of the laser for this test is a wavelength sweep across the entire range from 1522.13 nm to 1566.18 nm and at a power of 0 dBm which is shown in a Optical Spectrum Analyzer (Agilent 86140B) to visually highlight the characteristics of the laser in the frequency spectrum in Figure 4-2.
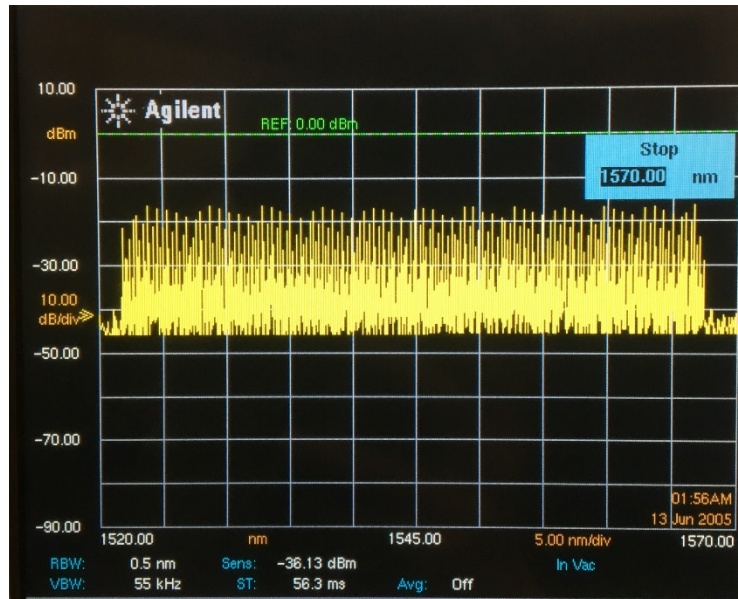
Figure 4-2 – Swept 1522.13 nm to 1566.18 nm output of laser shown in optical spectrum analyzer.

With the laser under test settings determined, the next step was to determine the method of actually obtaining the interference fringes in order to use them to test the ranging capabilities of the swept laser. Luckily, the method of obtaining these interference fringes isn't too vastly different from obtaining linewidth.

As illustrated in Section 3.2 of Chapter 3, to obtain linewidth, an interferometer was used to split the laser source outputting a fixed wavelength into two different paths only to be brought together before being sent into a photodetector to be converted into electrical signals for the electrical spectrum analyzer. The interferometer used in that experiment had a very large delay of $3.5\,\mu s$ in one path compared to the other path.

In order to obtain interference fringes, the setup is almost the same except the laser source is swept across a range of frequencies and is split into two paths with a much smaller path length difference. For ranging purposes, this path length difference would be the distance one would hope to measure.

Qualitatively explained, the laser is sweeping frequencies linearly across a range, just like a radar would in FMCW. Recalled from before in Section 1.2 of Chapter 1, the radar in FMCW will be able to determine the distance between itself and an object, knowing when it sent out a certain frequency in its sweep and being able to calculate the time difference when it detects that certain frequency at the receiver. With that time difference it is able to calculate distance knowing the speed of its signals. The concept of this interference fringe test for the laser is similar in that the sweeping laser source is split into two different paths by the interferometer. There will be a path length difference, so one path will have a delay. Comparing to the radar FMCW concept, the shorter path can be seen as the frequency that is being sent out by the transmitter, and the longer path can be seen as frequency that is being sent to the receiver after reflecting off the object to be detected. After being split

by the interferometer and traveling through different path
lengths, this will lead to two different frequencies, due
to the sweep, coming together at the end of the
interferometer to combine with each other constructively
and destructively, which will create interference fringes.
The spacing between the interference fringe peaks will
indicate the delta wavelength of the sweep $\Delta\lambda$, depending on
the path length difference ΔL, and knowing the velocity of
light in optical fiber v_g, this path length difference can
be found. How $\Delta\lambda$ is related to interference fringes is
illustrated in Figure 4-3.
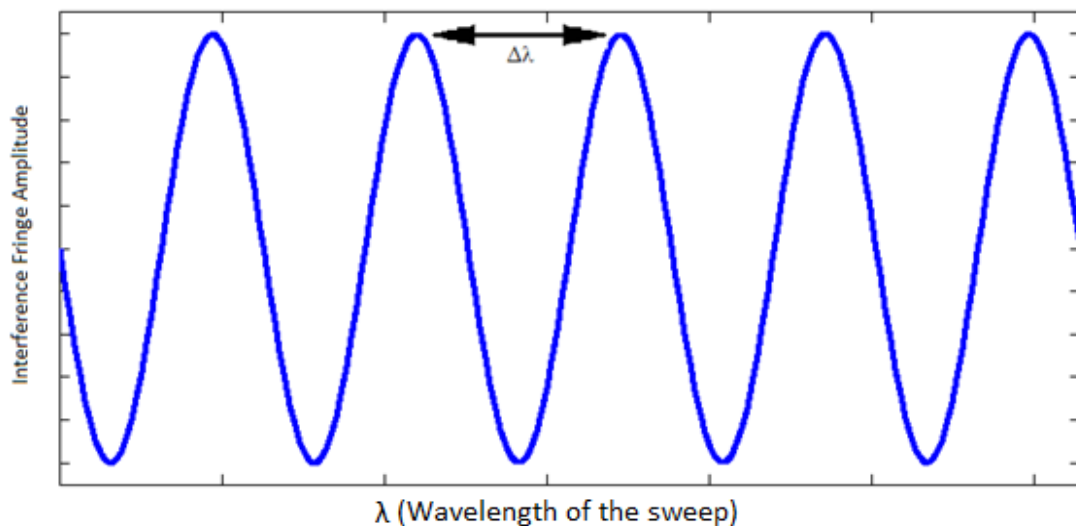
Figure 4-3 – The delta wavelength of the sweep $\Delta\lambda$ is the difference in the sweep of the laser between two peaks of the interference fringes.

The delta wavelength of the sweep $\Delta\lambda$ decreases with a ΔL increase of the interferometer. The rate at which $\Delta\lambda$ decreases is determined by the laser linewidth. A narrower laser linewidth will allow a larger ΔL (because the maximum ΔL is determined by the coherence length), before the $\Delta\lambda$ decreases to a point where peaks cannot be determined as the wavelengths combine completely destructively at the output of the interferometer. Figure 4-4 provides a visual representation of how interference fringes can change over increasing path length differences ΔL.
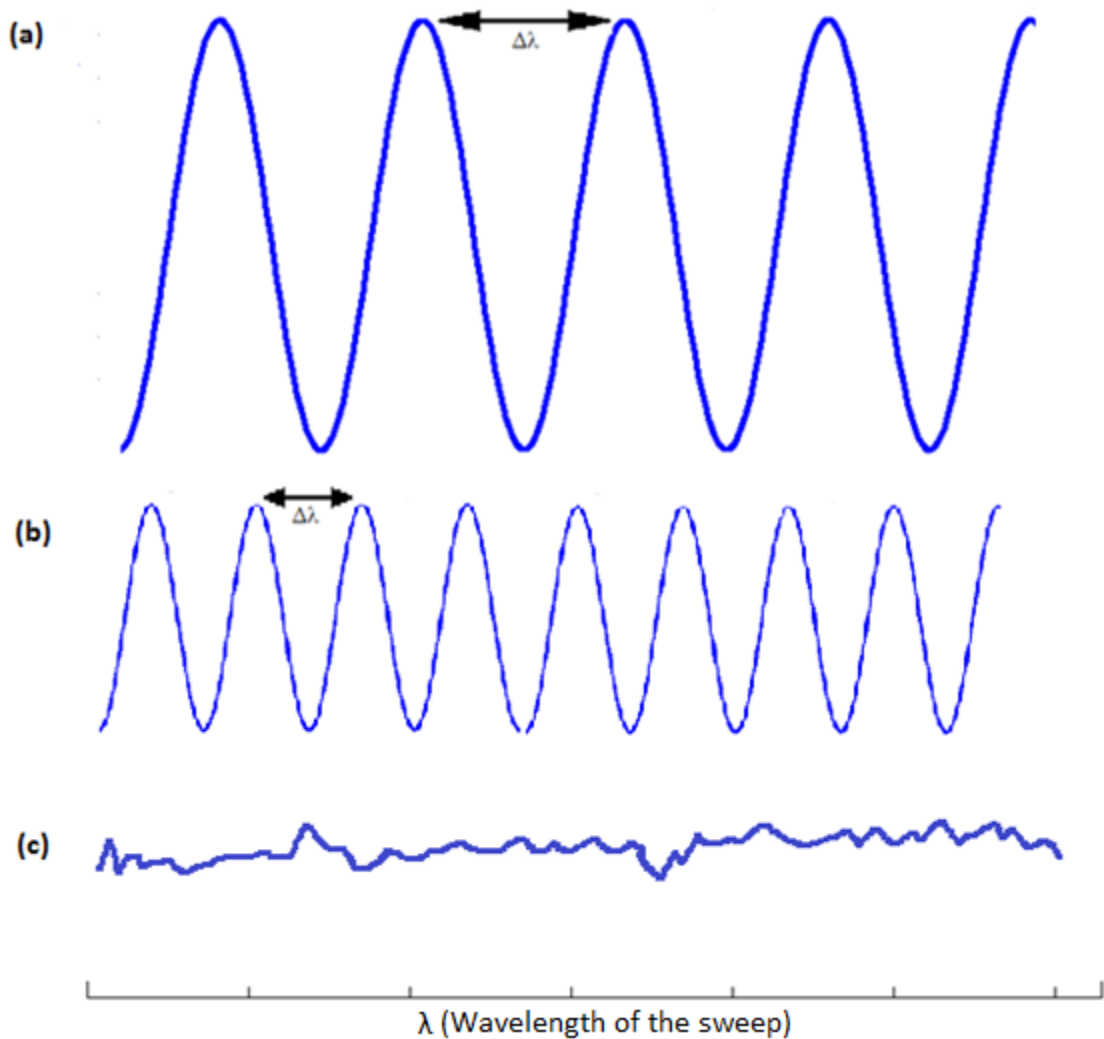
Figure 4-4 – Example of time domain interference fringes at (a) a small ΔL (b) a medium ΔL (c) a large ΔL.

Quantitatively explained, one can refer to the derivation of the relationship between $\Delta \lambda$ or delta frequency of the sweep Δf (known as the free spectral range of the interference fringes), and ΔL for a Mach-Zehnder interferometer, which is what was used for the linewidth measurements in Chapter 3, and is what is essentially created in the interference fringe test. In the Mach-

Zehnder, the laser is split into two different path lengths

at one end and is joined together at the other end, and

because the laser is sweeping, the phases are different as

can be illustrated in Figure 4-5.

$$\varphi_1 = \frac{2\pi}{\lambda} L_1$$

$$\varphi_2 = \frac{2\pi}{\lambda} L_2$$
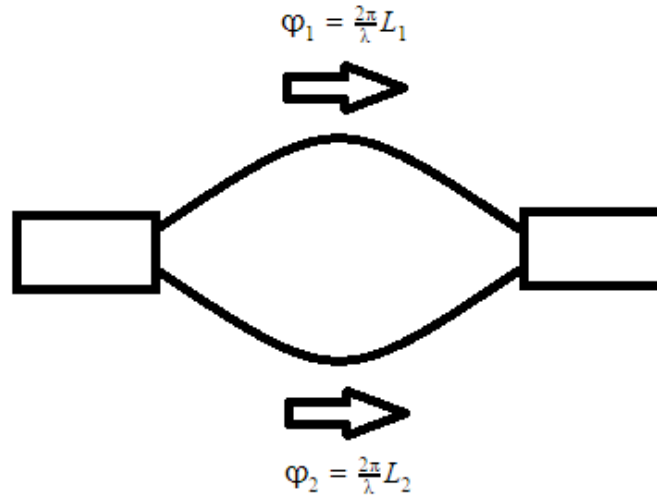
Figure 4-5 – Phase and length relationship across two different lengths.

Taking into account the phase relationship with length, and

how the phase changes with a sweeping wavelength, useful

equations which will allow one to find path length

difference from $\Delta\lambda$ or Δf is derived as follows:

$$\phi_1 = \frac{2\pi}{\lambda} L_1$$

$$\phi_2 = \frac{2\pi}{\lambda} L_2$$

$$\frac{\delta\phi_1}{\delta\lambda} = \frac{-2\pi L_1}{\lambda^2}$$

$$\frac{\delta\phi_2}{\delta\lambda} = \frac{-2\pi L_2}{\lambda^2}$$

$$\frac{\Delta\phi}{\Delta\lambda} = \frac{\delta\phi_1}{\delta\lambda} - \frac{\delta\phi_2}{\delta\lambda} = \frac{2\pi\Delta L}{\lambda^2} \; where \; \Delta L = |L_1 - L_2|$$

$$\frac{2\pi}{\Delta\lambda} = \frac{2\pi\Delta L}{\lambda^2}$$

$$group \; velocity \; index \; n_g = 1.47, for \; optical \; fiber$$

$$velocity \; of \; light \; within \; fiber \; v_g = \frac{c}{n_g}$$

$$\Delta\lambda = \frac{\lambda^2}{\Delta L} = \frac{v_g}{f_1} - \frac{v_g}{f_2} = \frac{v_g\Delta f}{f^2}$$

$$\frac{\lambda^2}{\Delta L} = \frac{v_g\Delta f}{f^2}$$

$$\frac{(v_g/f)^2}{\Delta L} = \frac{v_g\Delta f}{f^2}$$

$$\Delta L = \frac{v_g}{\Delta f}$$

The derivation can be summarized in three very useful equations:

$$Free \; Spectral \; Range \; FSR = \Delta f = \frac{v_g}{\Delta L} = v_g\frac{\Delta\lambda}{\lambda^2}$$

$$\Delta\lambda = v_g\frac{\Delta f}{f^2}$$

$$\Delta L = \frac{v_g}{\Delta f}$$

The equations above allows one to obtain the path length difference from the free spectral range of the interference fringes and the velocity of light in optical fiber.

The test setup to obtain interference fringes is very similar to how the linewidth test was setup in Section 3.2

of Chapter 3 except that these Mach-Zehnder type interferometers had to be made with much smaller path length differences then was presented in the off the shelf module that was used for the linewidth tests which had a $3.5\,\mu s$ delay. Because there was no off the shelf module available for path length differences which would successfully be able to test the relatively short path length difference as indicated by the range of coherence lengths as shown in Appendix A, the interferometers with these path length differences were made.

Two 1x2 couplers (Thorlabs TW1550R5A1) with a theoretical splitting ratio of 50/50 (50% one arm and 50% on the other) were used. These couplers had a bandwidth of 1550 nm ± 100 nm, which was perfect for the output wavelength range of this laser of 1522.13 nm to 1566.18 nm. With FC APC male connectors already available on the inputs and outputs of the couplers, interchanging lengths in between them was simply done using FC APC male to male adapters. The couplers and the adapters in the test layout can be found in Figure 4-6.
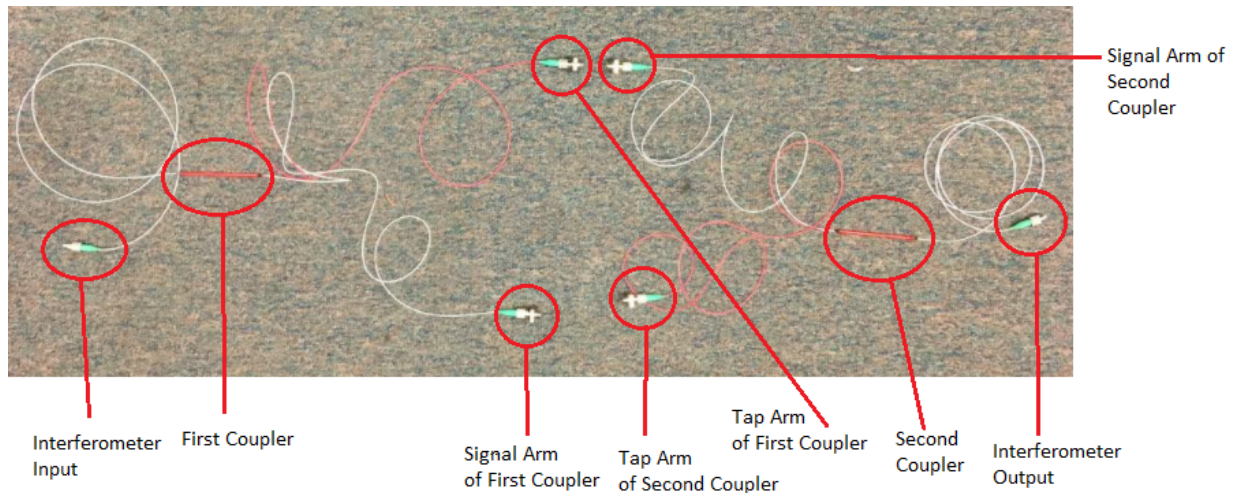
Figure 4-6 – Homemade Mach-Zehnder interferometer allowing for interchangeable lengths.

A polarization controller was also made to be able to plug into the homemade interferometer. Although light waves are able to vibrate in multiple planes, a polarization controller allows one to tune light waves to vibrate in one plane, which is preferable for consistency in test. The light directly output by the laser is polarized; however, the optical fiber is birefringent which alters the polarization. In order to try and reach maximum polarization, but more importantly, avoid destructive polarization differences when the two lights combine at the end of the interferometer with the second coupler, a polarization controller was made with a cardboard backplane. The dimensions and number of rotations were based off a 2 paddle polarization controller. This homemade polarization controller can be found in Figure 4-7.
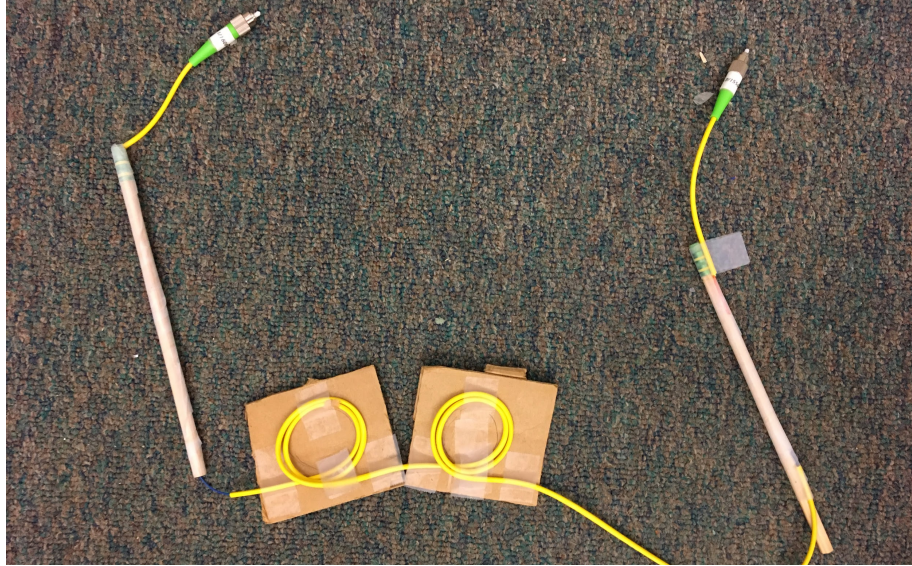
Figure 4-7 - Homemade two paddle polarization controller.

4.2 Interference Fringe Test

With a basic theoretical background and a method of capturing path length difference determined, the experimental setup to capture the interference fringes of swept wavelengths across the wavelength range able to be output by the Insight laser at different path length differences was begun.

The laser is connected to the homemade interferometer shown in Figure 4-7 and a variable path length difference is inserted into the interferometer. The output of the interferometer is plugged into an off the shelf photodetector (Insight BPD-1). The output of that photodetector is then plugged into an oscilloscope (Tektronix TDS 784A or the 5105 LABVIEW oscilloscope setup) so that the interference fringes can be seen. A visual

representation of the experimental setup for the interference fringe characterization of the Insight laser can be seen in Figure 4-8.
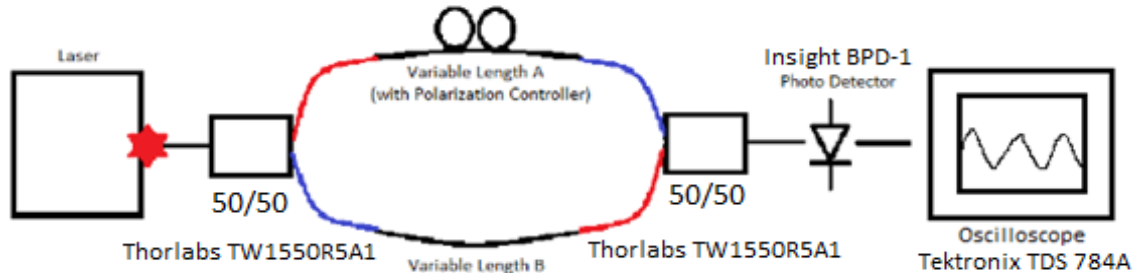
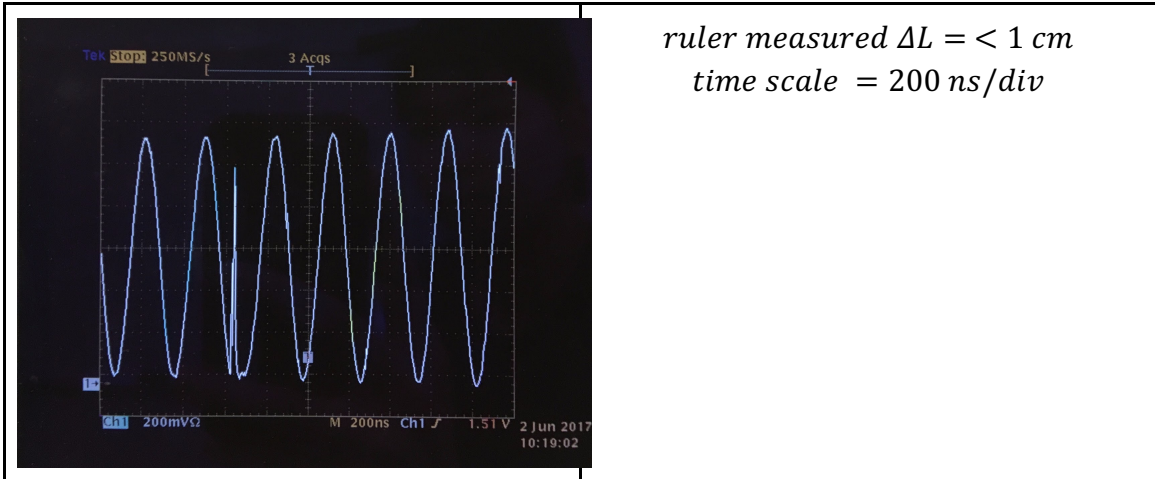**Figure 4-8 - Time domain interference fringe test setup.**

Using the interference fringe test setup as seen in Figure 4-8, 9 different path length differences were inserted. This ranged from very small ruler measured path length differences of < 1 cm (no observable measurable path length difference) to relatively larger ruler measured path length differences such as 187.5 cm. Figure 4-9 shows the interference fringes for a ruler measured path length difference of < 1 cm across the time scale for the laser to perform approximately 3 sweeps on the LABVIEW oscilloscope via use of a 5105 PCI Digitizer ADC and a 5105 Acquisition program. As can be observed by utilizing Waveform Graph 2 of the program, the time from 1523.13 nm to 1566.18 nm is around $60\,\mu s$.
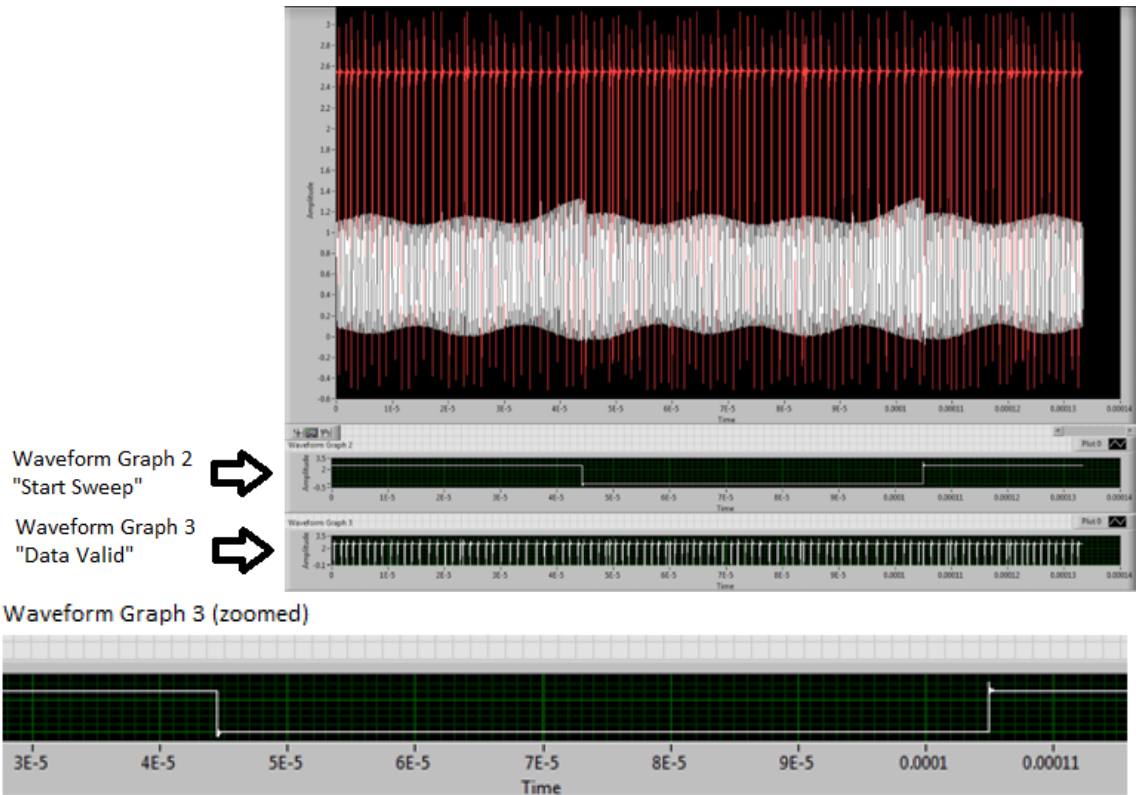
Figure 4-9 – Interference fringes as seen on 5105 Acquisition program across a time scale of around 3 laser sweeps for a ruler measured path length difference of < 1 cm.

Scaled to a much smaller time scale so that the interference fringe frequency is more visible for all of the path length differences, and utilizing the high bandwidth Tektronix oscilloscope rather than the 5105 setup due to its limited bandwidth capabilities, please refer to Appendix C for the results of this experiment in tabular format. Figure 4-10 highlights the format in which the data was taken for example purpose for a ruler measured path length difference ΔL of < 1 cm.
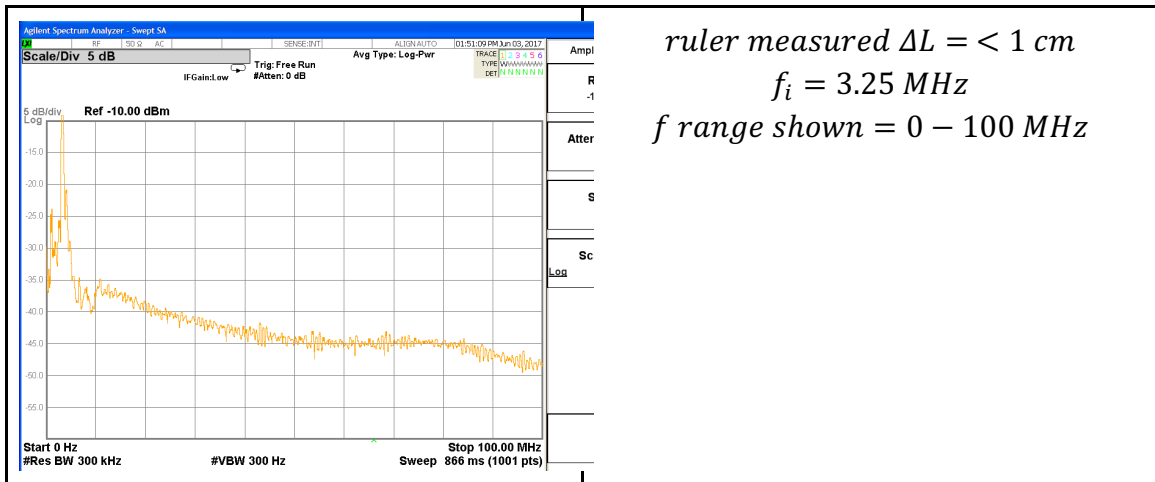
$$ruler\ measured\ \Delta L = < 1\ cm$$
$$time\ scale\ = 200\ ns/div$$

Figure 4-10 – Example of experimental data taken for ruler measured path length difference of < 1 cm in time domain interference fringe test.

With the time domain of the output of this experiment captured, in order to capture the frequency of these interference fringes f_i, a spectrum analyzer was utilized. This would not only allow one to capture the frequency of the interference fringes, but it would also allow one to observe the entire frequency spectrum and any harmonics that may present themselves. In order to do a frequency domain analysis, the output of the photodetector as seen in Figure 4-8 was connected to an off the shelf spectrum analyzer (Agilent Technologies N9000A). This frequency domain test setup can be seen in Figure 4-11.
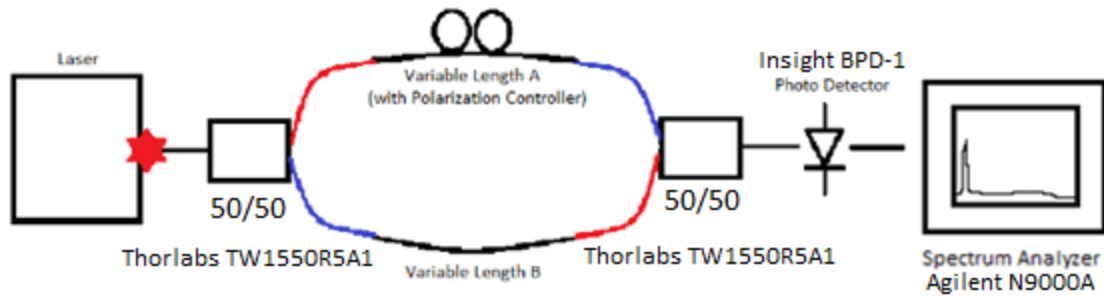
Figure 4-11 – Frequency domain interference fringe test setup.

The frequency domain test was done for all of the ruler measured path length differences that were tested in the time domain with the oscilloscope. The frequency at which there was peak power was recorded as the frequency of the interference fringe. Please refer to Appendix D for the results of this experiment in tabular format. Figure 4-12 highlights the format in which the data was taken for example purpose for a ruler measured path length difference ΔL of < 1 cm.

$$ruler\ measured\ \Delta L = < 1\ cm$$
$$f_i = 3.25\ MHz$$
$$f\ range\ shown = 0 - 100\ MHz$$

Figure 4-12 – Example of experimental data taken for ruler measured path length difference of < 1 cm in frequency domain interference fringe test.

4.3 Interference Fringe Test Calibration Method

With the equations necessary to find path length difference from the free spectral range Δf or $\Delta \lambda$ from Section 4.1, and the interference fringe time domain and frequency domain characteristics obtained from section 4.2, the next logical step would be to calculate exactly what path length differences are indicated by the interference fringes obtained and to see how well that lines up with the ruler measured path length differences.

In order to do this, the frequency of the interference fringes f_i must be associated with Δf or $\Delta \lambda$. This can be done a variety of ways including correlating the wavelength range of the sweep with the time it takes for one sweep, and calculating what sweep wavelength difference (or frequency difference) is correlated with a period of the

interference fringes. Another way, similar to a sort of calibration, is to take a known value of $\Delta\lambda$ from an already tested interferometer and find the f_i correlated with it. Because the time it takes for each laser sweep is constant, knowing how $\Delta\lambda$ and f_i relate for one case will allow one to calculate the $\Delta\lambda$ of the rest of the cases, if given just f_i of the other cases, by taking proportions.

Because there was an interferometer with a known $\Delta\lambda$ of 100 pm available, the second calibration method was chosen. The output of the laser was connected to the input of the calibration interferometer, and the output of the interferometer was then connected to both the oscilloscope and spectrum analyzer. The output of the calibration interferometer with a $\Delta\lambda$ of 100 pm in the time domain is shown in Figure 4-13, and the frequency domain of the same is shown in Figure 4-14.

**Figure 4-13 – Time domain output of calibration
interferometer with known 100 pm $\Delta\lambda$.**

**Figure 4-14 – Frequency domain output of calibration
interferometer with known 100 pm $\Delta\lambda$.**

Utilizing both Figure 4-13 and Figure 4-14, the frequency

of the interference fringes f_i is found to be 7.25 MHz.

Further, with the known 100 pm $\Delta\lambda$, the path length

difference that correlates with an f_i of 7.25 MHz can be found mathematically as follows:

$$\Delta\lambda = 100\text{pm}$$

$$\Delta f = (2.04x10^8 m/s) * [\frac{100pm}{(1545nm)^2}]$$

$$\Delta f = 8.546\ GHz$$

$$\Delta L = \frac{2.04x10^8 m/s}{(8.546GHz)}$$

$$\Delta L = 2.4\ cm$$

This allows one to correlate a ΔL of 2.4 cm with a f_i of 7.25 MHz, and also allows one to be able to find an unknown path length difference if provided a known f_i for the sweep settings of the laser used in this chapter as follows:

$$\frac{7.25MHz}{2.4cm} = \frac{f_i}{\Delta L}$$

$$\Delta L = f_i * \frac{2.4cm}{7.25MH\square}$$

4.4 Interference Fringe Test Results and Analysis

With a method of finding path length difference ΔL from interference fringe frequencies f_i as found in Section 4.3, the interference fringe frequencies captured in Appendix D were utilized to calculate experimental path length differences and were compared with the ruler measured path length differences.

As seen in Appendix D, for a ruler measured ΔL of < 1 cm, there is a f_i of 3.25 MHz. Thus the experimental ΔL can be found mathematically as follows according to Section 4.3:

$$\Delta L \ = \ f_i * \frac{2.4cm}{7.25MHz}$$

$$\Delta L \ = \ (3.25 \ MHz) * \frac{2.4cm}{7.25MHz}$$

$$\Delta L \ = 1.075 \ cm$$

This was done for all of the ruler measured path length differences and the comparison between the ruler measured ΔL and experimental ΔL (found from f_i) can be seen in Table 7.

Table 7 – Comparison of ruler measured ΔL and experimental ΔL (calculated from interference fringes frequency) for various path lengths.

Ruler Measured ΔL	Experimental ΔL
< 1 cm	1.075 cm
≈ 1 cm	3.145 cm
≈ 11.5 cm	17.66 cm
≈ 22.5 cm	36.4 cm
≈ 34 cm	54.8 cm
≈ 56.5 cm	87.7 cm
≈ 119 cm	191.3 cm
≈ 130.5 cm	209.7 cm
≈ 187.5 cm	N/A

Initial observations of Table 7 between the ruler measured and experimental path length differences show a large discrepancy between them that seems to get larger as the path length difference is increased. In order to get a visual of how the ruler measured ΔL and the experimental ΔL vary, they were both plotted. For the value of < 1 cm, a value of 0 was used for this purpose. This graph can be found in Figure 4-15.
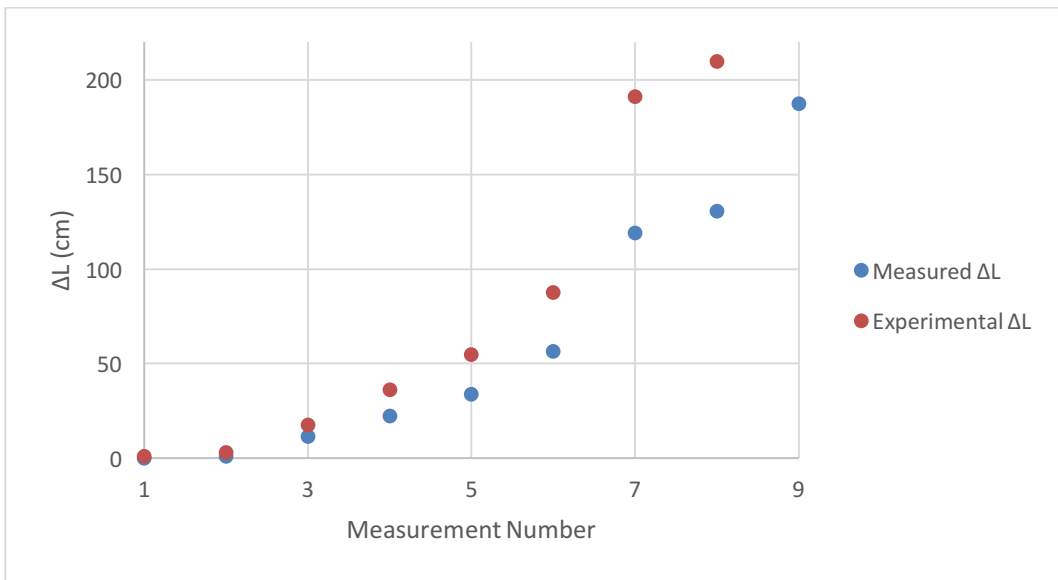
Figure 4-15 – Comparison of ruler measured ΔL and experimental ΔL for various path length measurements.

Although many more data points would have to be taken to speak with confidence, there seems to be an exponential increase in the error between the ruler measured and experimental path length differences as can be seen in the spacing between the two for each of the measurements as seen in Figure 4-15. Perhaps with more data points, the

mathematical model can be derived for the error and can be compensated so that the experimental and ruler measured match up together closer for a more accurate ranging.

Moving on to more about coherence time and coherence length, and how they hold up with the data that was found in Section 4.3, the max path length difference in which a frequency was discernible from the noise for this experiments was at a ruler measured ΔL of 130.5 cm. With the max coherence length found to be 129.92 cm found in Appendix A, 130.5 cm is a fraction of a cm longer than the max coherence length found from the linewidth test in Chapter 3. Though it must be stated that although the frequency is discernible in the spectrum analyzer, it is by such a slight amount that the opposite can be argued. Not to mention the fact that the time domain interference fringes is almost completely destructive such that one would have to look at the frequency domain to obtain a frequency for it. It is fair to say that at 130.5 cm, the coherence is being stretched. Nonetheless, there is also a possibility there may be a maximum coherence length (minimum linewidth) that was not seen in the specific wavelengths tested across the range of theoretically infinite wavelengths. The interference fringes for the path length difference of 130.5 cm can be seen in time domain

with the oscilloscope in Figure 4-16 and in frequency

domain with the spectrum analyzer in Figure 4-17.
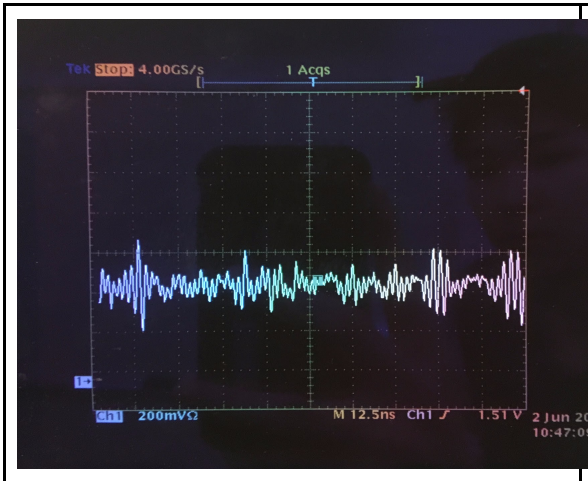
$ruler\ measured\ \Delta L \approx 130.5\ cm$
$time\ scale\ = 12.5\ ns/div$

Figure 4-16 - Barely discernible interference fringes at a ruler measured path length difference of 130.5 cm.
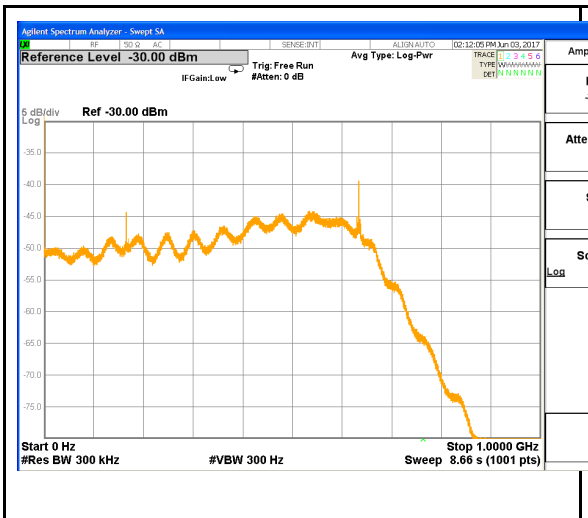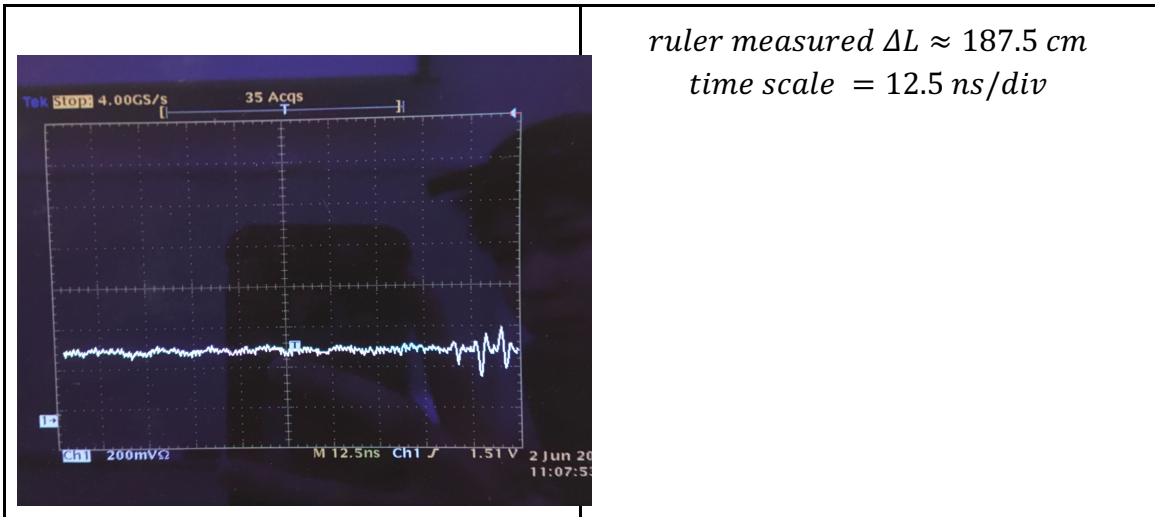

$ruler\ measured\ \Delta L \approx 130.5\ cm$
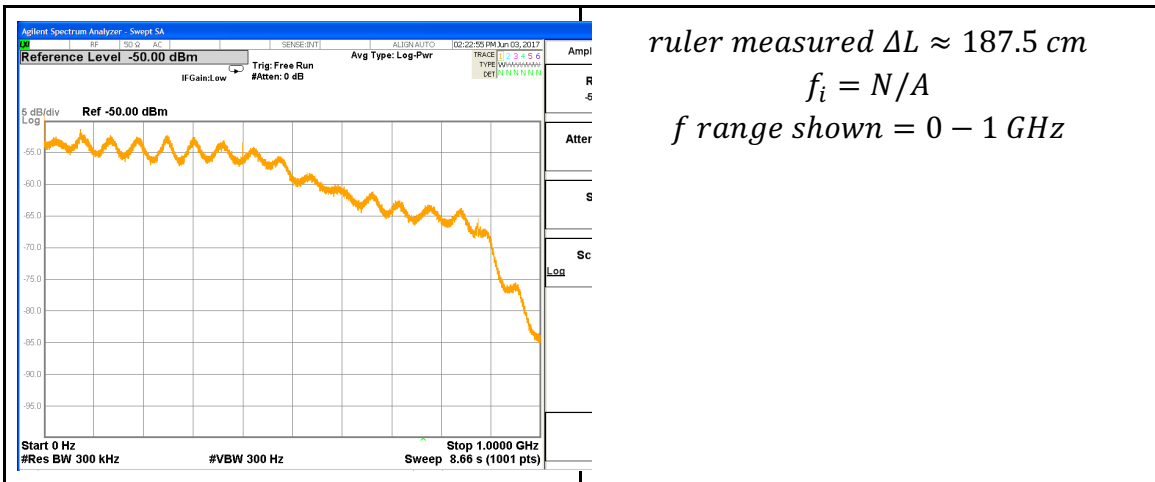$f_i = 633.57\ MHz$
$f\ range\ shown = 0 - 1\ GHz$

Figure 4-17 - Barely discernible frequency of interference fringes at a ruler measured path length difference of 130.5 cm.

In the larger ΔL of 187.5 cm that was also tested,

there was neither a discernible waveform in the time domain

as seen in Figure 4-18 nor a discernible frequency peak

above the noise floor as seen in Figure 4-19. As such, the

f_i is labeled as N/A and an experimental path length
difference cannot be calculated for this case.

$ruler\ measured\ \Delta L \approx 187.5\ cm$
$time\ scale\ = 12.5\ ns/div$

**Figure 4-18 - Indiscernible interference fringes at a ruler
measured path length difference of 187.5 cm.**

$ruler\ measured\ \Delta L \approx 187.5\ cm$
$f_i = N/A$
$f\ range\ shown = 0 - 1\ GHz$

**Figure 4-19 - Indiscernible frequency of interference
fringes at a ruler measured path length difference of 187.5
cm.**

Given that a path length difference of 187.5 cm is
approximately 57.5 cm longer than the maximum calculated
coherence length of 129.92 cm, it is understandable that
there is no discernable frequency.

Chapter 5. Conclusions

The Insight VT-DBR Akinetic laser source has been
characterized for ranging performance through both a
linewidth experiment and ranging experiments using
interference fringes. Conclusions on the experiments,
possible applications, and future work are presented. The
purpose of this study was to investigate into the
feasibility of using this laser for ranging purposes
similar to how the FMCW method works for radar in order to
combine the benefits of both a lidar and radar into one
FMCW lidar sensor. The overall goals of such a sensor are
outlined in Table 8.

Table 8 – Goals of the FMCW Lidar sensor within various parameters.

Parameter	Goal Value	Comments
Range/Sensitivity	100 m	Should be able to sense something like a stop sign at 100 m with adequate signal to noise ratio.
Distance Resolution	10 cm	N/A
Time to take a single data point.	$2\,\mu s$	Corresponds to taking 500 kSamples/s
Security of system against other lidars.	TBD	Must be able to work in an environment with many simultaneous LIDARs in operation, with little interference.
Security against intentional jamming.	TBD	Must still work even with intentional laser jamming signal.
Cost	TBD	Minimal part of autonomous system cost
Eye Safety	IEC Class 1	Class 1 lasers are very low risk and "safe under reasonably foreseeable use" [14].

5.1 Insight Laser Linewidth

In summary of the laser linewidth characterization performed in Chapter 3, the Insight VT-DBR akinetic laser was put through a linewidth test in which the purpose was

79

to find the magnitude and variation of linewidths across
its sweep range of 1522.13 to 1566.18 nm. This was done to
investigate where there may be lower linewidths across the
sweep range of the laser and what causes then. In order to
capture linewidths of the laser, the laser was placed into
fixed wavelength mode to output across the range in integer
wavelengths of 1523 nm to 1566 nm in steps of 1 nm. The
linewidth at these wavelengths were extracted using the
Delayed Self-Homodyne technique using a Mach-Zehnder
Interferometer. The largest linewidth captured was 300 MHz
at a fixed wavelength laser output of 1562 nm while the
smallest linewidth was captured to be 50 MHz found at fixed
wavelength laser outputs of 1523, 1525, 1539, 1545, and
1546 nm. With the linewidths obtained across the range of
the laser, the laser pump currents at these different
wavelengths were investigated in order to find a
correlation between the laser currents and the linewidth.

It was found that there was not a simple correlation
or obvious correlation as would be hoped between the laser
currents and the linewidth. However, there seems to be a
loose correlation, but a correlation nonetheless, between
the where one is in the wavelength range able to be output,
the currents at those wavelengths, and low linewidth.
Across the range of 1523 to 1566 nm, this experiment found

a somewhat linear, albeit low correlation, area of low
linewidths depending on the front mirror and back mirror
currents. It is suggested that the front mirror and back
mirror currents must both be within their respective area
of low linewidths for the overall laser to have a low
linewidth. The front mirror currents of low linewidths vs
high linewidths are shown in Figure 5-1 while the same
except for back mirror currents is shown in Figure 5-2.
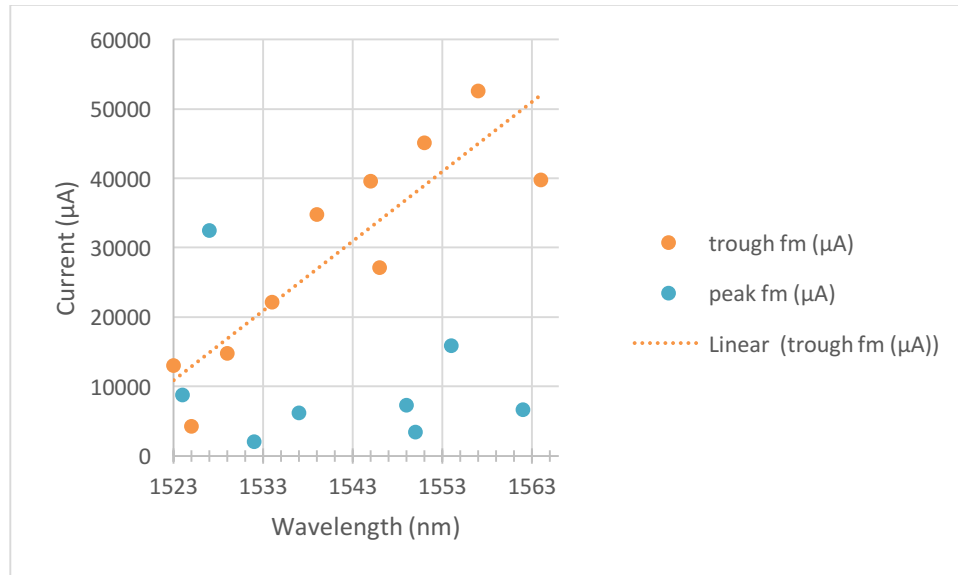
**Figure 5-1 – Low linewidth front mirror (trough fm) and
high linewidth front mirror (peak fm) currents plotted on
same graph to highlight deviation of high linewidth
currents from proposed trend of low linewidth currents.**
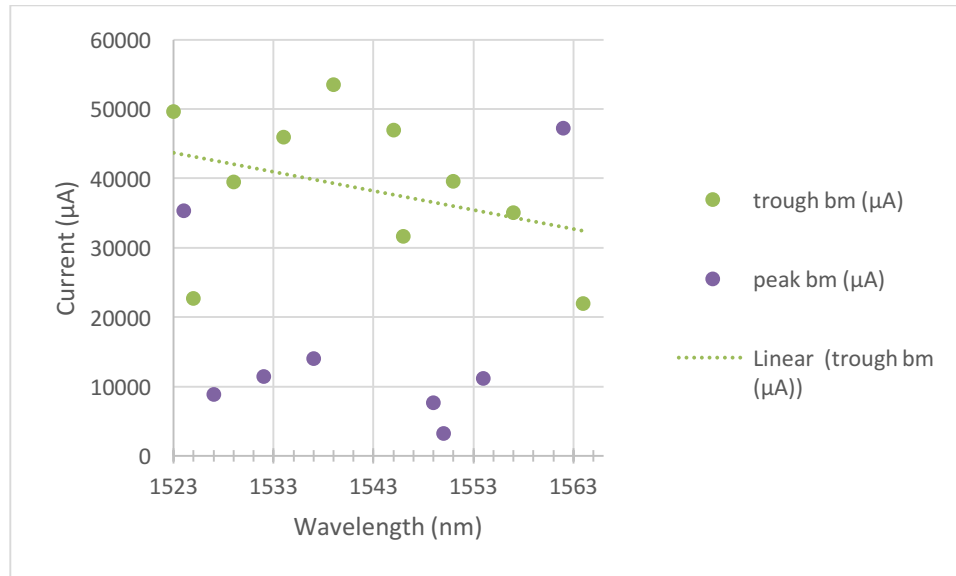
Figure 5-2 – Low linewidth back mirror (trough bm) and high linewidth back mirror (peak bm) currents plotted on same graph to highlight deviation of high linewidth currents from proposed trend of low linewidth currents.

Furthermore, as a precursor to the interference fringe experiment and to gain an understanding of the possible range of the laser in terms of ranging, coherence numbers were also calculated utilizing the linewidths captured with the minimum coherence time and coherence length of 1.061 ns and 21.65 cm respectively at the maximum linewidth found of 300 MHz, and with the maximum coherence time and coherence length of 6.366 ns and 129.92 cm respectively at the minimum linewidth found of 50 MHz. This is far from the goal range/sensitivity of 100 m as was outlined in Table 1 of Section 1.3 in Chapter 1. The linewidth required for 100 m within optical fiber requires a much narrower linewidth of 649.6 kHz. The linewidth of the laser needs to be

reduced by approximately 100 times to meet the 100 m goal outlined in Table 8.

5.2 Ranging with Insight Laser

In summary of the ranging with interference fringes experiment in Chapter 4, the Insight VT-DBR akinetic laser was put through a series of ranging tests with different path length differences of an interferometer in order to obtain interference fringes from which path length can be calculated. This was done to investigate the coherence lengths as was proposed by the linewidth experiment in Chapter 3, but was also to get an initial idea of how well the laser may work in terms of ranging. In order to capture the interference fringes of varying lengths, the laser was placed into swept wavelength mode across the the range of 1522.13 to 1566.18 nm. The interference fringes were extracted using a homemade Mach-Zehnder interferometer with interchangeable path length differences around the coherence length of the laser as was found in Chapter 4. The largest path length difference in this experiment in which a frequency of the interference fringes was discernible in the frequency spectrum was at a ruler measured path length difference of 130.5 cm which is very close to the max coherence length found in the linewidth experiment of 129.92 cm.

It was found that the interference fringes in this experiment was not very accurate in terms of larger path length differences. At a small ruler measured path length difference of < 1 cm (no observable measurable path length difference), the interference fringes indicated an experimental path length difference of 1.075 cm which is approximately 1 cm off from the ruler measured. However, as the ruler measured path length difference increases, the difference between the ruler measured and experimental increased as well. For example, at a ruler measured path length difference of 130.5 cm, the interference fringes indicated an experimental path length difference of 209.7 cm. This can be observed in Table 9, along with the rest of the path length differences tested.

Table 9 – The increase in error as the ruler measured path length ΔL difference increases.

Ruler Measured ΔL	Experimental ΔL
$< 1\ cm$	$1.075\ cm$
$\approx 1\ cm$	$3.145\ cm$
$\approx 11.5\ cm$	$17.66\ cm$
$\approx 22.5\ cm$	$36.4\ cm$
$\approx 34\ cm$	$54.8\ cm$
$\approx 56.5\ cm$	$87.7\ cm$

$\approx 119\ cm$	$191.3\ cm$
$\approx 130.5\ cm$	$209.7\ cm$
$\approx 187.5\ cm$	N/A

A visual representation of the error between the ruler measured path lengths and experimental path lengths can be seen in Figure 5-3.
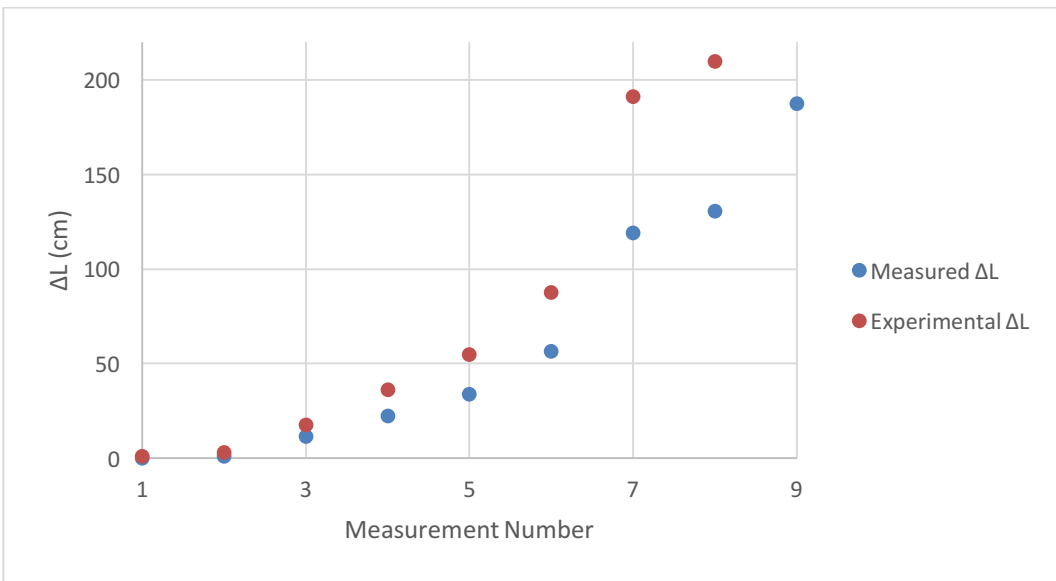
Figure 5-3 – Difference between the ruler measured path length differences and experimental path length differences as the ruler measured path length difference increases from Measurement Number 1 to 9.

Figure 5-3 suggests that the error between the ruler measured and experimental path length differences is increasing on a sort of exponential scale. If a mathematical model for the error can be found, it can be

used to compensate for the error found in ranging via interference fringes, making it much more accurate.

5.3. Future Work

This thesis was able to provide an initial investigation into the the possibility of the Insight VT-DBR akinetic laser source used for ranging, and the laser shows promise. Nonetheless, there is still much investigation that needs to be done.

First, although the linewidth characterization done in Chapter 3 gives one an idea of how the linewidth varies over the laser sweep range in 1 nm increments, it would not be unwise to take even more data points. For example, although the linewidth experiment captured a minimum linewidth of 50 MHz, there may be another wavelength output that provides an even narrower linewidth located between the 1 nm increments. Theoretically, within the range of the laser of 1522.13 and 1566.18 there are an infinite number of points that can be taken. As such, in order to make the data taking simpler on the user and more efficient, one might look into the possibility of implementing an automated system, whether it be by LabVIEW or another program. This would allow one to set up the delayed self-homodyne test and simply plug in the laser to the input of the test set up and take the output of the test setup into

a spectrum analyzer, and step through a smaller increment of waveforms to capture many more points in between the minimum and maximum wavelengths of the laser. Taking more linewidth data points and capturing the laser currents associated with these data points would allow a user to further define the range of the currents across the sweep that lead to good linewidths as was attempted in Chapter 3 with fewer linewidths.

Further work regarding linewidth, would be to find a method by which one can minimize the linewidth of the laser. With the current linewidths of the laser, the maximum coherence length is around 130 cm. In order for this sensor to be applicable to most systems, a range of 100 meters would be ideal. Beginning with the areas of lower linewidth to maximize effectiveness, one may want to implement a system similar to a phase-locked loop to minimize phase jumps thus allowing the linewidth to be narrower and the coherence length to be longer.

Second, although the interference fringe ranging test done in Chapter 4 was an initial investigation and was able to provide an idea of how the tunable laser would measure distance, there is much more that needs to be added on to this experiment to confidently come to the conclusion that

this laser would be successful in real world ranging applications.

The first area that needs to be investigated for ranging is to find out why the path length difference indicated by the interference fringes is not accurate to the ruler measured path length difference and how it can be fixed. What would really help in this aspect is also to take more data points to investigate if there is a mathematical relationship of the errors between the ruler measured and experimental. An off the shelf variable length interferometer would be extremely helpful in this case due to the fact that in the interferometer made in Chapter 4, one would have to be extremely careful with lengths due to the unpredictable lengths inherent in the process of fusion splicing, not to mention that it takes a very long time to make the variable lengths to be inserted into the interferometer of Chapter 4. If a mathematical model of the error can be found, the errors can be removed for agreement between the ruler measured and experimental path length differences.

The second area that needs to be done for ranging is for it to be done in air rather than in optical fiber as was the case in this thesis. Although for initial investigation optical fiber was used, the end goal is to

make this ranging possible in the open. This would bring in a variety of different factors into play such as scattering.

The third area to be investigated is how well the laser is able to perform ranging when the object is moving. In this thesis, the experiments were done with a constant path length difference, but it is necessary to investigate how the laser performs with a changing path length difference and see if it can detect the rate of change. This would be followed by an in the open test (not in optical fiber) with a moving object and analysis of if the laser can not only detect the object and how far it is away, but also how fast the object is moving. This would being in a variety of different factors into play such as the Doppler Effect.

BIBLIOGRAPHY

i[1]   "Journey — Waymo." *Waymo*. N.p., n.d. Web. 14 Oct. 2017.
 aaa   <https://waymo.com/journey/>.

 [2]   Alex Davies, "We Take a Ride in the Self-Driving Uber Now
       Roaming Pittsburgh." *Wired*. Conde Nast, 14 Sept. 2016.
       Web. 4 Jan. 2017. <https://www.wired.com/2016/09/self-
       driving-autonomous-uber-pittsburgh/>.

 [3]   Fred Lambert, "Tesla Announces All Production Cars Now
       Have Fully Self-driving Hardware." *Electrek*. N.p., 19 Oct.
       2016. Web. 7 Jan. 2017.
       <https://electrek.co/2016/10/19/tesla-fully-autonomous-
       self-driving-car/>.

 [4]   Alex Davies, "Turns Out the Hardware in Self-Driving Cars
       Is Pretty Cheap." *Wired*. Conde Nast, 10 May 2017. Web. 11
       May 2017. <https://www.wired.com/2015/04/cost-of-sensors-
       autonomous-cars/>.

 [5]   "Centimeter-accurate GPS for Self-driving Vehicles."
       Articles. N.p., n.d. Web. 24 Jan. 2017.
       <http://articles.sae.org/15067/>.

 [6]   "What Is an Ultrasonic Sensor?" *Ultrasonic Sensor | What
       Is an Ultrasonic Sensor?* N.p., n.d. Web. 23 Jan. 2017.
       <http://education.rec.ri.cmu.edu/content/electronics/boe/u
       ltrasonic_sensor/1.html>.

 [7]   "Odometry Sensors." *Title3.gif*. N.p., n.d. Web. 23 Jan.
       2017. <http://planning.cs.uiuc.edu/node576.html>.

 [8]   *United States Geological Survey*, N.p., n.d. Web. 13 May
       2017. <https://lta.cr.usgs.gov/lidar_digitalelevation>.

 [9]   "Autonomous Cars' Pick: Camera, Radar, Lidar? | EE Times."
       EETimes. N.p., n.d. Web. 30 Jan. 2017.
       <http://www.eetimes.com/author.asp?section_id=36&doc_id=13
       30069>.

[10]   Christian Wolff, *Radar Basics*. N.p., n.d. Web. 2 Feb.
       2017.
       <http://www.radartutorial.eu/02.basics/Frequency%20Modulat
       ed%20Continuous%20Wave%20Radar.en.html>.

[11]   Tobiasotto, "Principle of FMCW Radar." *LinkedIn
       SlideShare*. N.p., 26 July 2012. Web. 14 Feb. 2017.
       <https://www.slideshare.net/tobiasotto/principle-of-fmcw-
       radars>.

[12] *The Universe*, N.p., n.d. Web. 11 May 2017.
      <http://wps.pearsoned.com.au/sf3_2/130/33327/8531808.cw/-
      /8531815/index.html>.

[13] Christian Martens, "Sweep Stability Characterization of a
      Vernier-Tuned Distributed Bragg Reflector (VT-DBR) All-
      Semiconductor Tunable Swept Laser System at 1550 nm for
      Sensing Applications." California Polytechnic State
      University, San Luis Obispo, Thesis 2015.

[14] *Laser Standards and Classifications*. N.p., n.d. Web. 01
      June 2017.
      <https://www.rli.com/resources/articles/classification.asp
      x>.

[15] Jacob Egorov, "Wavelength accuracy study for high-density
      Fiber Bragg grating sensor systems using a Rapidly-Swept
      Akinetic-Laser source." California Polytechnic State
      University, San Luis Obispo, Thesis 2016.

[16] Gregory Bergdoll, "Characterization of two Vernier-Tuned
      Distributed Bragg Reflector (VT-DBR) Lasers used in Swept
      Source Optical Coherence Tomography (SS-OCT)." California
      Polytechnic State University, San Luis Obispo, Thesis
      2015.

[17] Dennis Derickson et al., "SGDBR single-chip wavelength
      tunable lasers for swept source OCT." in
      SPIE Digital Library, San Jose, 2008.

[18] M. Bonesi et al., "Akinetic all-semiconductor programmable
      swept-source at 1550 nm and 1310 nm with centimeters
      coherence length." Optics Express, vol. 22, no. 3, pp.
      2632-2655, 2014.

[19] M.P. Minneman, J. Ensher, M. Crawford, and D. Derickson,
      "All-semiconductor high-speed akinetic swept-source for
      OCT." in Proc. SPIE 8311, Optical Sensors and Biophotonics
      III, 831116 , 2011.

[20] Insight Photonics, "Atlas 3.7.0 User Manual".

[21] Dennis Derickson, "Fiber Optic Test and Measurement."
      Upper Saddle River Prentice-Hall, 1998. Print.

[22] Insight Photonics, [Factory Data].

[23] "Spectral Line Shape." *Wikipedia*. Wikimedia Foundation, 16
      Apr. 2017. Web. 01 June 2017.
      <https://en.wikipedia.org/wiki/Spectral_line_shape>.

APPENDICES

Appendix A. Captured Laser Linewidths

Video BW = 300 Hz
Resolution BW = 300 kHz
$f\ range\ shown = 0 - 1\ GHz$
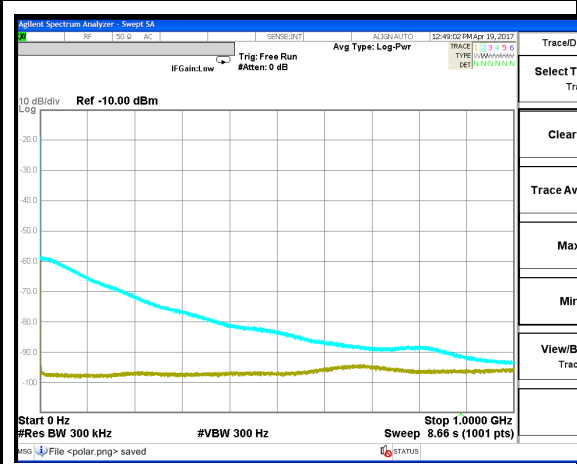
$wl\ = 1523\ nm$
$\Delta v\ = 50\ MHz$
$\tau_c = 6.366\ ns$
$L_c\ =\ 129.92\ cm$
$fm\ = 13016$
$bm\ = 49647$
$phase\ = 11712$
$soa\ =\ 14657$
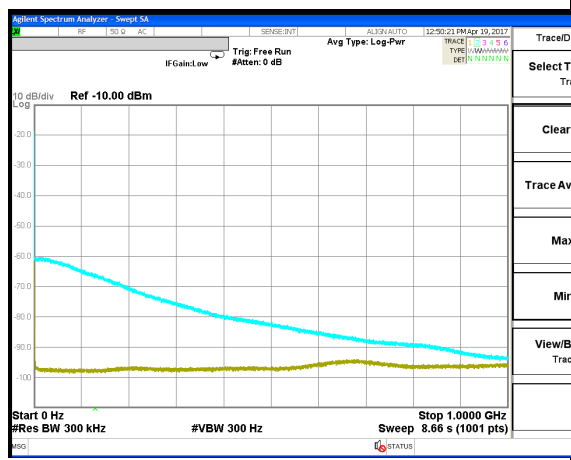
$wl\ = 1524\ nm$
$\Delta v\ =\ 85\ MHz$
$\tau_c\ = 3.745\ ns$
$L_c\ =\ 76.43\ cm$
$fm\ = 8689$
$m\ = 35317$
$phase\ = 10602$
$soa\ =\ 13899$
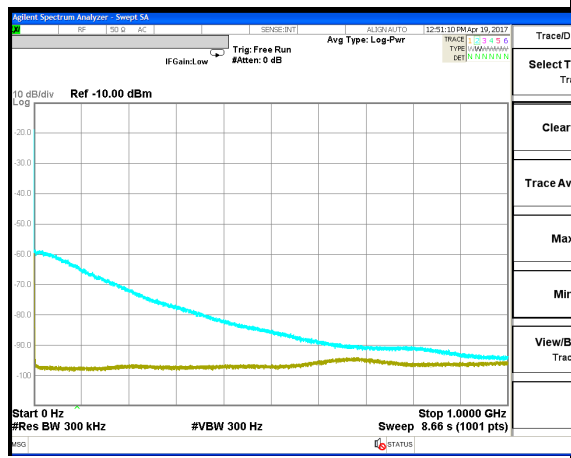
$wl\ = 1525\ nm$
$\Delta v\ = 50\ MHz$
$\tau_c = 6.366\ ns$
$L_c = 129.92\ cm$
$fm\ = 4173$
$bm\ = 22664$
$phase\ = 10276$
$soa\ = 13119$

$$wl \; = 1526 \, nm$$
$$\Delta v \; = \; 100 \, MHz$$
$$\tau_c = 3.183 \, ns$$
$$L_c \; = \; 64.96 \, cm$$
$$fm \; = 43725$$
$$bm \; = 15396$$
$$phase \; = 15538$$
$$soa \; = \; 13821$$
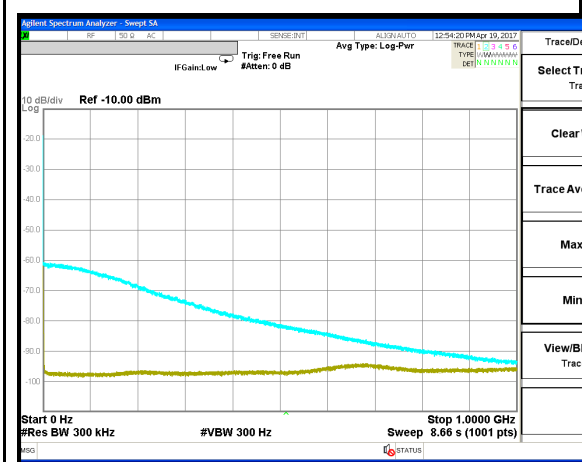
$$wl \; = 1527 \, nm$$
$$\Delta v \; = \; 130 \, MHz$$
$$\tau_c = 2.449 \, ns$$
$$L_c \; = \; 49.98 \, cm$$
$$fm \; = 32425$$
$$bm \; = 8872$$
$$phase \; = 14129$$
$$soa \; = 13233$$
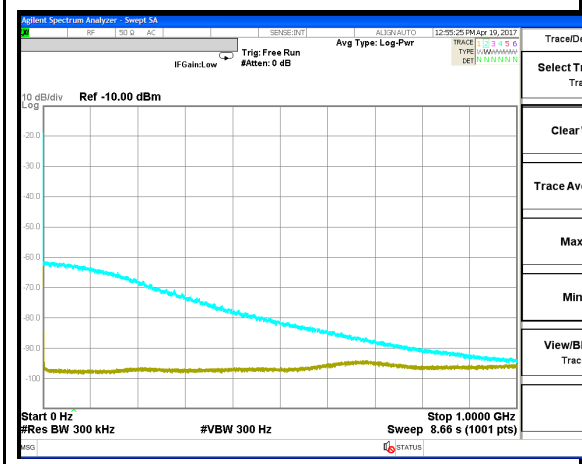
$$wl \; = 1528 \, nm$$
$$\Delta v \; = 125 \, MHz$$
$$\tau_c = 2.546 \, ns$$
$$L_c \; = 51.96 \, cm$$
$$fm \; = 22274$$
$$bm \; = 4265$$
$$phase \; = 13441$$
$$soa \; = 12667$$
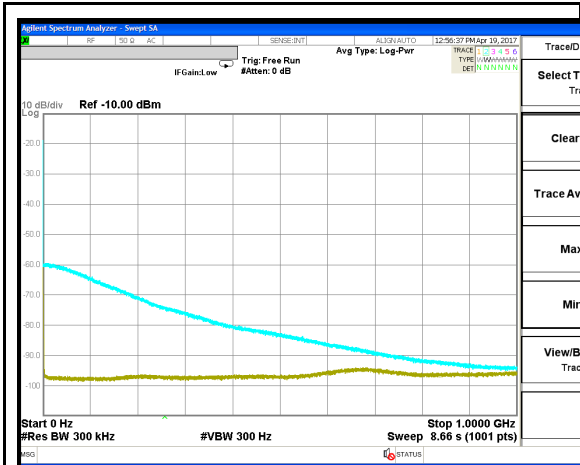
$wl\ = 1529\ nm$
$\Delta v\ =\ 75\ MHz$
$\tau_c\ = 4.244\ ns$
$L_c = 86.61\ cm$
$fm\ = 14717$
$bm\ = 39474$
$phase\ = 8864$
$soa\ = 12563$
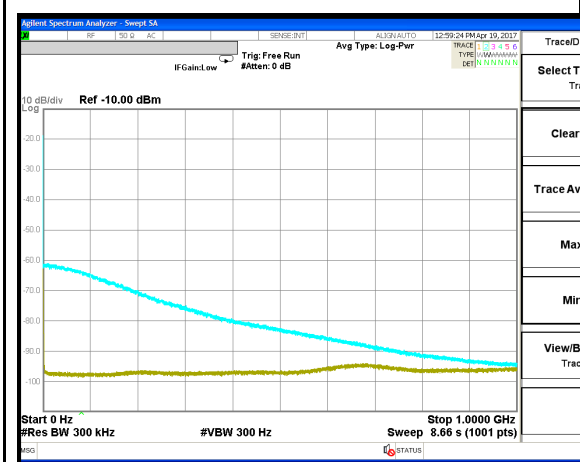
$wl\ = 1530\ nm$
$\Delta v\ =\ 100\ MHz$
$\tau_c\ = 3.183\ ns$
$L_c =\ 64.96\ cm$
$fm\ = 9395$
$bm\ =\ 27618$
$phase\ = 7264$
$soa\ =\ 12136$
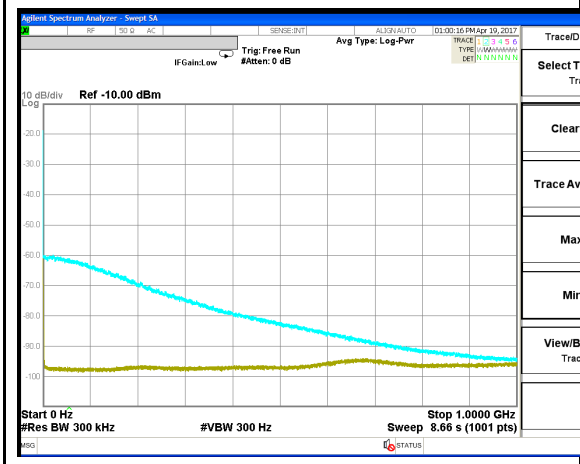
$wl\ = 1531\ nm$
$\Delta v\ = 100\ MHz$
$\tau_c\ = 3.183\ ns$
$L_c =\ 64.96\ cm$
$fm\ = 4898$
$bm\ = 17744$
$phase\ = 6899$
$soa\ =\ 11696$

$wl\ = 1532\ nm$
$\Delta v\ = 140\ MHz$
$\tau_c = 2.274\ ns$
$L_c =\ 46.41\ cm$
$fm\ =\ 2022$
$bm\ =\ 11437$
$phase\ = 5732$
$soa\ =\ 11264$
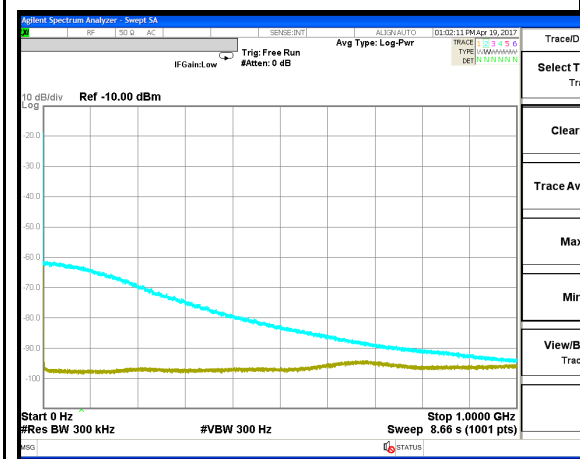
$wl\ = 1533\ nm$
$\Delta v\ = 115\ MHz$
$\tau_c = 2.768\ ns$
$L_c =\ 56.49\ cm$
$fm\ = 33960$
$bm\ =\ 5780$
$phase\ = 31581$
$soa\ =\ 12069$
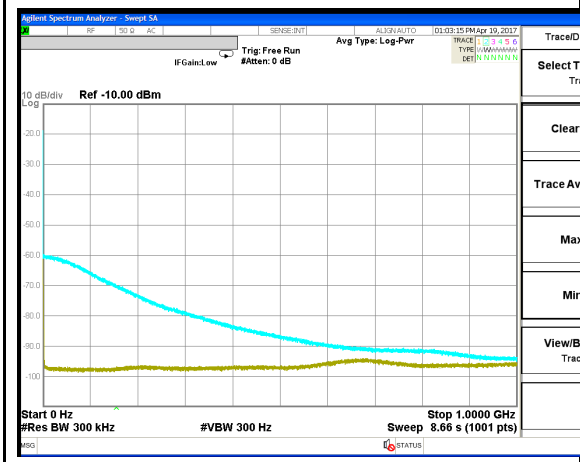
$wl\ = 1534\ nm$
$\Delta v\ = 75\ MHz$
$\tau_c = 4.244\ ns$
$L_c = 86.61\ cm$
$fm\ = 22116$
$bm\ = 45904$
$phase\ = 7610$
$soa\ = 11932$
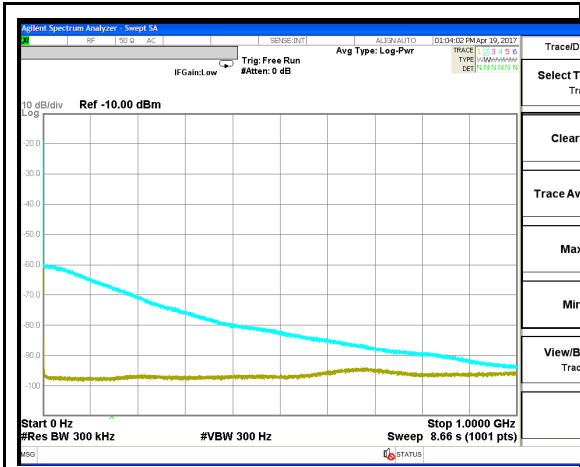
$wl\ = 1535\ nm$
$\Delta v\ = 80\ MHz$
$\tau_c = 3.979\ ns$
$L_c = 81.2\ cm$
$fm\ = 15742$
$bm\ = 32907$
$phase\ = 46252$
$soa\ = 11924$
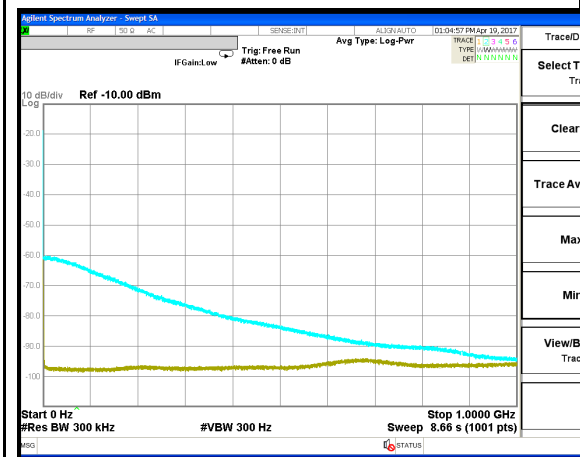
$wl\ = 1536\ nm$
$\Delta v\ = 80\ MHz$
$\tau_c = 3.979\ ns$
$L_c =\ 81.2\ cm$
$fm\ = 9897$
$bm\ = 21193$
$phase\ = 18251$
$soa\ = 11359$
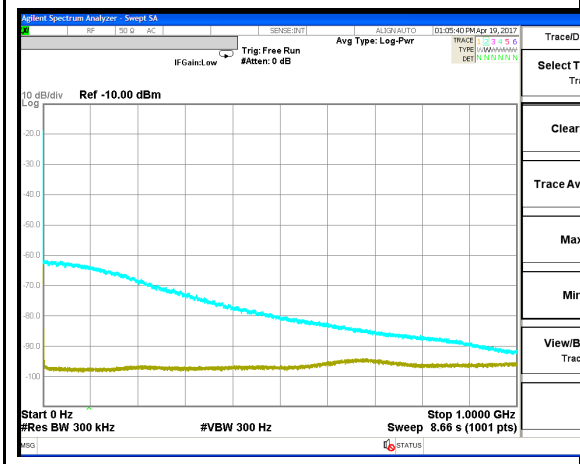
$wl\ = 1537\ nm$
$\Delta v\ = 150\ MHz$
$\tau_c = 2.122\ ns$
$L_c = 43.31\ cm$
$fm\ = 6108$
$bm\ = 14066$
$phase\ = 14583$
$soa\ = 10958$
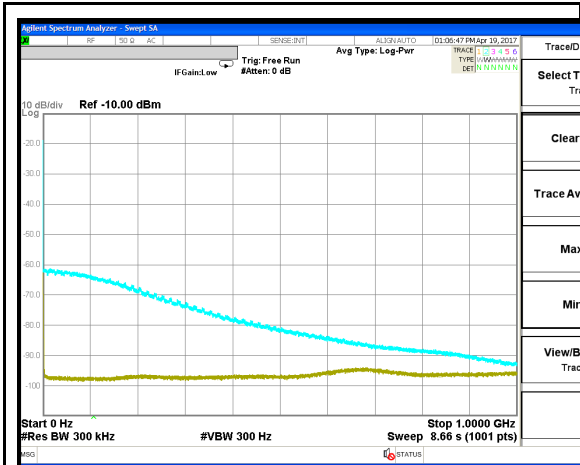
$wl\ = 1538\ nm$
$\Delta v\ = 125\ MHz$
$\tau_c = 2.546\ ns$
$L_c = 51.96\ cm$
$fm\ = 2299$
$bm\ = 7220$
$phase\ = 15071$
$soa\ = 10569$
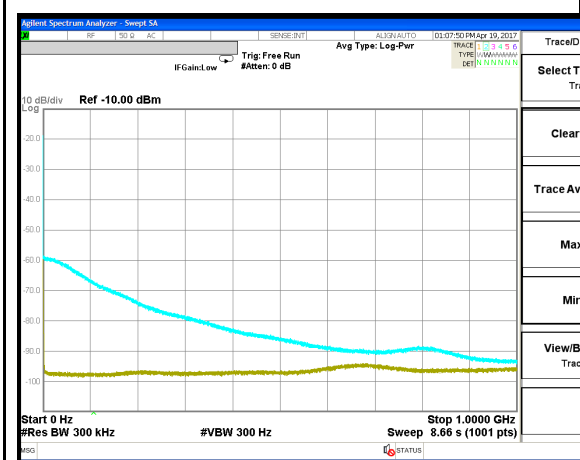
$wl\ = 1539\ nm$
$\Delta v\ = 50\ MHz$
$\tau_c = 6.366\ ns$
$L_c = 129.92\ cm$
$fm\ = 34746$
$bm\ = 53504$
$phase\ = 16493$
$soa\ = 11849$
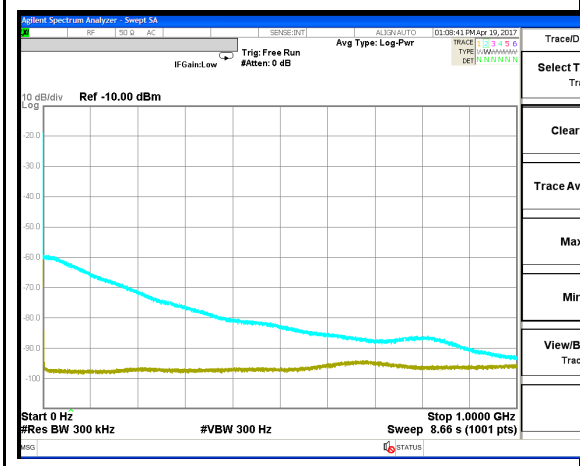
$wl\ = 1540\ nm$
$\Delta v\ = 55\ MHz$
$\tau_c = 5.787\ ns$
$L_c =\ 118.1\ cm$
$fm\ = 25850$
$bm\ = 39301$
$phase\ = 14324$
$soa\ = 11456$
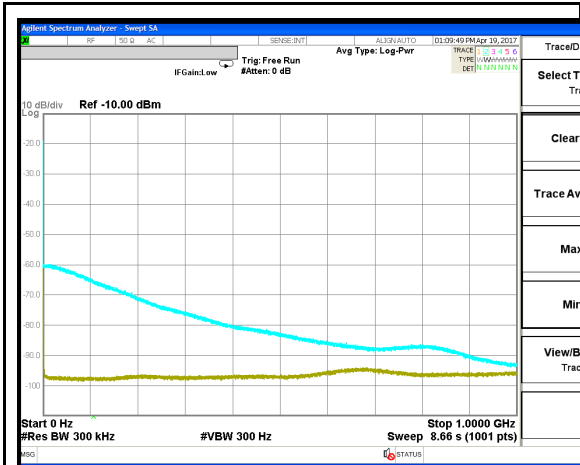
$$wl \ = 1541 \ nm$$
$$\Delta v \ = \ 80 \ MHz$$
$$\tau_c = 3.979 \ ns$$
$$L_c \ = \ 81.2 \ cm$$
$$fm \ = 17602$$
$$bm \ = 26305$$
$$phase \ = 14758$$
$$soa \ = 11035$$
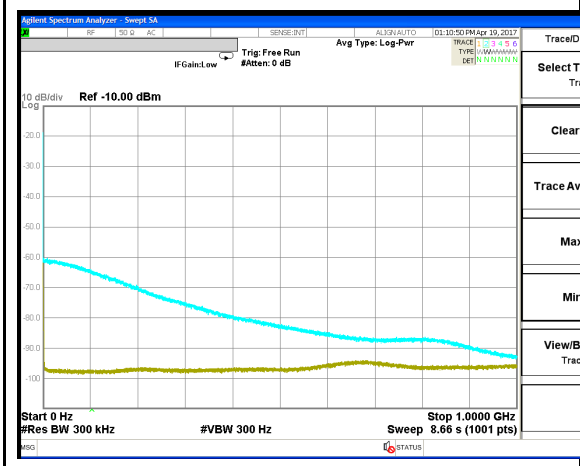
$$wl \ = 1542 \ nm$$
$$\Delta v \ = 90 \ MHz$$
$$\tau_c = 3.537 \ ns$$
$$L_c \ = 72.18 \ cm$$
$$fm \ = 11316$$
$$bm \ = 17043$$
$$phase \ = 14503$$
$$soa \ = 10686$$
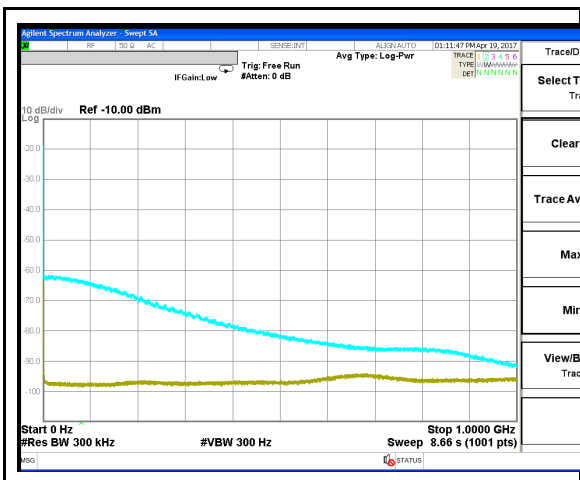
$$wl \ = 1543 \ nm$$
$$\Delta v \ = 115 \ MHz$$
$$\tau_c = 2.768 \ ns$$
$$L_c = 56.49 \ cm$$
$$fm \ = 6339$$
$$bm \ = 9848$$
$$phase \ = 11499$$
$$soa \ = 10282$$
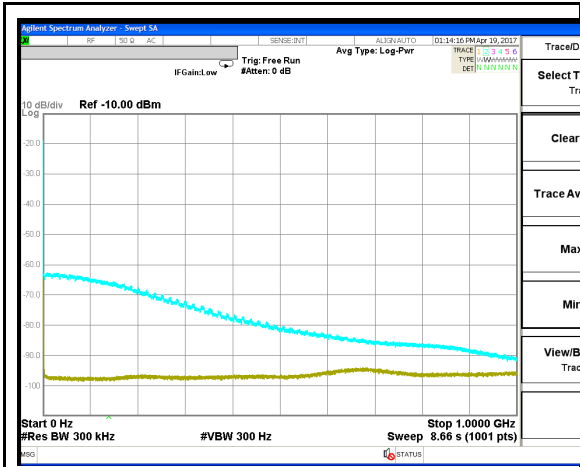
$$wl \ = 1544\ nm$$
$$\Delta v \ = 140\ MHz$$
$$\tau_c = 2.274\ ns$$
$$L_c = \ 46.41\ cm$$
$$fm \ = 2834$$
$$bm \ = 4711$$
$$phase \ = 10339$$
$$soa \ = 9849$$
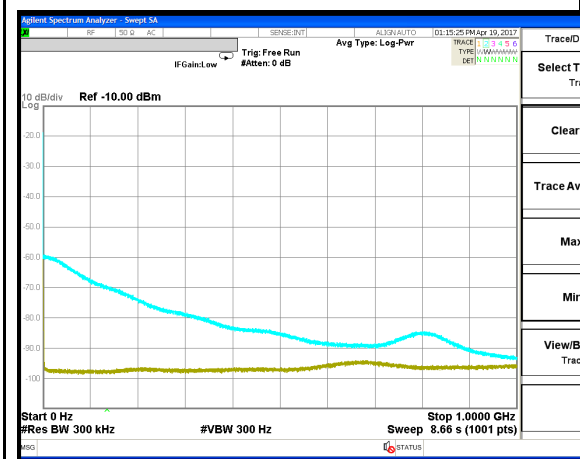
$$wl \ = 1545\ nm$$
$$\Delta v \ = 50\ MHz$$
$$\tau_c = 6.366\ ns$$
$$L_c = 129.92\ cm$$
$$fm \ = 39503$$
$$bm \ = 46982$$
$$phase \ = 12729$$
$$soa \ = 11218$$
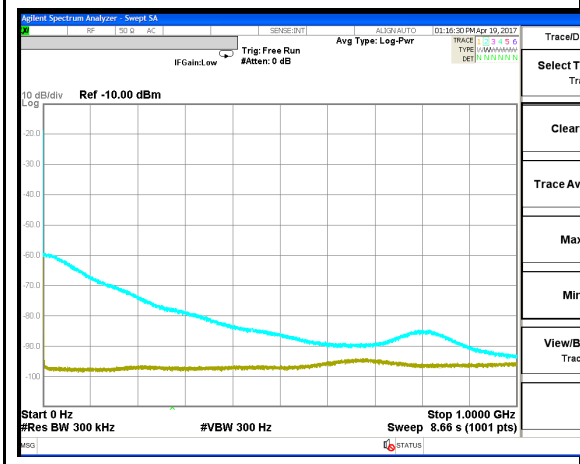
$$wl \ = 1546\ nm$$
$$\Delta v \ = 50\ MHz$$
$$\tau_c = 6.366\ ns$$
$$L_c = 129.92\ cm$$
$$fm \ = 27048$$
$$bm \ = 31647$$
$$phase \ = 13278$$
$$soa \ = 10796$$

$wl\ = 1547\ nm$
$\Delta v\ =\ 80\ MHz$
$\tau_c = 3.979\ ns$
$L_c = 81.2\ cm$
$fm\ = 19605$
$bm\ = 22286$
$phase\ = 29276$
$soa\ = 10577$
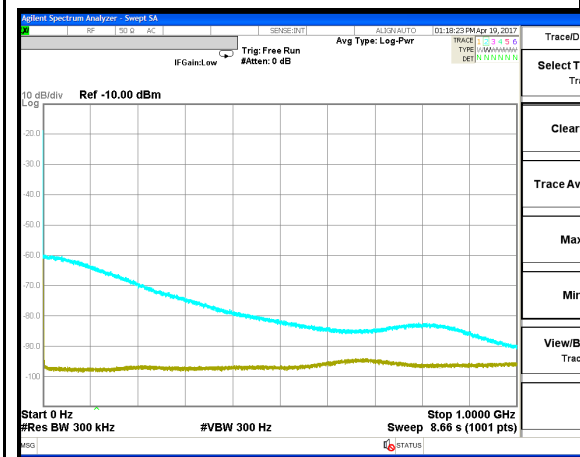
$wl\ = 1548\ nm$
$\Delta v\ = 100\ MHz$
$\tau_c = 3.183\ ns$
$L_c =\ 64.96\ cm$
$fm\ = 11883$
$bm\ = 13593$
$phase\ = 31370$
$soa\ = 10600$
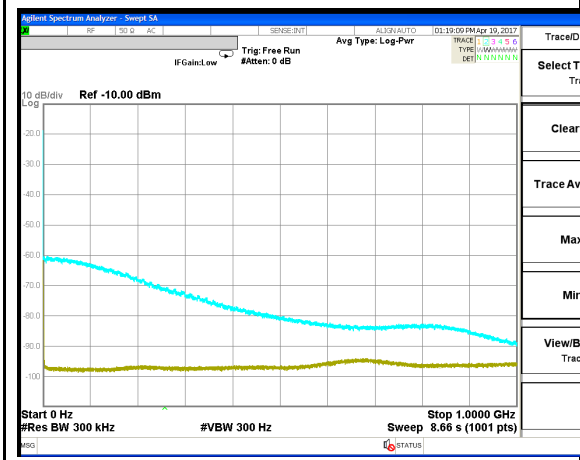
$wl\ = 1549\ nm$
$\Delta v\ = 145\ MHz$
$\tau_c = 2.195\ ns$
$L_c = 44.8\ cm$
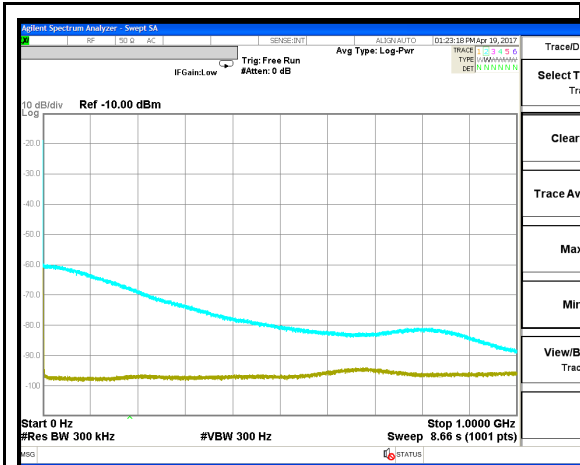$fm\ = 7220$
$bm\ = 7629$
$phase\ = 31801$
$soa\ = 10086$
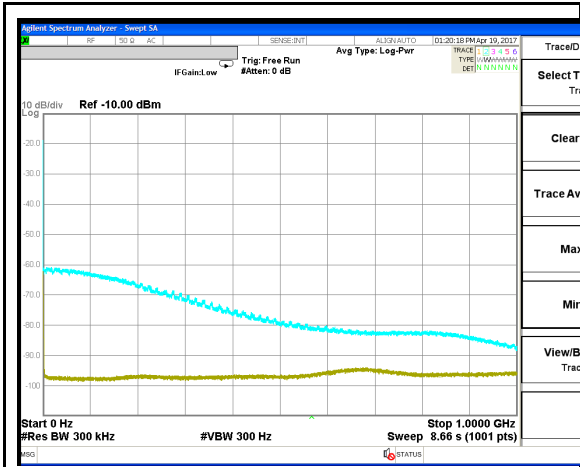
$wl\ = 1550\ nm$
$\Delta v\ = 145\ MHz$
$\tau_c = 2.195\ ns$
$L_c = 44.8\ cm$
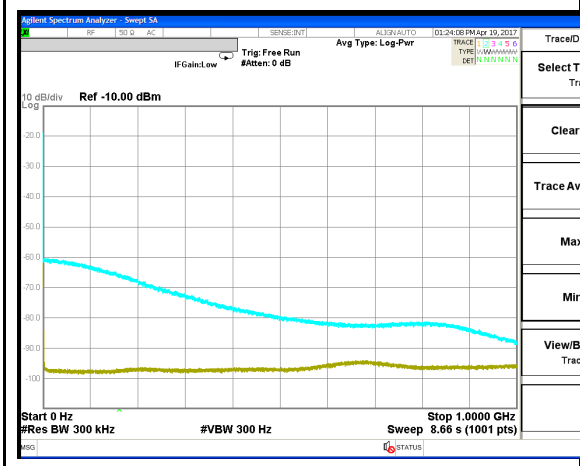$fm\ = 3377$
$bm\ = 3213$
$phase\ = 29276$
$soa\ = 10050$
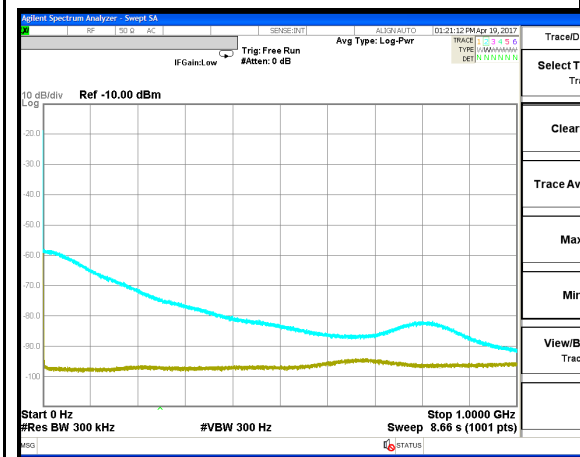
$wl\ = 1551\ nm$
$\Delta v\ = 60\ MHz$
$\tau_c = 5.305\ ns$
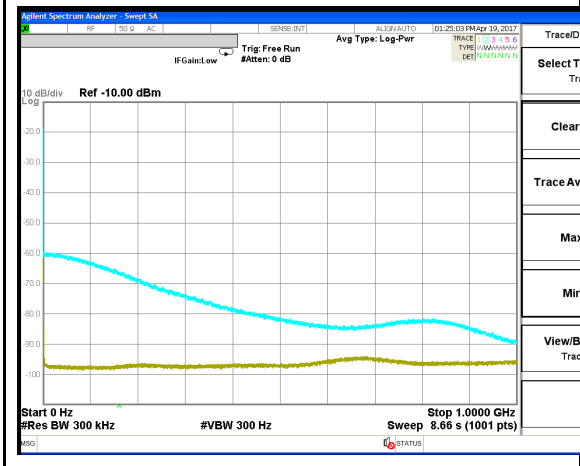$L_c =\ 108.27\ cm$
$fm\ = 45088$
$bm\ = 39538$
$phase\ = 9810$
$soa\ = 10567$
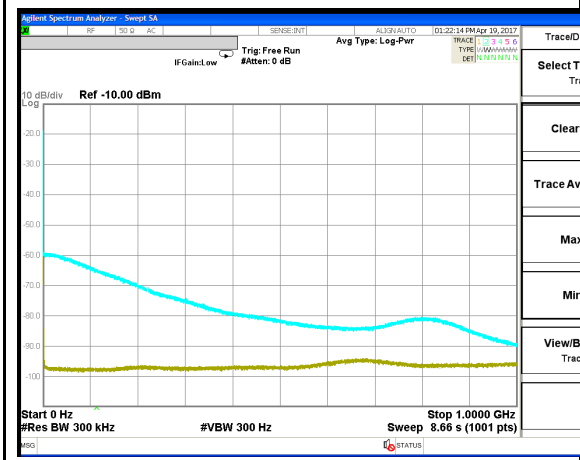
$wl\ = 1552\ nm$
$\Delta v\ = 80\ MHz$
$\tau_c = 3.979\ ns$
$L_c = 81.2\ cm$
$fm\ = 33830$
$bm\ = 28172$
$phase\ = 56822$
$soa\ = 10443$

$$wl\ = 1553\ nm$$
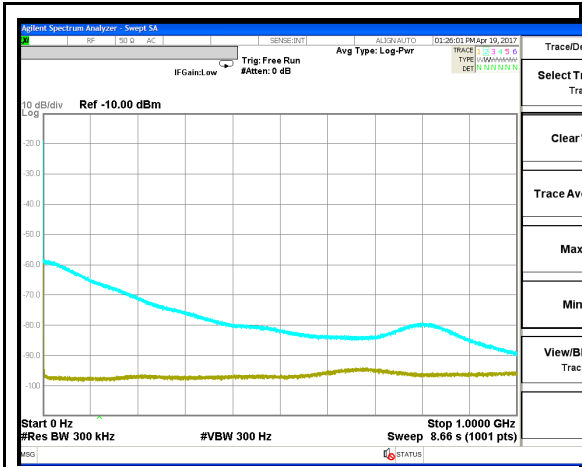$$\varDelta v\ = 100\ MHz$$
$$\tau_c = 3.183\ ns$$
$$L_c = 64.96\ cm$$
$$fm\ = 23726$$
$$bm\ = 18353$$
$$phase\ = 8944$$
$$soa\ = 9608$$

$$wl\ = 1554\ nm$$
$$\varDelta v\ = 115\ MHz$$
$$\tau_c = 2.768\ ns$$
$$L_c =\ 56.49\ cm$$
$$fm\ = 15857$$
$$bm\ = 11153$$
$$phase\ = 9362$$
$$soa\ = 9316$$

$$wl\ = 1555\ nm$$
$$\varDelta v\ = 110\ MHz$$
$$\tau_c = 2.894\ ns$$
$$L_c =\ 59.06\ cm$$
$$fm\ = 8605$$
$$bm\ = 5001$$
$$phase\ = 11165$$
$$soa\ = 8910$$

Panel 1

Agilent Spectrum Analyzer - Swept SA
SENSE:INT   AL3GN AUTO   01:26:01 PM Apr 19, 2017
RF   50 Ω   AC   Avg Type: Log-Pwr   TRACE 1 2 3 4 5 6   Trace/Det
TYPE W W W W W W
Trig: Free Run   DET N N N N N N   Select Trace
IFGain:Low   #Atten: 0 dB   Trace

10 dB/div   Ref -10.00 dBm   Clear W
Log

-20.0

-30.0   Trace Aver

-40.0

-50.0   Max H

-60.0

-70.0   Min H

-80.0

-90.0   View/Blar
Trace
-100

M
1
Start 0 Hz   Stop 1.0000 GHz
#Res BW 300 kHz   #VBW 300 Hz   Sweep 8.66 s (1001 pts)
MSG   STATUS

$$wl = 1557\,nm$$
$$\Delta v = 65\,MHz$$
$$\tau_c = 4.897\,ns$$
$$L_c = 99.94\,cm$$
$$fm = 52534$$
$$bm = 35049$$
$$phase = 16698$$
$$soa = 10696$$

Panel 2

Agilent Spectrum Analyzer - Swept SA
SENSE:INT   AL3GN AUTO   01:27:00 PM Apr 19, 2017
RF   50 Ω   AC   Avg Type: Log-Pwr   TRACE 1 2 3 4 5 6   Trace/Det
TYPE W W W W W W
Trig: Free Run   DET N N N N N N   Select Trace
IFGain:Low   #Atten: 0 dB   Trace

10 dB/div   Ref -10.00 dBm   Clear W
Log

-20.0

-30.0   Trace Aver

-40.0

-50.0   Max H

-60.0

-70.0   Min H

-80.0

-90.0   View/Blar
Trace
-100

M
1
Start 0 Hz   Stop 1.0000 GHz
#Res BW 300 kHz   #VBW 300 Hz   Sweep 8.66 s (1001 pts)
MSG   STATUS

$$wl = 1558\,nm$$
$$\Delta v = 95\,MHz$$
$$\tau_c = 3.351\,ns$$
$$L_c = 68.39\,cm$$
$$fm = 38973$$
$$bm = 24404$$
$$phase = 16472$$
$$soa = 10277$$

Panel 3

Agilent Spectrum Analyzer - Swept SA
SENSE:INT   AL3GN AUTO   01:28:00 PM Apr 19, 2017
RF   50 Ω   AC   Avg Type: Log-Pwr   TRACE 1 2 3 4 5 6   Trace/Det
TYPE W W W W W W
Trig: Free Run   DET N N N N N N   Select Trace
IFGain:Low   #Atten: 0 dB   Trace

10 dB/div   Ref -10.00 dBm   Clear W
Log

-20.0

-30.0   Trace Aver

-40.0

-50.0   Max H

-60.0

-70.0   Min H

-80.0

-90.0   View/Blar
Trace
-100

M
1
Start 0 Hz   Stop 1.0000 GHz
#Res BW 300 kHz   #VBW 300 Hz   Sweep 8.66 s (1001 pts)
MSG   STATUS

$$wl = 1559\,nm$$
$$\Delta v = 95\,MHz$$
$$\tau_c = 3.351\,ns$$
$$L_c = 68.39\,cm$$
$$fm = 27077$$
$$bm = 15359$$
$$phase = 21790$$
$$soa = 9822$$
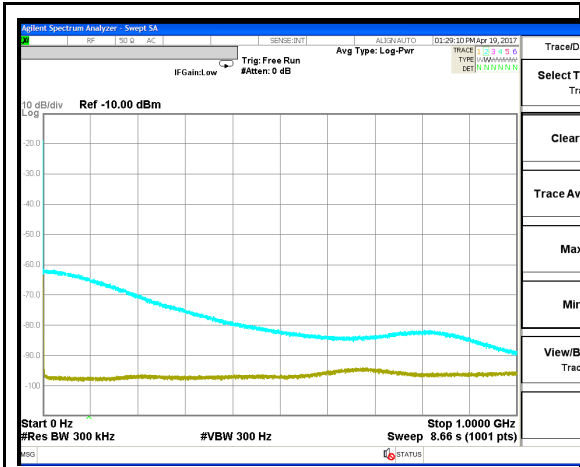
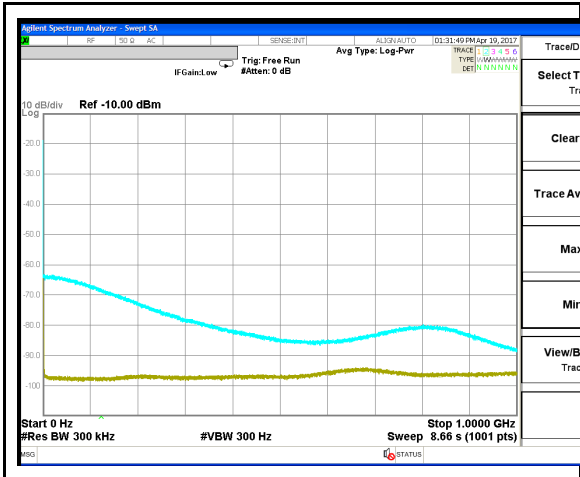$$wl = 1560\ nm$$
$$\Delta v = 95\ MHz$$
$$\tau_c = 3.351\ ns$$
$$L_c = 68.39\ cm$$
$$fm = 17764$$
$$bm = 8494$$
$$phase = 28083$$
$$soa = 9495$$
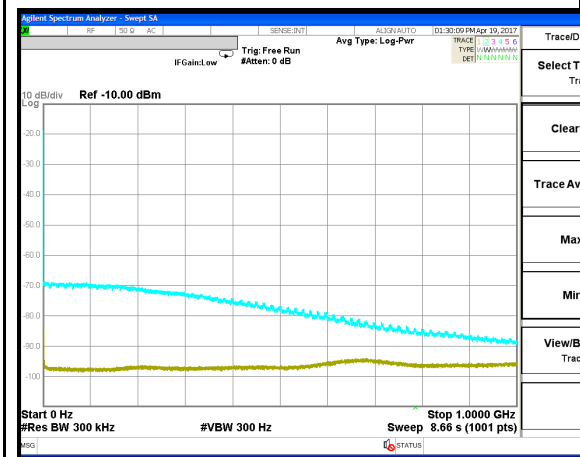
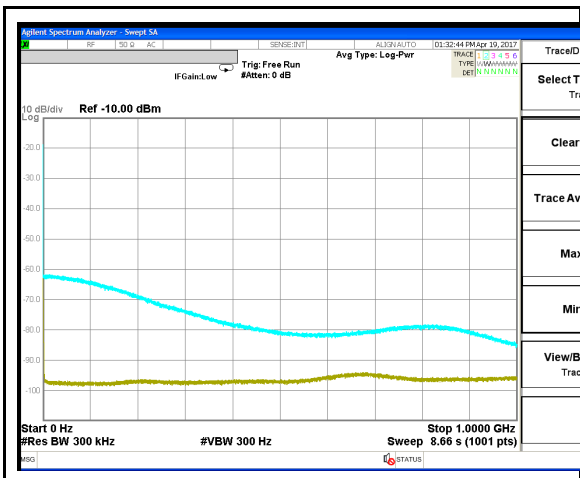$$wl = 1562\ nm$$
$$\Delta v = 300\ MHz$$
$$\tau_c = 1.061\ ns$$
$$L_c = 21.65\ cm$$
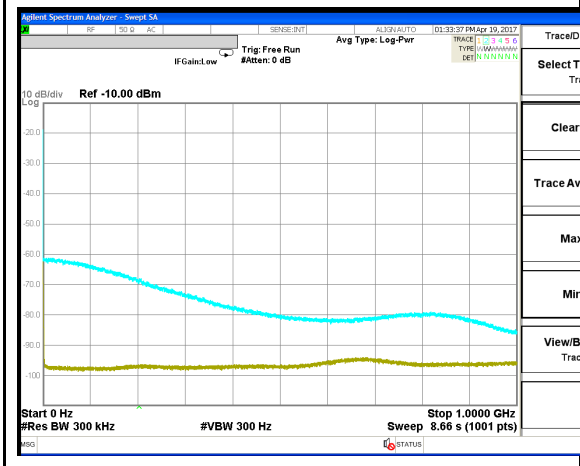$$fm = 6572$$
$$bm = 47277$$
$$phase = 11626$$
$$soa = 9787$$
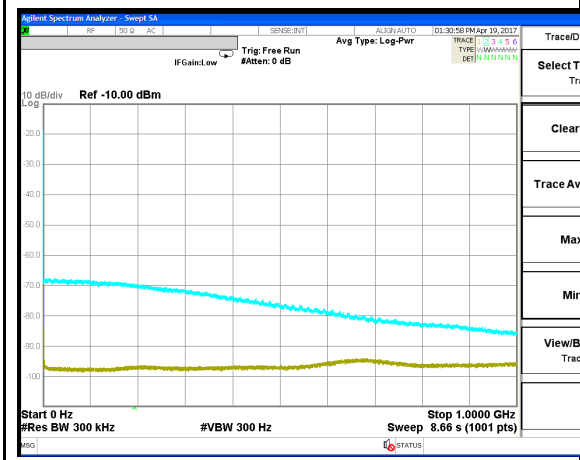
$$wl = 1563\ nm$$
$$\Delta v = 290\ MHz$$
$$\tau_c = 1.098\ ns$$
$$L_c = 22.41\ cm$$
$$fm = 2715$$
$$bm = 31196$$
$$phase = 15063$$
$$soa = 9736$$

$$wl\ = 1564\ nm$$
$$\Delta v\ = 100\ MHz$$
$$\tau_c = 3.183\ ns$$
$$L_c = 64.96\ cm$$
$$fm\ = 39771$$
$$bm\ = 21950$$
$$phase\ = 19923$$
$$soa\ = 10987$$

$$wl\ = 1565\ nm$$
$$\Delta v\ = 125\ MHz$$
$$\tau_c = 2.546\ ns$$
$$L_c = 51.96\ cm$$
$$fm\ = 29805$$
$$bm\ = 13905$$
$$phase\ = 19948$$
$$soa\ = 10630$$

$$wl\ = 1566\ nm$$
$$\Delta v\ = 120\ MHz$$
$$\tau_c = 2.653\ ns$$
$$L_c = 54.14\ cm$$
$$fm\ = 20252$$
$$bm\ = 6830$$
$$phase\ = 21046$$
$$soa\ = 10240$$

Appendix B. Laser Lineshapes

Laser Wavelength	Experimental Laser Lineshape	Lorentzian Laser Lineshape
$1523\ nm$	$\Delta v = 50\ MHz$ $\Delta v_{10dB} = 160\ MHz$ $\Delta v_{20dB} = 350\ MHz$ $\Delta v_{30dB} = 700\ MHz$	$\Delta v = 50\ MHz$ $\Delta v_{10dB} = 150\ MHz$ $\Delta v_{20dB} = 497.5\ MHz$ $\Delta v_{30dB} = 1580\ MHz$
$1524\ nm$	$\Delta v = 85\ MHz$ $\Delta v_{10dB} = 200\ MHz$ $\Delta v_{20dB} = 400\ MHz$ $\Delta v_{30dB} = 850\ MHz$	$\Delta v = 85\ MHz$ $\Delta v_{10dB} = 255\ MHz$ $\Delta v_{20dB} = 845.7\ MHz$ $\Delta v_{30dB} = 2687\ MHz$
$1525\ nm$	$\Delta v = 50\ MHz$ $\Delta v_{10dB} = 169\ MHz$ $\Delta v_{20dB} = 335\ MHz$ $\Delta v_{30dB} = 600\ MHz$	$\Delta v = 50\ MHz$ $\Delta v_{10dB} = 150\ MHz$ $\Delta v_{20dB} = 497.5\ MHz$ $\Delta v_{30dB} = 1580\ MHz$
$1526\ nm$	$\Delta v = 100\ MHz$ $\Delta v_{10dB} = 230\ MHz$ $\Delta v_{20dB} = 470\ MHz$ $\Delta v_{30dB} = 875\ MHz$	$\Delta v = 100\ MHz$ $\Delta v_{10dB} = 300\ MHz$ $\Delta v_{20dB} = 995\ MHz$ $\Delta v_{30dB} = 3161\ MHz$
$1527\ nm$	$\Delta v = 130\ MHz$ $\Delta v_{10dB} = 250\ MHz$ $\Delta v_{20dB} = 490\ MHz$ $\Delta v_{30dB} = 870\ MHz$	$\Delta v = 130\ MHz$ $\Delta v_{10dB} = 390\ MHz$ $\Delta v_{20dB} = 1293.5\ MHz$ $\Delta v_{30dB} = 4109\ MHz$
$1528\ nm$	$\Delta v = 125\ MHz$ $\Delta v_{10dB} = 250\ MHz$ $\Delta v_{20dB} = 500\ MHz$ $\Delta v_{30dB} = 850\ MHz$	$\Delta v = 125\ MHz$ $\Delta v_{10dB} = 375\ MHz$ $\Delta v_{20dB} = 1243.7\ MHz$ $\Delta v_{30dB} = 3951\ MHz$
$1529\ nm$	$\Delta v = 75\ MHz$ $\Delta v_{10dB} = 185\ MHz$ $\Delta v_{20dB} = 380\ MHz$ $\Delta v_{30dB} = 725\ MHz$	$\Delta v = 75\ MHz$ $\Delta v_{10dB} = 225\ MHz$ $\Delta v_{20dB} = 746\ MHz$ $\Delta v_{30dB} = 2370.5\ MHz$
$1530\ nm$	$\Delta v = 100\ MHz$ $\Delta v_{10dB} = 200\ MHz$ $\Delta v_{20dB} = 459\ MHz$ $\Delta v_{30dB} = 825\ MHz$	$\Delta v = 100\ MHz$ $\Delta v_{10dB} = 300\ MHz$ $\Delta v_{20dB} = 995\ MHz$ $\Delta v_{30dB} = 3161\ MHz$
$1531\ nm$	$\Delta v = 100\ MHz$ $\Delta v_{10dB} = 215\ MHz$	$\Delta v = 100\ MHz$ $\Delta v_{10dB} = 300\ MHz$

|		
	$\Delta v_{20dB} = 440\ MHz$ $\Delta v_{30dB} = 750\ MHz$	$\Delta v_{20dB} = 995\ MHz$ $\Delta v_{30dB} = 3161\ MHz$
1532 nm	$\Delta v = 140\ MHz$ $\Delta v_{10dB} = 300\ MHz$ $\Delta v_{20dB} = 530\ MHz$ $\Delta v_{30dB} = 900\ MHz$	$\Delta v = 140\ MHz$ $\Delta v_{10dB} = 420\ MHz$ $\Delta v_{20dB} = 1393\ MHz$ $\Delta v_{30dB} = 4425\ MHz$
1533 nm	$\Delta v = 115\ MHz$ $\Delta v_{10dB} = 230\ MHz$ $\Delta v_{20dB} = 465\ MHz$ $\Delta v_{30dB} = 865\ MHz$	$\Delta v = 115\ MHz$ $\Delta v_{10dB} = 345\ MHz$ $\Delta v_{20dB} = 1144\ MHz$ $\Delta v_{30dB} = 3635\ MHz$
1534 nm	$\Delta v = 75\ MHz$ $\Delta v_{10dB} = 160\ MHz$ $\Delta v_{20dB} = 325\ MHz$ $\Delta v_{30dB} = 640\ MHz$	$\Delta v = 75\ MHz$ $\Delta v_{10dB} = 225\ MHz$ $\Delta v_{20dB} = 746\ MHz$ $\Delta v_{30dB} = 2370.5\ MHz$
1535 nm	$\Delta v = 80\ MHz$ $\Delta v_{10dB} = 195\ MHz$ $\Delta v_{20dB} = 415\ MHz$ $\Delta v_{30dB} = 850\ MHz$	$\Delta v = 80\ MHz$ $\Delta v_{10dB} = 240\ MHz$ $\Delta v_{20dB} = 796\ MHz$ $\Delta v_{30dB} = 2528.6\ MHz$
1536 nm	$\Delta v = 80\ MHz$ $\Delta v_{10dB} = 190\ MHz$ $\Delta v_{20dB} = 400\ MHz$ $\Delta v_{30dB} = 820\ MHz$	$\Delta v = 80\ MHz$ $\Delta v_{10dB} = 240\ MHz$ $\Delta v_{20dB} = 796\ MHz$ $\Delta v_{30dB} = 2528.6\ MHz$
1537 nm	$\Delta v = 150\ MHz$ $\Delta v_{10dB} = 270\ MHz$ $\Delta v_{20dB} = 550\ MHz$ $\Delta v_{30dB} = 1000\ MHz$	$\Delta v = 150\ MHz$ $\Delta v_{10dB} = 450\ MHz$ $\Delta v_{20dB} = 1492.5\ MHz$ $\Delta v_{30dB} = 4741\ MHz$
1538 nm	$\Delta v = 125\ MHz$ $\Delta v_{10dB} = 250\ MHz$ $\Delta v_{20dB} = 515\ MHz$ $\Delta v_{30dB} = 940\ MHz$	$\Delta v = 125\ MHz$ $\Delta v_{10dB} = 375\ MHz$ $\Delta v_{20dB} = 1243.7\ MHz$ $\Delta v_{30dB} = 3951\ MHz$
1539 nm	$\Delta v = 50\ MHz$ $\Delta v_{10dB} = 135\ MHz$ $\Delta v_{20dB} = 310\ MHz$ $\Delta v_{30dB} = 620\ MHz$	$\Delta v = 50\ MHz$ $\Delta v_{10dB} = 150\ MHz$ $\Delta v_{20dB} = 497.5\ MHz$ $\Delta v_{30dB} = 1580\ MHz$
1540 nm	$\Delta v = 55\ MHz$ $\Delta v_{10dB} = 175\ MHz$ $\Delta v_{20dB} = 375\ MHz$ $\Delta v_{30dB} = 890\ MHz$	$\Delta v = 55\ MHz$ $\Delta v_{10dB} = 165\ MHz$ $\Delta v_{20dB} = 796\ MHz$ $\Delta v_{30dB} = 2528.6\ MHz$

1541 nm	$\Delta v = 80\ MHz$ $\Delta v_{10dB} = 190\ MHz$ $\Delta v_{20dB} = 400\ MHz$ $\Delta v_{30dB} = 895\ MHz$	$\Delta v = 80\ MHz$ $\Delta v_{10dB} = 240\ MHz$ $\Delta v_{20dB} = 796\ MHz$ $\Delta v_{30dB} = 2528.6\ MHz$

1542 nm	$\Delta v = 90\ MHz$ $\Delta v_{10dB} = 215\ MHz$ $\Delta v_{20dB} = 440\ MHz$ $\Delta v_{30dB} = 930\ MHz$	$\Delta v = 90\ MHz$ $\Delta v_{10dB} = 270\ MHz$ $\Delta v_{20dB} = 895.5\ MHz$ $\Delta v_{30dB} = 2844.6\ MHz$
1543 nm	$\Delta v = 115\ MHz$ $\Delta v_{10dB} = 250\ MHz$ $\Delta v_{20dB} = 510\ MHz$ $\Delta v_{30dB} = > 1000\ MHz$	$\Delta v = 115\ MHz$ $\Delta v_{10dB} = 345\ MHz$ $\Delta v_{20dB} = 1144\ MHz$ $\Delta v_{30dB} = 3635\ MHz$
1544 nm	$\Delta v = 140\ MHz$ $\Delta v_{10dB} = 315\ MHz$ $\Delta v_{20dB} = 590\ MHz$ $\Delta v_{30dB} = > 1000\ MHz$	$\Delta v = 140\ MHz$ $\Delta v_{10dB} = 420\ MHz$ $\Delta v_{20dB} = 1393\ MHz$ $\Delta v_{30dB} = 4425\ MHz$
1545 nm	$\Delta v = 50\ MHz$ $\Delta v_{10dB} = 130\ MHz$ $\Delta v_{20dB} = 325\ MHz$ $\Delta v_{30dB} = 880\ MHz$	$\Delta v = 50\ MHz$ $\Delta v_{10dB} = 150\ MHz$ $\Delta v_{20dB} = 497.5\ MHz$ $\Delta v_{30dB} = 1580\ MHz$
1546 nm	$\Delta v = 50\ MHz$ $\Delta v_{10dB} = 130\ MHz$ $\Delta v_{20dB} = 320\ MHz$ $\Delta v_{30dB} = 885\ MHz$	$\Delta v = 50\ MHz$ $\Delta v_{10dB} = 150\ MHz$ $\Delta v_{20dB} = 497.5\ MHz$ $\Delta v_{30dB} = 1580\ MHz$
1547 nm	$\Delta v = 80\ MHz$ $\Delta v_{10dB} = 215\ MHz$ $\Delta v_{20dB} = 450\ MHz$ $\Delta v_{30dB} = 1000\ MHz$	$\Delta v = 80\ MHz$ $\Delta v_{10dB} = 240\ MHz$ $\Delta v_{20dB} = 796\ MHz$ $\Delta v_{30dB} = 2528.6\ MHz$
1548 nm	$\Delta v = 100\ MHz$ $\Delta v_{10dB} = 215\ MHz$ $\Delta v_{20dB} = 450\ MHz$ $\Delta v_{30dB} = 1000\ MHz$	$\Delta v = 100\ MHz$ $\Delta v_{10dB} = 300\ MHz$ $\Delta v_{20dB} = 995\ MHz$ $\Delta v_{30dB} = 3160.7\ MHz$
1549 nm	$\Delta v = 145\ MHz$ $\Delta v_{10dB} = 250\ MHz$ $\Delta v_{20dB} = 515\ MHz$ $\Delta v_{30dB} = > 1000\ MHz$	$\Delta v = 145\ MHz$ $\Delta v_{10dB} = 435\ MHz$ $\Delta v_{20dB} = 1442.7\ MHz$ $\Delta v_{30dB} = 4583\ MHz$

1550 nm	$\Delta v = 145\ MHz$ $\Delta v_{10dB} = 310\ MHz$ $\Delta v_{20dB} = 610\ MHz$ $\Delta v_{30dB} => 1000\ MHz$	$\Delta v = 145\ MHz$ $\Delta v_{10dB} = 435\ MHz$ $\Delta v_{20dB} = 1442.7\ MHz$ $\Delta v_{30dB} = 4583\ MHz$
1551 nm	$\Delta v = 60\ MHz$ $\Delta v_{10dB} = 150\ MHz$ $\Delta v_{20dB} = 340\ MHz$ $\Delta v_{30dB} = 920\ MHz$	$\Delta v = 60\ MHz$ $\Delta v_{10dB} = 180\ MHz$ $\Delta v_{20dB} = 597\ MHz$ $\Delta v_{30dB} = 1896.4\ MHz$
1552 nm	$\Delta v = 80\ MHz$ $\Delta v_{10dB} = 185\ MHz$ $\Delta v_{20dB} = 400\ MHz$ $\Delta v_{30dB} = 1000\ MHz$	$\Delta v = 80\ MHz$ $\Delta v_{10dB} = 240\ MHz$ $\Delta v_{20dB} = 796\ MHz$ $\Delta v_{30dB} = 2528.6\ MHz$
1553 nm	$\Delta v = 100\ MHz$ $\Delta v_{10dB} = 220\ MHz$ $\Delta v_{20dB} = 500\ MHz$ $\Delta v_{30dB} => 1000\ MHz$	$\Delta v = 100\ MHz$ $\Delta v_{10dB} = 300\ MHz$ $\Delta v_{20dB} = 995\ MHz$ $\Delta v_{30dB} = 3160.7\ MHz$
1554 nm	$\Delta v = 115\ MHz$ $\Delta v_{10dB} = 250\ MHz$ $\Delta v_{20dB} = 540\ MHz$ $\Delta v_{30dB} => 1000\ MHz$	$\Delta v = 115\ MHz$ $\Delta v_{10dB} = 345\ MHz$ $\Delta v_{20dB} = 1144\ MHz$ $\Delta v_{30dB} = 3635\ MHz$
1555 nm	$\Delta v = 110\ MHz$ $\Delta v_{10dB} = 225\ MHz$ $\Delta v_{20dB} = 450\ MHz$ $\Delta v_{30dB} => 1000\ MHz$	$\Delta v = 110\ MHz$ $\Delta v_{10dB} = 330\ MHz$ $\Delta v_{20dB} = 1094.5\ MHz$ $\Delta v_{30dB} = 3476.8\ MHz$
1557 nm	$\Delta v = 65\ MHz$ $\Delta v_{10dB} = 165\ MHz$ $\Delta v_{20dB} = 365\ MHz$ $\Delta v_{30dB} = 990\ MHz$	$\Delta v = 65\ MHz$ $\Delta v_{10dB} = 195\ MHz$ $\Delta v_{20dB} = 646.7\ MHz$ $\Delta v_{30dB} = 2054.5\ MHz$
1558 nm	$\Delta v = 95\ MHz$ $\Delta v_{10dB} = 215\ MHz$ $\Delta v_{20dB} = 485\ MHz$ $\Delta v_{30dB} => 1000\ MHz$	$\Delta v = 95\ MHz$ $\Delta v_{10dB} = 285\ MHz$ $\Delta v_{20dB} = 945\ MHz$ $\Delta v_{30dB} = 3002.7\ MHz$
1559 nm	$\Delta v = 95\ MHz$ $\Delta v_{10dB} = 225\ MHz$ $\Delta v_{20dB} = 510\ MHz$ $\Delta v_{30dB} => 1000\ MHz$	$\Delta v = 95\ MHz$ $\Delta v_{10dB} = 285\ MHz$ $\Delta v_{20dB} = 945\ MHz$ $\Delta v_{30dB} = 3002.7\ MHz$
1560 nm	$\Delta v = 95\ MHz$ $\Delta v_{10dB} = 230\ MHz$	$\Delta v = 95\ MHz$ $\Delta v_{10dB} = 285\ MHz$

	$\Delta v_{20dB} = 490\ MHz$ $\Delta v_{30dB} => 1000MHz$	$\Delta v_{20dB} = 945\ MHz$ $\Delta v_{30dB} = 3002.7\ MHz$
1562 nm	$\Delta v = 300\ MHz$ $\Delta v_{10dB} = 550\ MHz$ $\Delta v_{20dB} => 1000MHz$ $\Delta v_{30dB} => 1000MHz$	$\Delta v = 300\ MHz$ $\Delta v_{10dB} = 900\ MHz$ $\Delta v_{20dB} = 2985\ MHz$ $\Delta v_{30dB} = 9482\ MHz$
1563 nm	$\Delta v = 290\ MHz$ $\Delta v_{10dB} = 585\ MHz$ $\Delta v_{20dB} => 1000\ MHz$ $\Delta v_{30dB} => 1000\ MHz$	$\Delta v = 290\ MHz$ $\Delta v_{10dB} = 870\ MHz$ $\Delta v_{20dB} = 2885.5\ MHz$ $\Delta v_{30dB} = 9166\ MHz$

1564 nm	$\Delta v = 100\ MHz$ $\Delta v_{10dB} = 230\ MHz$ $\Delta v_{20dB} = 460\ MHz$ $\Delta v_{30dB} => 1000\ MHz$	$\Delta v = 100\ MHz$ $\Delta v_{10dB} = 300\ MHz$ $\Delta v_{20dB} = 995\ MHz$ $\Delta v_{30dB} = 3160.7\ MHz$
1565 nm	$\Delta v = 125\ MHz$ $\Delta v_{10dB} = 260\ MHz$ $\Delta v_{20dB} = 930\ MHz$ $\Delta v_{30dB} => 1000\ MHz$	$\Delta v = 125\ MHz$ $\Delta v_{10dB} = 375\ MHz$ $\Delta v_{20dB} = 1243.7\ MHz$ $\Delta v_{30dB} = 3951\ MHz$
1566 nm	$\Delta v = 120\ MHz$ $\Delta v_{10dB} = 260\ MHz$ $\Delta v_{20dB} = 600\ MHz$ $\Delta v_{30dB} => 1000MHz$	$\Delta v = 120\ MHz$ $\Delta v_{10dB} = 360\ MHz$ $\Delta v_{20dB} = 1194\ MHz$ $\Delta v_{30dB} = 3793\ MHz$
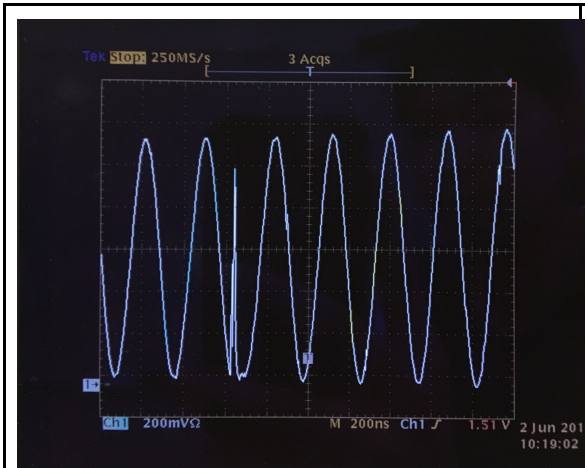
ruler measured $\Delta L = < 1\ cm$

time scale $= 200\ ns/div$
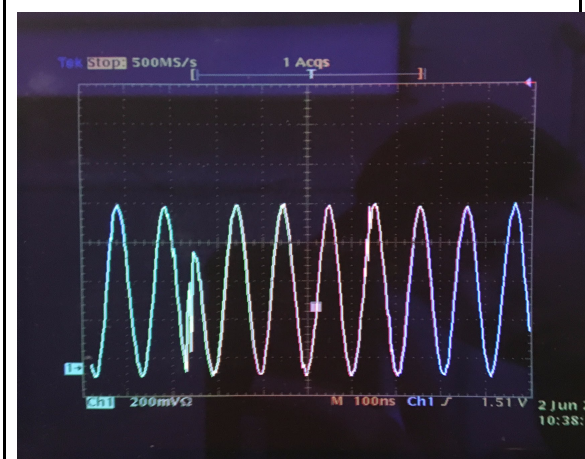
ruler measured $\Delta L \approx 1\ cm$

time scale $= 100\ ns/div$
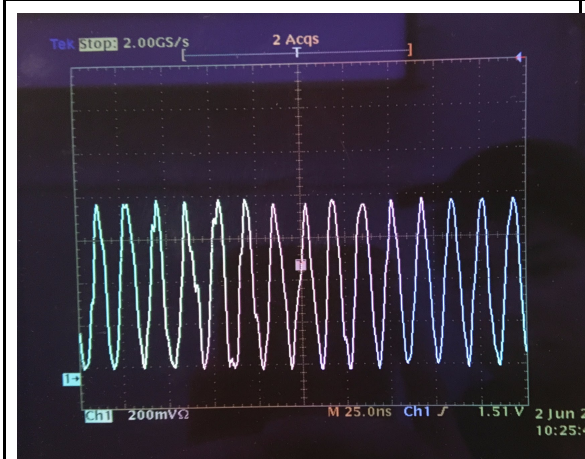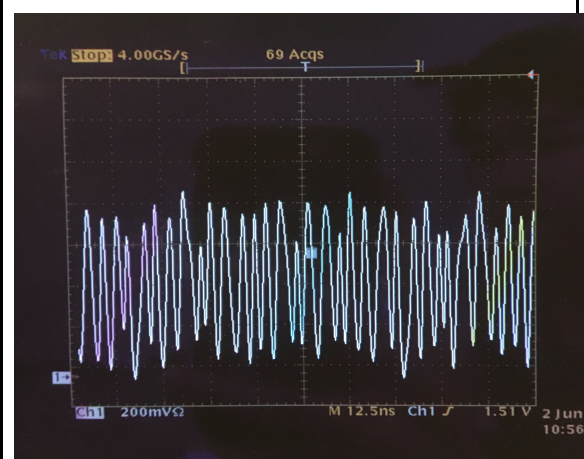

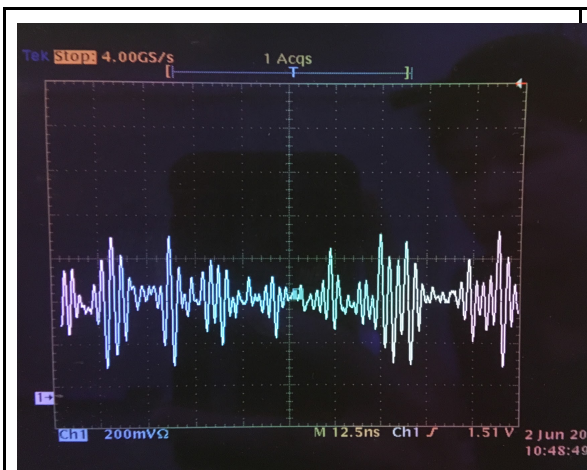*ruler measured* $\Delta L \approx 11.5\ cm$

time scale $= 25\ ns/div$
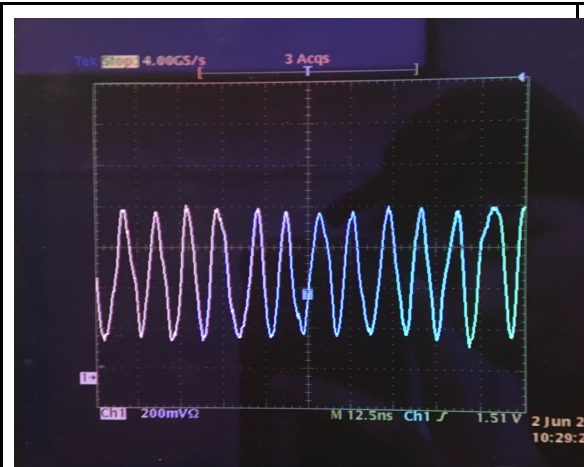
ruler measured $\Delta L \approx 22.5\ cm$

time scale $= 12.5\ ns/div$
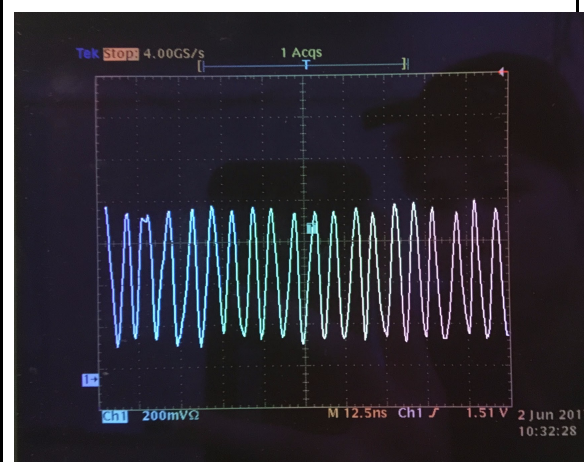
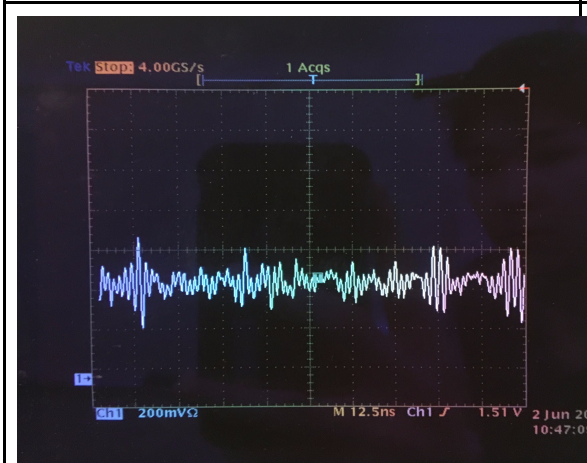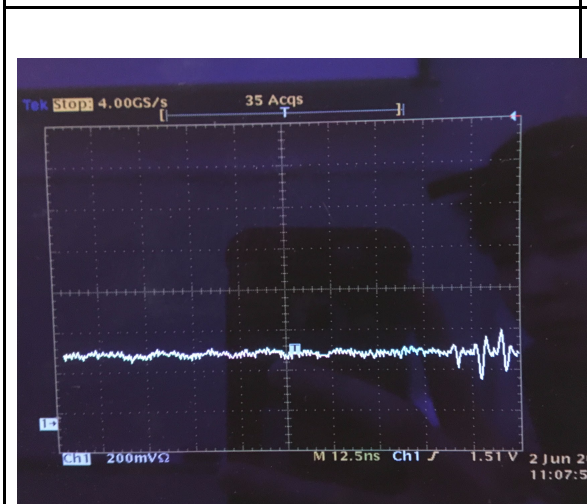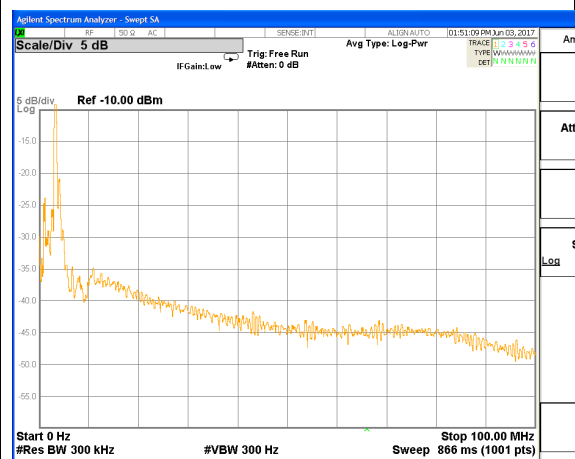*ruler measured* $\Delta L \approx 34\ cm$

time scale $= 12.5\ ns/div$

ruler measured $\Delta L \approx 56.5\ cm$

time scale $= 12.5\ ns/div$

ruler measured $\Delta L \approx 119\ cm$

time scale $= 12.5\ ns/div$

ruler measured $\Delta L \approx 130.5\ cm$

time scale $= 12.5\ ns/div$

ruler measured $\Delta L \approx 187.5\ cm$

time scale $= 12.5\ ns/div$

Appendix D. Frequency Domain Interference Fringes

Video BW = 300 Hz Resolution BW = 300 kHz	
	$ruler\ measured\ \Delta L =\ < 1\ cm$ $f_i = 3.25\ MHz$ $f\ range\ shown = 0 - 100\ MHz$
	$ruler\ measured\ \Delta L \approx 1\ cm$ $f_i = 9.5\ MHz$ $f\ range\ shown = 0 - 100\ MHz$
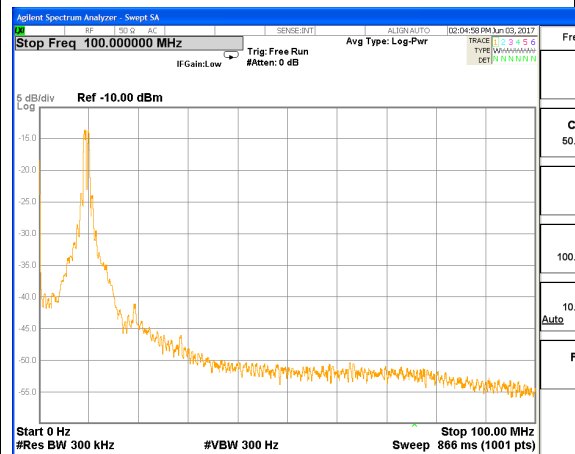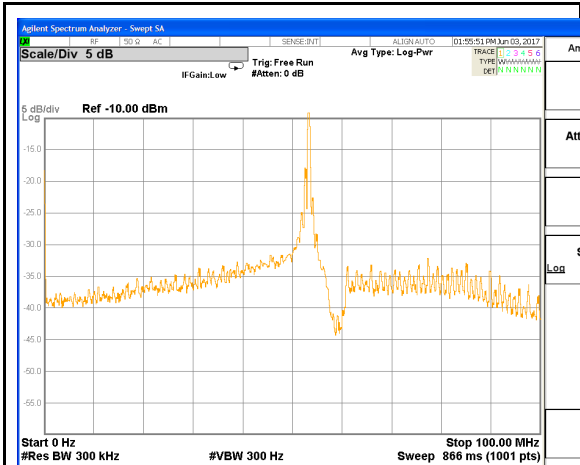
$ruler\ measured\ \Delta L \approx 11.5\ cm$

$f_i = 53.35\ MHz$

$f\ range\ shown = 0 - 100\ MHz$
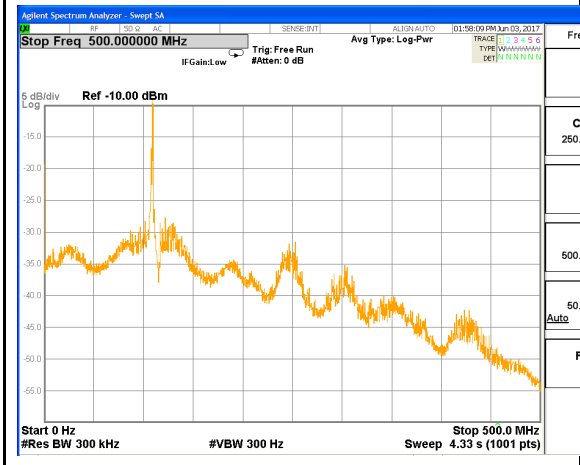
$ruler\ measured\ \Delta L \approx 22.5\ cm$
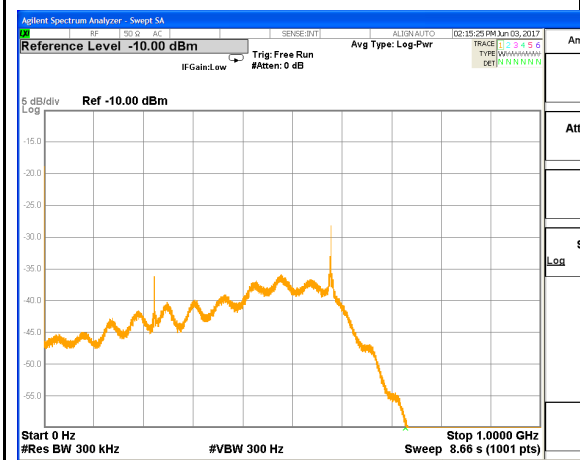
$f_i = 110\ MHz$

$f\ range\ shown = 0 - 500\ MHz$
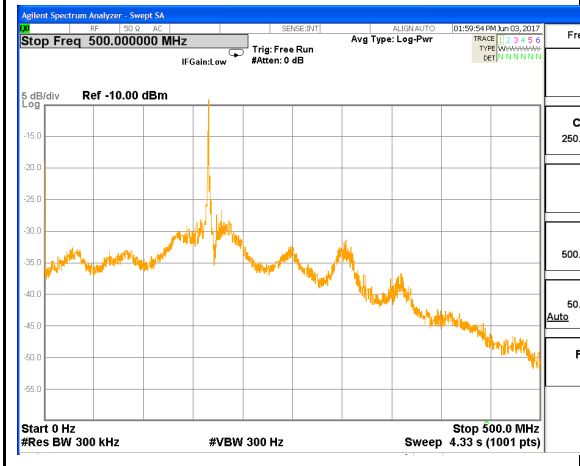
$ruler\ measured\ \Delta L \approx 34\ cm$

$f_i = 165.54\ MHz$

$f\ range\ shown = 0 - 500\ MHz$
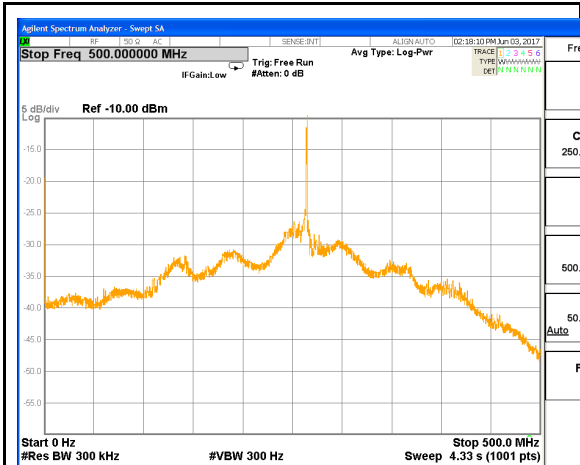
$$ruler\ measured\ \Delta L \approx 56.5\ cm$$

$$f_i = 264.89\ MHz$$

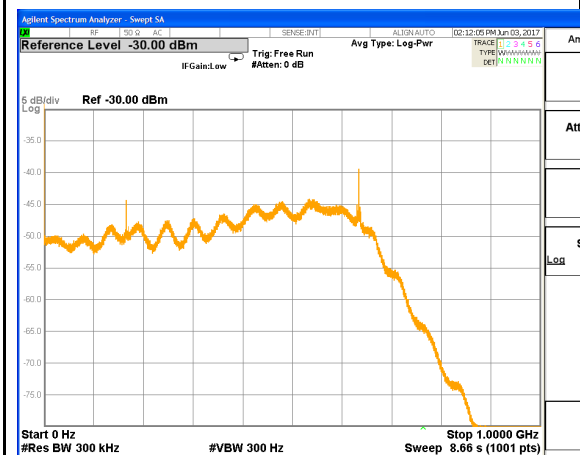$$f\ range\ shown = 0 - 500\ MHz$$

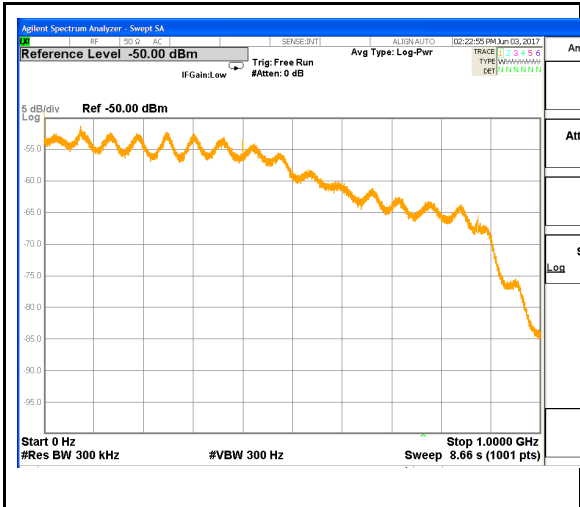$$ruler\ measured\ \Delta L \approx 119\ cm$$

$$f_i = 577.8\ MHz$$

$$f\ range\ shown = 0 - 1\ GHz$$

$$ruler\ measured\ \Delta L \approx 130.5\ cm$$

$$f_i = 633.57\ MHz$$

$$f\ range\ shown = 0 - 1\ GHz$$

$ruler\ measured\ \Delta L \approx 187.5\ cm$

$$f_i = N/A$$

$$f\ range\ shown = 0 - 1\ GHz$$